PHOTOPHYSICAL PROPERTIES OF CATIONIC AND

NEUTRAL DYES CONFINED IN ZEOLITE LTL:

EXPERIMENTAL AND THEORETICAL STUDIES

Wilaiporn Insuwan

A Thesis Submitted in Partial Fulfillment of the Requirements for the

Degree of Doctor of Philosophy in Chemistry

Suranaree University of Technology

Academic Year 2013

สมบัติทางกายภาพเชิงแสงของสีย้อมที่เป็นแคตไอออนและเป็นกลาง
ที่ถูกกักขังในซีโอไลต์แอลทีแอล: การทดลองและการศึกษาเชิงทฤษฎี

นางสาววิไลพร อินสุวรรณ

วิทยานิพนธ์นี้เป็นส่วนหนึ่งของการศึกษาตามหลักสูตรปริญญาวิทยาศาสตรดุษฎีบัณฑิต
สาขาวิชาเคมี
มหาวิทยาลัยเทคโนโลยีสุรนารี
ปีการศึกษา 2556

PHOTOPHYSICAL PROPERTIES OF CATIONIC AND

NEUTRAL DYES CONFINED IN ZEOLITE LTL:

EXPERIMENTAL AND THEORETICAL STUDIES

Suranaree University of Technology has approved this thesis submitted in partial fulfillment of the requirements for the Degree of Doctor of Philosophy.

Thesis Examining Committee

_____

(Assoc. Prof. Dr. Jatuporn Wittayakun)

Chairperson

_____

(Asst. Prof. Dr. Kunwadee Rangsriwatananon)

Member (Thesis Advisor)

_____

(Asst. Prof. Dr. Sanchai Prayoonpokarach)

Member

_____

(Asst. Prof. Dr. Thanaporn Manyum)

Member

_____

(Asst. Prof. Dr. Siriporn Jungsuttiwong)

Member

_____   _____

(Prof. Dr. Sukit Limpijumnong)   (Assoc. Prof. Dr. Prapun Manyum)

Vice Rector for Academic Affairs   Dean of Institute of Science

วิไลพร อินสุวรรณ : สมบัติทางกายภาพเชิงแสงของสีย้อมที่เป็นแคตไอออนและเป็นกลาง
ที่ถูกกักขังในซีโอไลต์แอลทีแอล : การทดลองและการศึกษาเชิงทฤษฎี
(PHOTOPHYSICAL PROPERTIES OF CATIONIC AND NEUTRAL DYES
CONFINED IN ZEOLITE LTL: EXPERIMENTAL AND THEORETICAL STUDIES)
อาจารย์ที่ปรึกษา : ผู้ช่วยศาสตราจารย์ ดร.กุลวดี รังษีวัฒนานนท์, 194 หน้า

ส่วนแรกของวิทยานิพนธ์เกี่ยวข้องกับการสังเคราะห์ซีโอไลต์แอลทีแอลที่มีสัณฐานวิทยา
แตกต่างกันภายใต้การพิจารณาพารามิเตอร์ต่างๆเช่นความเป็นด่าง ความเจือจาง ปริมาณอลูมิเนียม
ออกไซด์และซิลิกอนไดออกไซด์ซีโอไลต์แอลทีแอลในรูปของโปรตอน (H-LTL) และ
โพแทสเซียม (K-LTL) ที่มีสัณฐานแบบฮ็อกกี้น้ำแข็งและแบบทรงกลมมาใช้เป็นโฮสต์เพื่อการเข้า
ไปอยู่ของสีย้อมประจุบวก (อะคลิดีน ไฮโดรคลอไรด์ และอะคลิฟราวีน ไฮโดรคลอไรด์) และสี
ย้อมที่เป็นกลาง (ทรานส์-เอโซเบนซีนและทรานส์-สตีลบีน)ที่ทำหน้าที่เป็นเกสต์ที่จะเข้าไปอยู่ใน
ช่องของซีโอไลต์สีย้อมที่อยู่ในซีโอไลต์แอลทีแอลทำหน้าที่เป็นเสาอากาศเทียมซึ่งมีบทบาทสำคัญ
สำหรับการรับแสงและลำเลียงแสงไปยังโมเลกุลเป้าหมายเช่นสารกึ่งตัวนำประโยชน์ของซีโอไลต์
แอลทีแอลก็คือการป้องกันไม่ให้เกิดการรวมตัวของสีย้อมถึงแม้ว่าสีย้อมจะมีความความเข้มข้นสูง
และเป็นผลทำให้โมเลกุลของสีย้อมมีสมบัติทางแสงที่ดีเยี่ยม ดังนั้นการออกแบบวัสดุที่ดีได้ต้อง
เข้าใจถึงสมบัติเชิงสเปกโทรสโกและ สมบัติทางกายภาพเชิงแสงของแต่ละสีย้อมเรืองแสง

ส่วนที่สองของวิทยานิพนธ์คือการทดลองและการศึกษาเชิงทฤษฎีของสมบัติทางกายภาพเชิง
แสงของสีย้อมประจุบวกที่อยู่ในซีโอไลต์แอลทีแอลในรูปโปรตอน และในรูปโพแทสเซียมที่มี
สัณฐานแบบฮ็อกกี้น้ำแข็งและแบบทรงกลมการสังเกตสมบัติเชิงสเปกโทรสโกปีของทั้งสองสีซึ่ง
ให้ผลที่สอดคล้องกับการคำนวณทางทฤษฎีซึ่งในการคำนวณใช้ระเบียบวิธีทฤษฎีฟังก์ชันความ
หนาแน่น (DFT) และทฤษฎีฟังก์ชันความหนาแน่นที่ขึ้นกับเวลา (TD-DFT)สมบัติทางกายภาพเชิง
แสงของสีย้อมมีความไวต่อสภาวะแวดล้อมของซีโอไลต์แอลทีแอลโดยไม่ขึ้นกับลักษณะทาง
สัณฐานวิทยา สีย้อมที่อยู่ในซีโอไลต์แอลทีแอลสามารถถ่ายโอนพลังงานภายในซีโอไลต์โดยกลไก
ของfluorescence resonance energy transfer (FRET)จากอะคลิดีน ไฮโดรคลอไรด์ที่เป็นตัวให้
พลังงานไปยังอะคลิฟราวีน ไฮโดรคลอไรด์ที่เป็นตัวรับพลังงานได้สำเร็จ

นอกจากสีย้อมประจุบวกแล้วเรายังได้ศึกษาสมบัติทางกายภาพเชิงแสงของสีย้อมที่เป็น
กลางเช่น ทรานส์-เอโซเบนซีน พบว่าข้อมูลการทดลองสอดคล้องกับผลการคำนวณ โดยที่สีย้อมที่
อยู่ในสารละลายจะมีโครงสร้างแบบระนาบ ในขณะที่อยู่ในซีโอไลต์แอลทีแอลจะถูกบังคับด้วย
โครงสร้างของซีโอไลต์ทำให้เกิดการบิดเบี้ยวเนื่องจากผลกระทบของการจำกัดในซีโอไลต์

นอกจากนี้ยังสามารถตรวจพบการเปล่งแสงฟลูออเรสเซนส์ของโปรโตเนต*ทรานส์*-เอโซเบนซีนที่
อยู่ในซีโอไลต์แอลทีแอลในรูปโปรตอนเท่านั้นในขณะที่*ทรานส์*-เอโซเบนซีนที่อยู่ในซีโอไลต์แอล
ทีแอลในรูปโพแทสเซียมไม่สามารถตรวจพบการเรืองแสงได้

ในส่วนสุดท้ายเป็นการศึกษาไอโซเทอร์มของการดูดซับของอะคลิดีนไฮโดรคลอไรด์
และอะคลิฟาวีนไฮโดรคลอไรด์ที่ดูดซับในซีโอไลต์แอลทีแอลในรูปโปรตอน และในรูป
โพแทสเซียมเพื่อที่จะทำการประมาณปริมาณของสีที่ถูกดูดซับสูงสุดในซีโอไลต์แอลทีแอลปริมาณ
การดูดซับสูงสุดของอะคลิฟาวีนไฮโดรคลอไรด์และอะคลิดีนไฮโดรคลอไรด์ในซีโอไลต์แอลที
แอลในรูปโปรตอน และในรูปโพแทสเซียม อยู่ในช่วงร้อยละ4.03-6.44 และร้อยละ0.45-2.80
ตามลำดับจากสมบัติทางกายภาพเชิงแสงของสีย้อมทั้งสองสามารถใช้เป็นวัสดุเสาอากาศเทียม
ซึ่งอะคลิดีนไฮโดรคลอไรด์และอะคลิฟาวีนไฮโดรคลอไรด์ทำหน้าที่เป็นตัวให้และตัวรับตามลำดับ
แต่อย่างไรก็ตามบนพื้นฐานของความสามารถในการดูดซับของสีย้อมเหล่านี้เราแนะนำว่าอะคลิดีน
ไฮโดรคลอไรด์และอะ คลิฟาวีนไฮโดรคลอไรด์ใช้เป็นตัวให้และตัวรับพลังงานที่ไม่สามารถ
นำมาใช้ได้อย่างมีประสิทธิภาพเนื่องจากว่าระบบของเสาอากาศเทียมจะมีประสิทธิภาพสูงถ้าซี
โอไลต์ แอลทีแอลมีปริมาณของตัวให้ (อะคลิดีนไฮโดรคลอไรด์)จำนวนสูงกว่าเมื่อเปรียบเทียบกับ
ตัวรับ (อะคลิฟาวีนไฮโดรคลอไรด์)

สาขาวิชาเคมี   ลายมือชื่อนักศึกษา_____
ปีการศึกษา 2556   ลายมือชื่ออาจารย์ที่ปรึกษา_____

WILAIPORN INSUWAN : PHOTOPHYSICAL PROPERTIES OF

CATIONIC AND NEUTRAL DYES CONFINED IN ZEOLITE LTL :

EXPERIMENTAL AND THEORETICAL STUDIES. THESIS ADVISOR :

ASST. PROF. KUNWADEE RANGSRIWATANANON, Ph.D. 194 PP.

ZEOLITE LTL/PHOTOPHYSICAL PROPERTIES/CATIONIC DYE/NEUTRAL
DYE/ADSORPTION ISOTHERM

The first part of the thesis work involved synthesis of zeolite LTL with different

morphologies under consideration of various parameters, such asalkalinity, dilution,

Al_2O_3 and SiO_2 content. Zeolites LTL (K-LTL and H-LTL) with ice hockey and

round shape were used as hosts for an insertion of cationic dyes (acridine

hydrochloride, Ac and acriflavine hydrochloride, AF) and neutral dyes (*t*-azobenzene

and stillbene) as the guest molecules into the zeolite channels. The dyes loaded on the

zeolite LTL acted as artificial antenna materials that play a key role for light

harvesting and transporting to a target molecule, such as a semiconductor. The

advantage of the zeolite LTL is being able to prevent aggregation of the dye even at a

high concentration. As a result, the dye molecules may exhibit excellent optical

activities. To design optimized materials, it is necessary to understand the

spectroscopic and photophysical properties of each fluorescent dye.

The second part of the thesis work includedexperimental and theoretical studies

of the photophysical properties of cationic dyes loaded on (K-LTL and H-LTL) with

ice hockey and round shapes. The observed spectroscopic properties of these two dyes

(AF and Ac) confirm thetheoretical calculations, in which density function theory

IV

(DFT) and time dependent density function theory (TD-DFT) were employed. Their photophysical properties were sensitive to the microenvironment of zeolite LTL, independent of their morphologies. Moreover, we also demonstrate that the dye loaded on the zeolite LTL couldtransfer energy within the zeolite by a fluorescence resonance energy transfer (FRET) mechanismfrom Ac (donor) to AF (acceptor).

Besides cationic dyes, the neutral dye,*t*-azobenzene, wasinvestigated. The photophysical properties of *t*-azobenzene from the experimental data are correlated with the calculation results. The dye in solution can be relaxed into the planar structure, while in zeotite LTL it is constrained by the framework and is therefore twisted due to the confinement effects in zeolite. Moreover, the fluorescence was detected only from protonated *t*-azobenzene incorporated into H-LTL, while no fluorescence was detected from*t*-azobenzene confined in K-LTL framework.

In the last part, adsorption isotherms of Ac and AF on the zeolite LTL (H-LTL and K-LTL) were obtained in order to estimate the amount of the dyesadsorbed onthe zeolite LTL. The maximum loading (Θ_{max})of AF and Ac on H-LTL and K-LTL was in the range of 4.03-6.44% and 0.45-2.80%, respectively. Based on the photophysical properties of the two dyes, they can be utilized as artificial antenna materials, in which Ac and AF act asa donor and an acceptor, respectively. However, based on the adsorption capability of these dyes, it could be suggested that Ac and AF are not an effective donor-acceptor pair in the zeolite LTL, becausean antenna system would perform efficiently if the zeolite LTL contained a higher amount of thedonor (Ac)than the acceptor (AF).

School of Chemistry　　　　　Student's Signature_____

Academic Year 2013　　　　　Advisor's Signature_____＿_____

ACKNOWLEDGEMENTS

CONTENTS

CONTENTS (Continued)

CONTENTS (Continued)

CONTENTS (Continued)

CONTENTS (Continued)

CONTENTS (Continued)

CONTENTS (Continued)

CONTENTS (Continued)

Page

LIST OF TABLES

LIST OF TABLES (Continued)

LIST OF TABLES (Continued)

LIST OF FIGURES

LIST OF FIGURES (Continued)

LIST OF FIGURES (Continued)

LIST OF FIGURES (Continued)

LIST OF FIGURES (Continued)

LIST OF FIGURES (Continued)

LIST OF FIGURES (Continued)

LIST OF FIGURES (Continued)

LIST OF SCHEME

LIST OF ABBREVIATIONS

Ac   acridine hydrochloride

AF   acriflavine hydrochloride

a unit cell dimensions

b unit cell dimensions

c unit cell dimensions

cm^{-1} wavenumber (per centimeter)

C_0 and C_e concentrations of dyes in solution at initial and equilibrium, respectively

d_z diameter of the crystal in nanometer

FT-IR   Fourier transform infrared

FRET   Fluorescence resonance energy transfer

g   gram

HOMO   highest occupied molecular orbital

i   ice hockey shape

I_0 and I intensities of photon before and after the sample, respectively

K_L Langmuir constant

L   optical path length

LSC   luminesescenced solar concentrators

LTL   Linde Type L

LUMO   lowest unoccupied molecular orbital

M   molar

LIST OF ABBREVIATIONS (Continued)

mL	milliliter
mM	millimolar
M_z	molar mass of pure potassium zeolite K-LTL (2883 g/mol)
M_D	molar mass of the dye.
nm	namometer
n_D^+	number of molecules intercalated
n_s	number of sites available in zeolite LTL
p_z	density of the zeolite crystal
qe	amount of dye adsorbed at equilibrium.
q_m	maximum adsorption monolayer capacity
r	round shape
R	ideal gas constant
R^2	R-squared
SEM	Scanning electron microscopy
T	temperature
V	volume of the solution.
W_z	amount of zeolite LTL in grams
$\Delta G°$	change in standard Gibbs free energy
$\Delta H°$	change in standard enthalpy
$\Delta S°$	change in standard entropy
Θ_{max}	maximum loading
μm	micrometer

LIST OF ABBREVIATIONS (Continued)

ρ   occupation probability of dyes molecule

λ_{abs} absorption maximum wavelength

λ_{emis} emission maximum wavelength
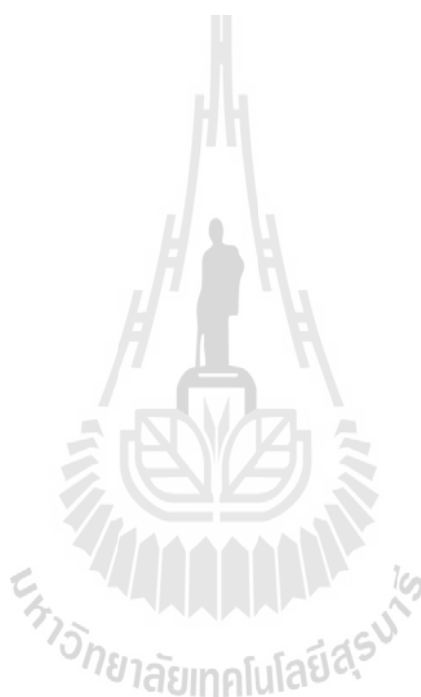
CHAPTER I

INTRODUCTION

1.1 Significance of the study

Zeolites are appealing inorganic microporous frameworks that possess a large variety of well-defined internal structure such as uniform cages, cavities or channel (Suib, 1993). A useful feature of zeolites is their ability to intercalate guest molecules within the intra void space, resulting in the modification of their properties. Especially, zeolite LTL has been employed in photochemical research (Yoon, 1993; Calzafferi et al., 2000). Because the zeolite LTL has a one-dimentional channel with 0.71 nm in diameter. Therefore, it can be filled with suitable organic guests, like fluorescent dye molecules. The encapsulation of organic fluorophores into the channel of zeolite LTL can avoid the formation of aggregates, improving the chemical, thermal, and photochemical stability of the dyes, and enforcing them to align in a colinear geometry and be distributed uniformly along the narrow channel. In contrast to the large spherical supercages allows to movement of guest molecules and heterogeneous distribution. Many types of dye have been incorporated into zeolite LTL such as thionine, methyl viologen, pyronine, oxonine and resorufin (Hennessy et al., 1999; Calzaferri and Gfeller, 1992; Gfeller, Megelski, Calzaferri, 1999; Brühwiler, Gfeller, Calzaferri, 1998). Dye-loaded zeolite systems allow various applications as microlaser (Calzaferri et al., 2002), optical switches (Hoffmann,

Resch-Genger, and Marlow, 2003), chemical sensors (Misra, Misra, Joshi, and Pant, 1999) and artificial antenna systems (Pauchard, Devaux, and Calzaferri, 2000). The main problem in the design of fluorescent dye in various applications is linked to the photophysical behavior of dyes in solid state. Generally, dyes are strongly fluorescent when dissolved in organic solvents at low concentration, but they lose their fluorescence upon aggregation in high concentration and solid state. This is due to the intermolecular interactions that take place in solid state and open deactivation pathways that compete with the fluorescence process (Birks, 1970; Silinsh, 1980). Therefore, in this work we focus on how to synthesize various morphologies of pure zeolite LTL which may affect zeolitic physicochemical properties. The adsorption and photophysical studies of dyes onto zeolite LTL have been studied as well in order to provide the information on the interaction of dyes and zeolite that plays a determining role to photonic artificial antenna system. Moreover, in this work besides the experimentation, the calculation has been studied as well.

1.2 Research objectives

1. To synthesize pure zeolite LTL by hydrothermal method.

2. To characterize the physical and chemical properties of the zeolite LTL.

3. To study the adsorption interaction and photophysical properties of dyes loaded zeolite LTL.

4. To study the structure and arrangement of dyes within H-LTL and K-LTL by calculation method.

5. To study the adsorption isotherms of cationic dyes (acriflavine hydrochloride and acridine hydrochloride) onto zeolite LTL (H-LTL and K-LTL with ice hockey and round shape).

1.3 Scope and limitations of the study

1. The syntheses of pure zeolite LTL are carried out by hydrothermal method and varied the initial gel compositions (alkalinity, dilution, Al_2O_3 and SiO_2 content) which affect the crystallinity, crystal shapes and crystal sizes.

2. The products are characterized by XRD, SEM, FT-IR and the particle size distribution techniques.

3. The zeolite host-guest systems have been focused on three areas: (i) incorporation processes of dye molecules into zeolites, (ii) investigation of photophysical properties, and (iii) to assist the experimental analysis of these host-guest systems, computational methods have been carried out to explore the interaction of dyes with extraframework cations of the hosts as well as photophysical properties of these dyes incorporated in the channel of zeolite LTL (H-LTL and K-LTL including ice hockey and round shape). In this study, acridine hydrochloride and acriflavine hydrochloride are selected as cationic dyes and neutral dye are *t*-azobenzene and *t*-stillbene. The structures of these dyes are shown in Figure 1.1. Due to their molecular sizes, low sublimation temperature (*t*-azobenzene and *t*-stilbene) and photochemical and thermal stability, these dyes are favorable for insertion into the zeolite LTL channel.

4. Dyes (acriflavine hydrochloride and acridine hydrochloride) adsorbed onto

zeolite LTL (H-LTL and K-LTL) are performed with the different temperatures (30, 40 and 50 °C) and the adsorption thermodynamic parameters are determined.

Acridine hydrochloride (Ac)   Acriflavine hydrochloride (AF)

t-stillbene   *t*-azobenzene
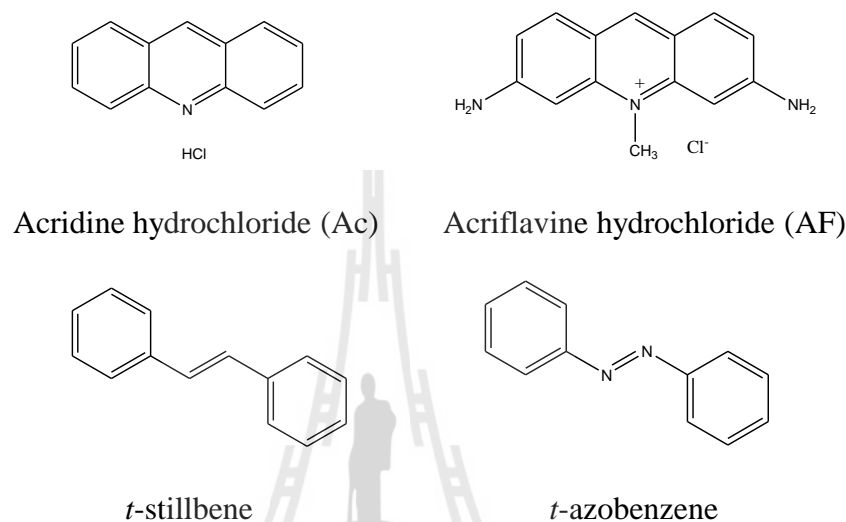
Figure 1.1 The structures of the selected dye molecules for insertion into zeolite LTL.

1.4 Zeolite LTL as a host

Zeolites are microporous crystalline aluminosilicates, composed of TO_4 (T = Si, Al) with O atoms arranging in tetrahedra. For a completely siliceous structure, combination of TO_4 (T = Si) units in this fashion leads to silica (SiO_2), which is an uncharged solid. Upon incorporation of Al into the silica framework, the +3 charge on the Al makes the framework negatively charged, and requires the presence of extraframework cations (inorganic and organic cations can satisfy this requirement) within the structure to keep the overall framework neutral. The zeolite composition can be best described as having three compositions.

$$M^{m+}{}_{n/m} \qquad \cdot \qquad [Si_{1-n}\,Al_nO_2] \qquad \cdot \qquad n\,H_2O$$

extraframework cations   framework   sorbed phase
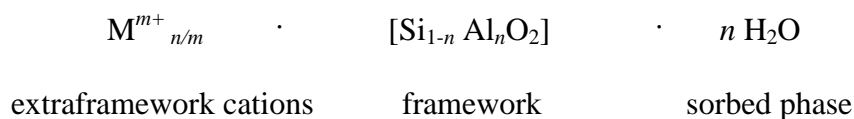
The extraframework cations are ion exchangeable and give rise to the rich ion-exchange chemistry of these materials. The novelty of zeolites stems from their microporosity as a result of the topology of the framework (Auerbach, Carrado, and Dutta, 2003).

Zeolite LTL (framework topology code LTL) was first described in 1968 and is one of a relatively small number of zeolites in which access to the internal pore volume is controlled by apertures that contain 12 T atoms (T = tetrahedral species: Si, Al, Ga, etc.) and 12 shared apical oxygen atoms (Newsam, 1989). The crystal structure of zeolite LTL has been determined from powder X-ray diffraction (XRD) at room temperature. The zeolite LTL is hexagonal with unit cell dimensions of a = 18.4 Å and c = 7.5 Å. Its framework density is 16.3T/1000 Å (Xu, Pang, Yu, Huo, and Chen, 2007). The structure has been refined assuming space group P6/mmm. The aluminosilicate framework is based upon the polyhedral cages which are formed by five 6-membered and six 4-membered rings and are found in cancrinite cage. These cavities are linked through the planes of their upper and lower 6-membered ring, thus forming columns in which hexagonal prisms and polyhedra alternate, and which run parallel to the c axis. The rings have free diameter of 7.1 Å in narrowest part and 12.6 Å in the widest part. The number of channels can be calculated from $0.265(d_c)^2$, where d_c is the diameters of the cylinder in nanometers. Zeolite LTL has five different cation sites, namely, A is the center of D6R, B is in the center of cancrinite cage, C lies midway between the centers of two adjacent cancrinite cage, and D is inside the main channel near the wall of the eight-membered ring. Furthermore, in case of

dehydrated zeolite LTL has cation site is located between site A (see Figure 1.2) (Minkowski, Pansu, Takano, and Calzaferri, 2006; Palomino et al., 1997; Ohgushi, Matsuo, Satoh, and Matsumoto, 2009; Burton and Lobo, 1999).
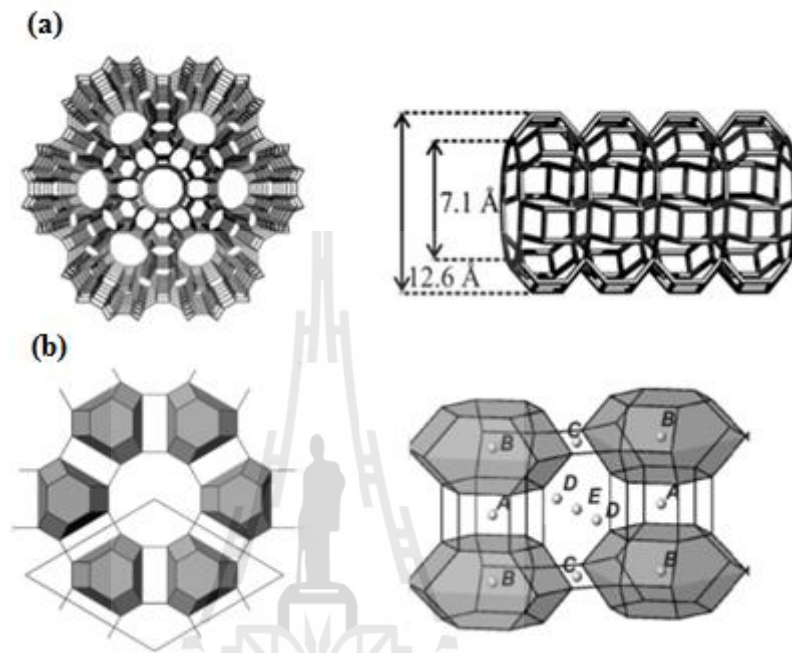
Figure 1.2 (a) Structure of zeolite LTL and framework side view of a main channel, (b) the cancrinite cages highlighted as polyhedra and the different cation site positions A to E (Hashimoto, 2003).

It is possible to tune the length, the diameter and the respect ratio (length to diameter ratio) of zeolite LTL crystals within a large range. Crystals ranging from 30 to 7 micrometer length were synthesized by Calzaferri et al. In addition they also calculated the number of parallel channels in the crystal as follows (Calzaferri and Devaux, 2010):

$$n_{ch} = \frac{\pi(\frac{d_z}{2})^2}{|a|^2 \sin(60)} = \frac{\pi}{2\sqrt{3}}(\frac{d_z}{|a|})^2 \tag{1}$$

where d_z is the diameter of the crystal in nanometer and $|a|$ is the length of the primitive vector.

Using the values of zeolite LTL the equation can be simplified to

$$n_{ch} = 0.267(d_z)^2 \tag{2}$$

A zeolite LTL crystal of 600 nm in diameter gives rise to about 96,000 parallel channels.

$$n_{u.c} = (\frac{m_z}{M_Z}) \tag{3}$$

The number of unit cells (in mol) in m_z grams of zeolite LTL can be calculated as follows Where m_z is the molar mass of a unit cells, $M_z = 2883$ g/mol for pure potassium zeolite LTL. 10 mg of pure potassium zeolite L contains 3.47×10^{-6} mol unit cells.

1.5 Dyes as guest molecules

Dye molecules at high concentrations have a tendency to aggregate. Aggregates are highly undesirable, since they quench the luminescence as a rule. Inside the channels of zeolite LTL, molecules are prevented from building dimmers or passing each other due to spatial restrictions imposed by the zeolite. High concentrations of monomeric dye can be obtained. Neutral as well as cationic dyes can be inserted into the channels of zeolite LTL; neutral dyes from gas phase and cationic ones by means of ion exchange. Dye molecules can be divided into three types that can be inserted into the channels of zeolite LTL (Calzaferri et al., 2002) (i) Molecules that are small enough to fit into a unit cell such as biphenyl, 4-hydroxy-TEMPO, 9-fluorenone, and methyl viologen (MV^{2+}). For molecules of type (i) not only translational but also

large-amplitude modes can be activated. (ii) Molecules that the size makes it hard to guess their positions and orientations in the channel. Oxonine, pyronine, and thionine are molecules of this type. (iii) Molecules which are large that they have no other choice but to align along the c-axis. Many examples fit into this category. The light-sensitive diphenylhexatriene (DPH) is one of them. From the whole volume of the zeolite, only a part, the channel, is available for guest species. Therefore, it is convenient to introduce a parameter bearing the information on dye concentration but based on purely geometrical (space-filling) properties of the zeolite as a host which extent the zeolite channels are filled with dye molecules. The loading, or occupation probability, ρ of a dye-zeolite LTL material is defined as follows (Calzaferri and Devaux, 2010);

$$\rho = \frac{\text{number of occupied sites}}{\text{total amount of sites}} \tag{4}$$

From (Eq 4) one gets the following expression to calculate the loading, if the weight m_z and m_D are zeolite and dye in grams;

$$\rho = \frac{m_D}{M_D}\left(\frac{M_Z n_s}{m_z}\right) \tag{5}$$

Where M_D is the molar mass of the dye. It ranges of (p) from 0 for an empty zeolite to 1 for a fully one. The dye concentration of a dye-zeolite material c(ρ) can be expressed as a function of loading (Calzaferri and Devaux, 2010);

$$c(\rho) = \frac{p_Z \, \rho}{M_Z n_S} \tag{6}$$

Where p_z is the density of the zeolite crystal, M_z is the molar mass of one unit cell, n_s is the number of unit cells that form one site, and c(p) is expressed in units of mol/L.

Inserting the values for potassium zeolite LTL (p_z = 2.17 g/cm^3, M_z = 2883g/mol), one obtains

$$c(\rho) = 0.752 \frac{\rho}{n_S} \tag{7}$$

1.6 Dye-loaded zeolite LTL materials

Plant photosynthesis is the conversion of light into chemical energy. Light is absorbed by photonic antenna systems consisting of a few hundred chlorophyll molecules. These systems allow fast energy transfer from an electronically excited molecule to an unexcited neighbor molecule in such a way that the excitation energy reaches the reaction center with high probability. In natural antenna the formation of aggregates is prevented by fencing the chlorophyll molecules in polypeptide cages. Systems with similar properties can be prepared by inserted dyes inside a microporous material that the cavities can uptake only monomers of dye without aggregates (Calzaferri and Devaux, 2010). This system zeolite LTL was equivalent to polypeptide cages and dye molecule comparable to chlorophyll molecules. Especially, zeolite LTL has been using as a host due to its crystals consisting of one-dimensional channels which are filled with dye molecules. The dye-filled zeolite LTL crystals are used as light-harvesting antenna. Designing optimized materials for these applications and designing the devices themselves requires a profound knowledge of their spectroscopic and photophysical properties. When the dye-loaded zeolite LTL was irradiated, a small portion of the energy release is disperse as vibrations throughout the molecules, the rest of the energy is emitted as fluorescence. This allows them to transfer the excitation energy directly without alteration into light from molecule to

molecule. Recently, Veiga-Gutierrez and co-workers (2012) have applied these method to prepare hockey-punk shaped crystals that most of them are standing on their base which yield monolayer with 95% standing crystals instead of cylindrical shape. Then dyes were filled. This method was allowing efficient transport of electronic excitation energy towards the zeolite LTL substrate interface. The supramolecular organization of the dyes inside the channel is considered as a first stage. It allows light harvesting within a certain volume of a dye-loaded zeolite LTL and radiationless energy transport to the end of the crystal that will be focused in this work. The second stage of organization is the coupling to an acceptor fluorophore at the ends of the zeolite LTL channel. The acceptor has to accept excitation energy from the dyes inside the channel but they are not able to pass it back. The third stage of organization is attached onto the surface of photonic device such as semiconductor, it is possible that the energy will be transferred from the dye to the semiconductor, achieving the goal of exciting the semiconductor (Figure 1.3.). Moreover, such antenna materials open possibilities for the design of a silicon based solar cell (Calzaferri et al., 2006) and luminescent solar concentrators (LSC) (Koeppea, Bossart, Calzaferri, and Sariciftci, 2007), where the excitation energy can only migrate in one direction towards the zeolite-semiconductor interface.

1.6.1 Solar cells sensitized by dye loaded zeolite LTL antenna

A dye-loaded zeolite LTL composites prepared as a monodirectional antenna would open possibilities for a different type of sensitized solar cell. In regular dye solar cells, light is directly absorbed by the sensitizer dye, exciting an electron from the HOMO level to the LUMO level. Then, electrons from the excited state of

dye are injected into the conduction band of TiO_2. A major disadvantage in such cells is that very few dyes can absorb a broad spectral range of the solar spectrum and dye molecules have to be regenerated by a redox couple. Moreover, reducing the amount of costly ruthenium (dye) and conducting glass or plastic are needed to produce a dye-sensitized solar cell (DSSCs).

First stage (a)

Second stage (b)
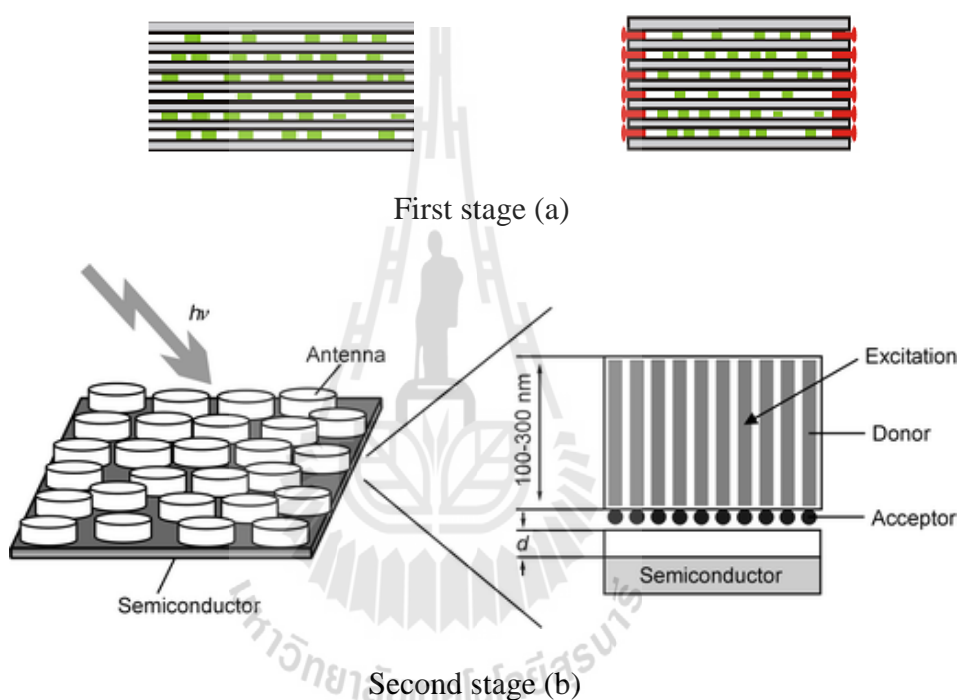
Figure 1.3 Two stages of organization; (a) Dye-loaded zeolite LTL crystal and antenna system with acceptor molecules as external traps (b) Energy Transfer (EnT) from a photonic antenna to a semiconductor (Calzaferri and Devaux, 2010).

Dye loaded zeolite LTL prove the general feasibility of enhancing light absorption and broadening the absorption spectrum by the addition of antenna material, effectively increasing the number of photons harvested by the dye-sensitized solar cell. The antenna effect, as it is found in natural photosynthetic system, is an

attractive tool to increase light absorption of solar cells. Dye-loaded zeolite LTL antenna consists of zeolite LTL as a host and incorporated luminescent dyes as donor and acceptor molecule into the channels of the crystal. Using fluorescence resonance energy transfer (FRET) to transfer energy from donor to acceptor provides a new way for enhancing the performance of dye-sensitized solar cell (Buhbut et al., 2010). In the present, dye-loaded zeolite LTL can act as additional light harvester absorbing the light. Light is absorbed by the donor molecules which became to excited molecules. The excitation energy then migrates radiationlessly among the inserted dyes towards the acceptor molecules. From there, FRET to the semiconductor takes place across a very thin insulating layer. The injected electronic excitation energy can now be used for driving the charge-separation process in the active medium. Finally, the resulting electrical current is collected through appropriate contacts (Figure 1.3).

1.6.2 Luminescent solar concentrators (LSC)

A LSC is to concentrate light with an inexpensive polymer-based device into efficient photovoltaic cells (Goetzberger and Greubel, 1977). It is a transparent plate containing with luminescent chromophores (dyes or phosphores). When light hits the face of the plate, the dyes absorb it and reemitted light at longer wavelengths or lower energy level. A substantial part of the longer wavelength light is trapped by total internal reflection and guided to the edges of the LSC plate, at which it can be convert to electricity by a photovoltaic device. Recently, some work has been presented that it can be coupled to solar cell that shown in Figure 1.4 (Calzaferri, Li, and Brühwiler, 2008). A major disadvantage in old LSC is reflection loss caused by the overlap between the absorption and emission spectra of the chromophores. Self-

absorption is the key problem that has to be solved in order to develop commercially viable LSC products (Calzaferri et al., 2011). The conception of an advanced LSC with reduced self-absorption is based on dye-zeolite inclusion compounds (Brühwiler et al., 2009). The channel of zeolite LTL are filled with a large number of donor molecules, which absorb the incident light and subsequently transport the electronic excitation energy to a comparatively small number of acceptor dyes by means of FRET. As the donor molecules are not able to absorb the acceptor luminescence, photons emitted by the acceptor molecules can travel through the LSC with low self-absorption losses.
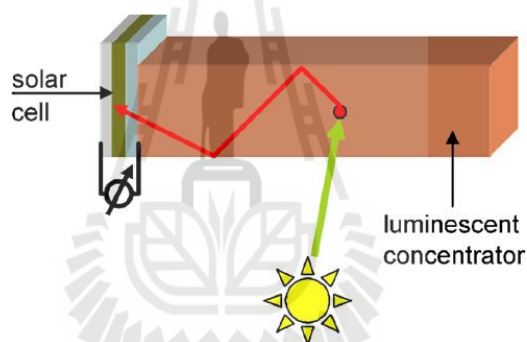
Figure 1.4 Schematic showing the working principle of a luminescent concentrator. Light is absorbed by dyes inside the concentrator and funnelled to the solar cell via a waveguiding structure (Koeppea, Bossart, Calzaferri, and Sariciftci, 2007).

Apart from an efficient FRET between donor and acceptor dyes, the donor-to-acceptor ratio (d/a) needs to be high to reduce self-absorption. Calzaferri, G et al. have considerably improved this system by increasing the d/a to 52, by optimizing the light-harvesting and FRET efficiency (Calzaferri et al., 2011). This is an important proof for the feasibility of the high donor-to-acceptor ratios required for the reduction of self-absorption.

1.7 Adsorption

The term "adsorption" was created by Kayser in 1881 to describe the increase in concentration of gas molecules in neighboring solid surfaces. Adsorption is a process that occurs when a gas or liquid solute accumulates on the surface of a solid or a liquid (adsorbent), forming a molecular or atomic film (the adsorbate). Adsorption can occur due to deficiency on the surface because the atoms are not wholly surrounded by other atoms. Thus it is energetically favorable for them to bond with whatever happens to be available. The adsorption is generally classified into 2 types namely, physisorption and chemisorption.

Adsorption is usually described through isotherms, that is, functions which connect the amount of adsorbate on the adsorbent, with its pressure (if gas) or concentration (if liquid). One can find in literature several models describing process of adsorption, namely Langmuir isotherm and Freundlich isotherm (Hameed, Ahmad, and Aziz, 2007).

1.7.1 Langmuir isotherm

This isotherm described adsorbate-adsorbent systems in which the extent of adsorbate coverage is limited to one molecular layer at or before a relative pressure of unity is reached. Langmuir isotherm was derived on the following well-known assumption:

- Molecules are adsorbed at a fixed number of well-defined localized sites.

- Each site can occupy one adsorbate molecule.

- All sites are energetically equivalent.

- There is no interaction between molecules adsorbed on neighbouring
sites.

The chemical reaction for monolayer adsorption can be described as follows:

$$A + S \rightleftharpoons AS \qquad (8)$$

where AS is a solute molecule bound to a surface site on S, A is unadsorbed solute
molecule and S is unoccupied solid surface.

From (Eq. 8) the equilibrium constant (K_{ads}) is given by:

$$K_{ads} = \frac{[AS]}{[A][S]} \qquad (9)$$

where [A] is the concentration of solute molecule and [S] and [AS] are two-
dimensional analogs of concentration. The complete form of the Langmuir isotherm
in terms of surface coverage (Θ) is defined as the number of sites of the surface which
are covered with solute molecules.

Thus, (1 - Θ) is the fraction of the surface which is unoccupied by solute molecule.

$$\frac{[AS]}{[S]} = \frac{\Theta}{(1-\Theta)} \qquad (10)$$

From (Eq 9), express [A] as C and rewrite (Eq. 2) as

$$K_{ads} = \frac{\Theta}{C(1-\Theta)} \qquad (11)$$

By rearranging (Eq. 11), the final form of the Langmuir adsorption isotherm is
obtained.

$$\Theta = \frac{K_{ads}C}{1 + K_{ads}C} \qquad (12)$$

If define Y as the amount of mole of adsorbate per mass of adsorbent and Y_{max} as the
maximal adsorption, then:

$$\Theta = \frac{Y}{Y_{max}} \tag{13}$$

Finally, the Langmuir isotherm can be expressed as:

$$\frac{C}{Y} = \frac{1}{K_{ads}Y_{max}} + \frac{C}{Y_{max}} \tag{14}$$

where K_{ad} is the equilibrium constant, C is concentration of solute molecule at equilibrium, Y is the amount of mole of adsorbate per mass of adsorbent and Y_{max} is the maximal adsorption corresponding to complete monolayer coverage on the adsorbent surface.

1.7.2 Adsorption thermodynamic properties

In several cases, the enthalpy can be obtained by performing adsorption experiments at different temperatures. Those results are used to calculate the equilibrium constant at various temperatures. In this research Gibbs-Helmholtz equation (Eq 15) was used to calculate the changes of Gibbs' free energy (Rytwo and Ruiz-Hitzky, 2003):

$$\left(\frac{\partial}{\partial T}\left(\frac{\Delta G}{T}\right)\right)_P = \frac{-\Delta H}{T^2} \tag{15}$$

where ΔG and ΔH are the difference in Gibbs' free energy and enthalpy between the final and the initial state. As at equilibrium, $\Delta G = 0$, from (Eq. 15) can relate the equilibrium constant can be related to the standard free energy of the reaction as follows:

$$\Delta G^\circ = -RT\ln K \tag{16}$$

By combining (Eq. 15) and (Eq. 16) the Van't Hoff equation is obtained:

$$\left(\frac{\partial \ln K}{\partial T}\right)_P = \frac{\Delta H^\circ}{T^2 R} \tag{17}$$

where ΔH° is the enthalpy of the reaction at standard pressure. In addition ΔH° can be assumed constant over the temperature range of an experiment and a plot of ln K vs 1/T provides a convenient estimate of ΔH°. Form the slope of the line which is equal to $-\Delta H^\circ/R$.

1.8 Absorption and fluorescence spectroscopy

Absorption and fluorescence spectroscopy can be used to quantify different sample properties, such as concentrations and photophysical properties of the dyes. The basic processes are absorption of photons by dye molecules and the subsequent emission of fluorescence photons.
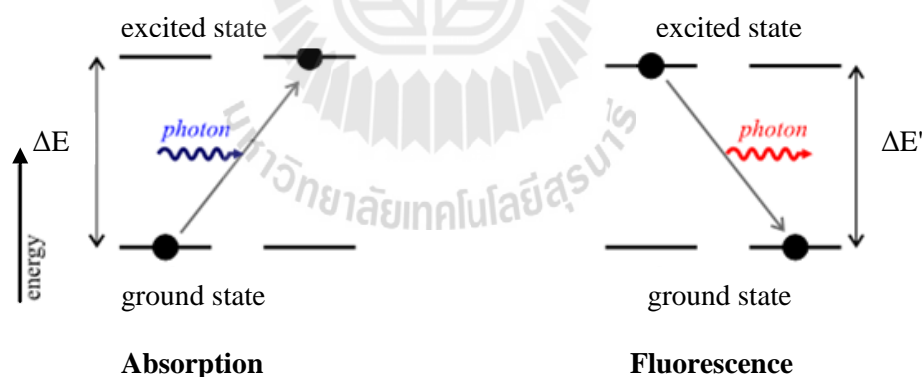
Figure 1.5 Absorption of an incident photon and emission of a fluorescence photon in a simplified fluorophore electronic state system (Lakowicz, 1999).

Figure 1.5 gives an overview of these processes. In a simplified picture, the fluorophore is described by two electronic states which are separated by an energy gap ΔE.

Absorption: When an incident photon hits a dye molecule in its ground state, the dye may be brought into its excited state. The photon is absorbed during this process, as its energy is used to excite the dye. This process only takes place if the photon energy equals the energy gap between the ground and excited state: $E_{photon} = \Delta E$.

Fluorescence: If an excited dye molecule returns to its ground state the energy $\Delta E'$ has to be deposited somewhere. One possible process is the emission of a (fluorescence) photon, carrying the energy $\Delta E'$. Although there are other possibilities to deposit $\Delta E'$, there is a class of dyes where fluorescence is the dominant path.

1.8.1 Absorption and the Lambert-Beer law

The Lambert-Beer law describes the effect of the absorption process, when light passes through some material. It connects the expected decrease in transmitted light (absorbance) with the properties of the material. Figure 1.6 shows a basic setup for absorption measurements using the Lambert-Beer law.
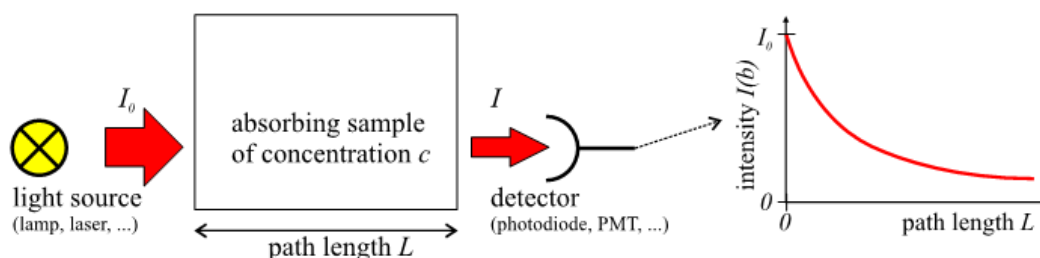
Figure 1.6 Setup of an absorption measurement (Lakowicz, 1999).

The law may be written in terms of the absorption A which is defined as the logarithmic relative decrease of intensity:

$$A = \log_{10}\left(\frac{I_0}{I}\right) \tag{18}$$

Where I_0 and I are the intensities before and after the sample.

$$A = \varepsilon(\lambda) \cdot L \cdot c \tag{19}$$

Where c is the sample concentration and L is the optical path length. The wavelength dependent coefficient $\varepsilon(\lambda)$ is called molar absorptivity and is given in units of $M^{-1}cm^{-1}$. The absorptivity may also be used to identify different components in the sample. This is usually done in an absorption spectrometer (Figure 1.7). Measurement I_0 in a reference sample to get rid of any influence by the solvent are performed. Thus the measurement of the absorption is absolute, independent of the spectrometer, being the comparison of two measured intensities.
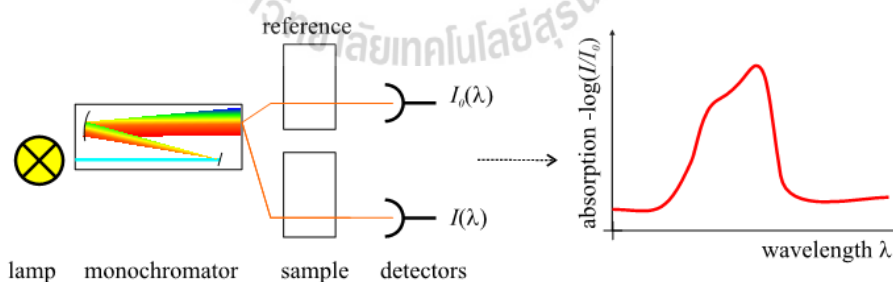
Figure 1.7 Absorption spectrometer (Lakowicz, 1999).

1.8.2 Absorbing Species

Molecules with σ bonds only

Molecule like CH_4, all bonds in methane are σ bonds and the only transition possible is the σ-σ* transition. However, the σ-σ* transition requires very high energy which occurs in vacuum UV.

Molecules with n electrons

Electrons in the valence shell that are not used up in chemical bonds are referred to as nonbonding electrons (n electrons).

Molecules with π bonds

Absorption of radiation by an alkene, containing a double bond, can result in σ−σ* or π−π* transitions. The σ−σ* transition is not useful but the π−π* turned is very useful since it requires reasonable energy and has good absorptivity. There are a number of transitions possible involving the bonding and the nonbonding electrons. The generalized molecular orbital energy level diagram and possible transitions for organic compounds is given in Figure 1.8.
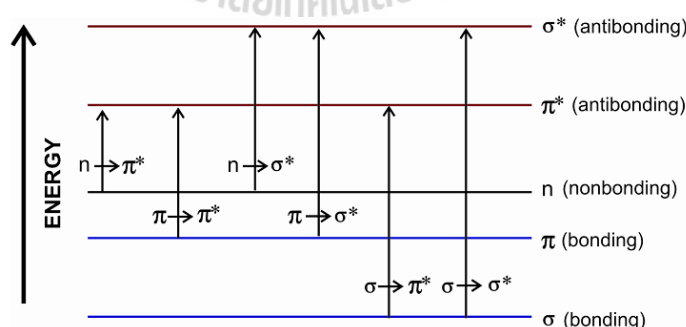
Figure 1.8 Generalised molecular orbital energy level diagram and possible transitions for organic compounds (Lakowicz, 1999).

1.8.3 Important terms and definitions

Chromophore

The energy of radiation being absorbed during excitation of electrons from ground state to excited state primarily depends on the nuclei that hold the electrons together in a bond. The group of atoms containing electrons responsible for the absorption is called chromophore.

Shifts in the absorption spectrum

Bathochromic shift is a change of spectral band position in the Absorption or emission spectrum of a molecule to a longer wavelength (lower absorption or emission spectrum of a molecule to frequency). This can occur because of a change in environmental conditions such as, a change in solvent polarity will result in solvatochromism.

Hypsochromic shift is referred to as blue shift in photochemistry. The blue shift is the phenomenon that the frequency of an electromagnetic wave emitted by a source moving towards the observer is shifted towards the blue side of the electromagnetic spectrum (that is, its wavelength is decreased).

Solvent effects

Highly pure, non-polar solvents such as saturated hydrocarbons do not interact with solute molecules either in the ground or excited state and the absorption spectrum of a compound in these solvents is similar to the one in a pure gaseous state. However, polar solvents such as water, alcohols etc. may stabilize or destabilize the molecular orbitals of a molecule either in the ground state or in excited state and the spectrum of a compound in these solvents may significantly vary from the one recorded in a hydrocarbon solvent. In case of π - π^* transitions, the excited

states are more polar than the ground state and the dipole-dipole interactions with solvent molecules lower the energy of the excited state more than that of the ground state. Therefore a polar solvent decreases the energy of π - π^* transition. In case of n - π^* transitions, the polar solvents form hydrogen bonds with the ground state of polar molecules more readily than with their excited states. Therefore, in polar solvents the energies of electronic transitions are increased (see Figure 1.9).
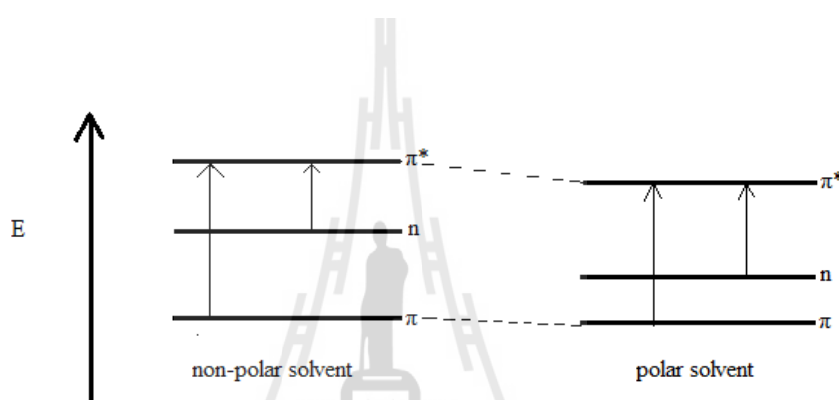
Figure 1.9 Molecular orbital energy level diagram and possible transitions for organic compounds in non-polar and polar solvent (Lakowicz, 1999).

1.9 Fluorescence

Fluorescence is the result of a three-stage process in the electron shell of certain molecules (generally polyaromatic hydrocarbons or heterocycles) called fluorophores or fluorescent dyes.
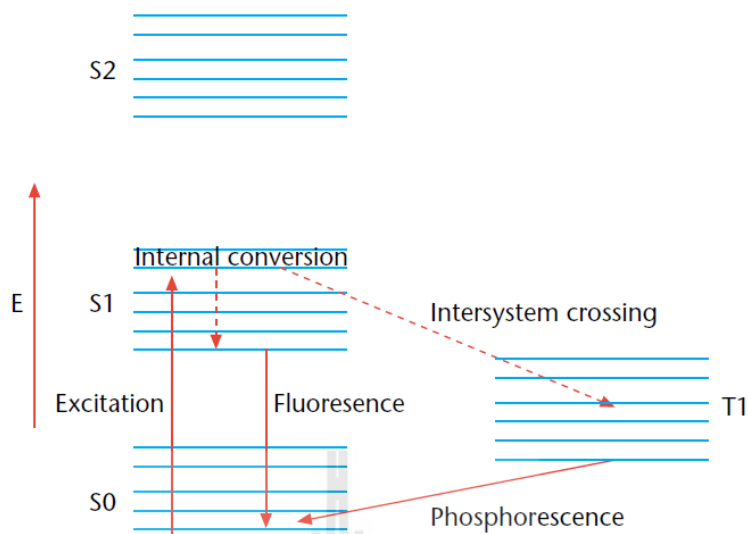
Figure 1.10 The Jablonski diagram of fluorophore excitation, radiative decay and nonradiative decay pathways (Lakowicz, 1999).

The processes involved in fluorescence are generated when a substance absorbs light energy at a short (higher energy) wavelength and then emits light energy at a longer (lower energy) wavelength. The length of time between absorption and emission is usually relatively brief, often on the order of 10^{-9} to 10^{-8} seconds. The history of a single fluorescence event can be shown by means of a Jablonski Diagram, named for the Ukranian born physicist Aleksander Jablonski (Figure 1.10) that E denotes the energy scale; S_0 is the ground singlet electronic state; S_1 and S_2 are the successively higher energy excited singlet electronic states. T_1 is the lowest energy triplet state. As shown, in stage 1 a photon of given energy $h\nu_{ex}$ is supplied from an outside source such as a laser or a lamp. The fluorescent molecule, lying in its ground energy state S_o, absorbs the energy creating an excited electronic singlet state S1. This excited state will last for a finite time, usually one to ten nanoseconds, during which

time the fluorescent molecule (fluorophore) undergoes conformational changes and can be subject to myriad potential interactions with its molecular environment. The first phase of Stage 2 is characterized by the fluorophore partially dissipating some of the absorbed energy creating a relaxed singlet state S_1. It is from this state that the fluorophore will enter the second phase, the emission of energy, $h\nu_{em}$ Finally, in Stage 3, the fluorophore will return to its ground state, S_o.

Fluorescence spectra

Fluorescence spectra can be measured in a fluorescence spectrometer (see Figure 1.11) which consists of a monochromized excitation light source (like the absorption spectrometer) and a detection channel, also with a monochromator. The detection channel is arranged perpendicularly to the excitation to suppress as much detection of the emission light as possible. Such a spectrometer may be used in two modes:

1. Detect emission spectra: Here the excitation wavelength is fixed and the detection wavelength is scanned over a given range. The results is the emission spectrum of the sample.

2. Detect excitation spectra: Here the detection wavelength is fixed to the emission maximum and the excitation wavelength is scanned. The result is an excitation spectrum of the sample.
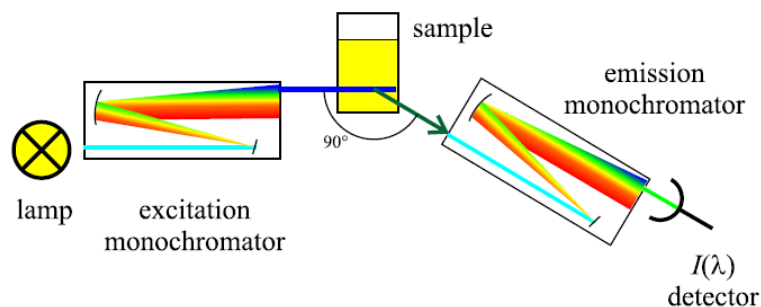
Figure 1.11 Principle of a fluorescence spectrometer. (Lakowicz, 1999).

1.10 Diffuse reflectance UV-Vis spectroscopy

Ground-state absorption spectra of solid opaque samples can experimentally be obtained using a procedure similar to the one used to perform absorption spectra of transparent samples. In the latter case one has to use the Beer-Lambert law to determine absorbances as a function of wavelength. In the case of solid samples, it is possible to determine the reflectance (R) as a function of the wavelength. In case of zeolites do not contain chromophores that absorb electromagnetic energy in the UV-Vis region of the spectrum. Consequently, optical probing of embedded guests is possible using diffuse reflectance techniques (Kortüm, 1969). These techniques measure the difference in the scatter light absorbed by a pure white surface reference and that absorbed by the embedded guest. In general, integrating spheres are used to collect the low intensity of scattered light generated by this method. The reflected light (R'_∞) is plotted according to the Kubelka–Munk equation (Eq. (20) to give an optical spectrum similar to the transmission spectrum obtained in normal UV-Vis absorption spectroscopy. The absorption coefficient (K), under conditions of low guest concentration and high standard surface area is proportional to the concentration of the embedded guest reminiscent of the Lambert–Beer Law.

$$F(R'_\infty) = \frac{(1-R'_\infty)^2}{2R'_\infty} = \frac{K}{S} \tag{20}$$

F (R'_∞) is called Kubelka-Munk function; R'_∞ is absolute reflectance of the sampled layer; K is the absorption coefficient and S is the scattering coefficient.

1.11 Fluorescence resonance energy transfer (FRET)

Fluorescence resonance energy transfer (FRET) is a process by which a fluorophore (donor), in an excited state, transfers its energy to a neighbouring molecule (acceptor) by nonradiative dipole–dipole interaction. The donor molecule typically emits at shorter wavelength which overlaps with the absorption spectrum of the acceptor (Figures 1.12 and 1.13). FRET was verified by Stryer and colleagues, in the late 1970's (Stryer, 1978).
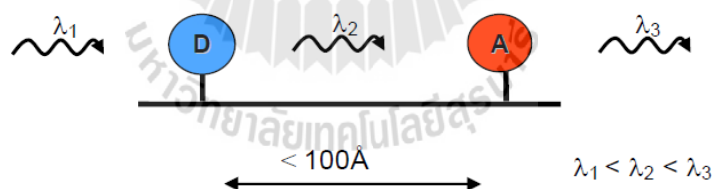
Figure 1.12 Principle of fluorescence resonance energy transfer (FRET) (Stryer, 1978).
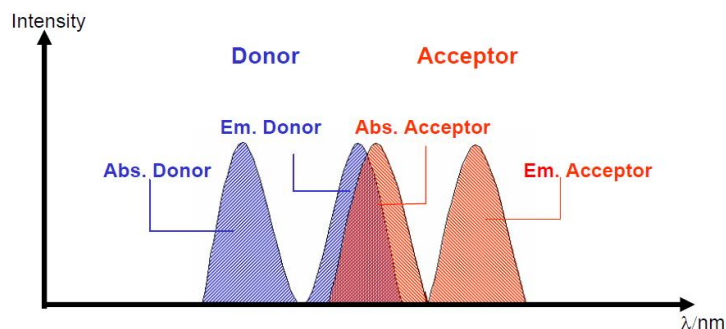
Figure 1.13 Spectral overlap of the donor and acceptor required for FRET (Stryer, 1978).

The molecular processes underlying FRET have been reviewed extensively and are illustrated in Figure 1.14 (Selvin, 1995; Clegg, 1992). The first step involves the absorption of energy by the donor molecule, resulting in its excitation from the ground state, S_0^D, to an excited singlet state, S_1^D. Several excited states are available to the donor; however, vibrational relaxation to S_1^D by internal conversion is rapid, ensuring that a majority of emission occurs from this state. Different energy states are possible for the excited donor, including spontaneous emission and nonradiative processes. If a suitable acceptor fluorophore is nearby, then nonradiative energy transfer between the donor and acceptor can occur. This transfer involves a resonance between the singlet-singlet electronic transitions of the two fluorophores, generated by coupling of the emission transition dipole moment of the donor and the absorption transition dipole moment of the acceptor. Thus, the efficiency of FRET and the range of distances over which it can be observed are determined by the spectral properties of a given donor- acceptor pair.
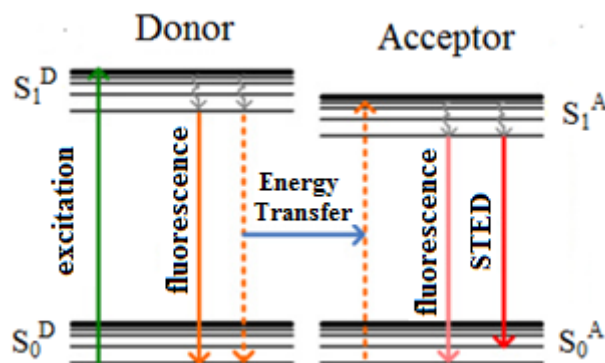
Figure 1.14 Jablonski diagram of FRET process (Selvin, 1995; Clegg, 1992).

The rate of energy transfer depends upon the extent of spectral overlap of the emission spectrum of the donor with the absorption spectrum of the acceptor (Figure 1.13), the quantum yield of the donor, the relative orientation of the donor and acceptor, transition dipoles and the distance between the donor and acceptor molecules.

$$k_{ET} = \frac{9000(\ln 10)\Phi_D}{128\pi^5 N_A n^4 \tau_D} G_{DA} J_{DA} \rho_D \rho_A \qquad (21)$$

k_{ET} is the rate constant for energy transfer, N_A is Avogadro's number in mol^{-1}, τ_D is the fluorescenc decay time of the donor, Φ_D is the fluorescence quantum yield of the donor, n is the refractive index of the medium, ρ_D and ρ_A are occupation probabilities of donor and acceptor molecule, G_{DA} is the geometrical factor and J_{DA} is the spectral overlap of the donor emission and the acceptor absorption spectra.

The most common application of FRET is to measure the distance between two sites of a macromolecule. If there is a single donor and acceptor and if the donor–acceptor distance does not change during the excited–state lifetime, then the donor–acceptor distance can be determined from the efficiency of the energy transfer. The

transfer efficiency (E) can be determined by steady–state measurements of the extent of donor quenching due to the acceptor (Lakowicz, 1999).

$$E = 1 - \frac{F_{DA}}{F_D} \tag{22}$$

$$E = 1 - \frac{\tau_{DA}}{\tau_D} \tag{23}$$

Where F is the relative fluorescence intensity in the absence (F_D) and presence (F_{DA}) of the acceptor, and τ is the lifetime (τ_D) in absence and (τ_{DA}) presence of the acceptor.

The study of the transfer of energy between donor and acceptor dye molecules has both theoretical practical important. Dye can play a major role in various fields. They are commonly used in biological and industrial. In photosynthesis, dyes transfer optical energy from one spectral region to another. There are many researches to study energy transfer from donor molecule to an acceptor molecule, for example. The excitation transfer in a laser dye mixure of rhodamine 6G and cresyl violet have been studied (Lin and Dienes, 1973). They found a Stern-Volmer quenching relaxation for the donor system. Some reserchers also study the excitation energy transfer from naphthalene derivatives (D) to acriflavine (A). Critical transfer distances (R_0) were measured experimentally for the donor-acceptor system. The experimental values of R_0 for the system were between 25 and 28 Å, and were in good agreement with theoretical values calculated from the absorption and fluorescence spectra (Ellis and Solomon, 1967). In addition the combination of a tuneable host morphology and possibility of obtaining highly organized molecular patterns of guest leads to a variety of potential applications which summarized in Table1.1.

Table 1.1 Some reported potential applications of FRET.

| Host materials | Dye molecules | | Application | Reference |
	Donor molecule	Acceptor molecule		
Nafion®	Acriflavine	Rhodamine 6G	pH sensor	Misra et al., 2002
Zeolite LTL	Atto-425	Atto-610	Encode markers for multiplexed bioassay	Busby et al., 2008
$[(Me_3Sn_4)Fe(CN)_6 \cdot 4H_2O]$	Neutral red or pyronine	Methylene blue or thionine	Artificial antenna	Mohamed et al., 2005
$[(R_3Sn)_4Fe(CN)_6]_n$ R = Me, n-bu or Ph	Rhodamine 6G	Methylene blue	Artificial antenna	Ibrahim and Etaiw, 2002
Zeolite LTL	Pyronine	Oxonine	Artificial antenna	Megelski and Calzaferri, 2001
Zeolite LTL	Pc 25	Oxonine	Artificial antenna	Li et al., 2006

1.12 References

Auerbach, S. M., Carrado, K. A., and Dutta, P. K. (2003). Handbook of zeolite science and technology. Marcel Dekker. New York. p. 1.

Brühwiler, D., Gfeller, N., and Calzaferri, G. (1998). Resorufin in the channels of zeolite L. **J. Phys. Chem. B**. 102(16): 2923-2929.

Brühwiler, D., Calzaferri, G., Torres, T., Ramm, J. H., Gartmann, N., Dieu, L.- Q., Lopez-Duarte, I., and Martinez-Diaz, M. V. (2009). Nanochannels for supramolecular organization of luminescent guests. **J. Mater. Chem**. 19: 8040-8067.

Birks, J. B. (1970). Photophysics of aromatic molecules, Wiley, London. pp. 53-56.

Buhbut, S., Itzhakov, S., Tauber, E., Shalom, M., Hod, I., Geiger, T., Garini, Y., Oron, D., and Zaban, A. (2010). Built-in quantum dot antennas in dye-sensitized solar cells. **ACS Nano**. 23(3): 1293-1298.

Burton, A., and Lobo, R. F. (1999). The role of barium cations in the synthesis of low silica LTL zeolites. **Micropor. Mesopor. Mater**. 33: 97-113.

Busby, M., Kerschbaumer, H., Calzaferri, G., and Cola, L. D. (2008). Orthogonally bifunctional fluorescent zeolite-L microcrystals. **Adv. Mater**. 20: 1614-1618.

Calzaferri, G., and Gfeller, N. (1992). Thionine in the cage of zeolite L. **J. Phys. Chem. A**. 96: 3428-3435.

Calzafferi, G., Brühwiler, D., Megelski, S., Pfenniger, M., Pauchard, M., Hennessy, B., Maas, H., Devaux, A., and Graf, U. (2000). Playing with dye molecules at the inner and outer surface of zeolite L. **Solid State Sci**. 2: 421-447.

Calzaferri, G., Pauchard, M., Maas, H., Huber, S., Khatyra, A., and Schaafsma, T. (2002). Photonic antenna system for light harvesting, transport and trapping. **J. Mater. Chem**. 12: 1-13.

Calzaferri, G., Maas, H., Pauchard, M., Pfeniger, M., Megelski, S., and Devaux, A. (2002). Supramolecularly organized dye molecules in the channels of zeolite L. **Adv. Photochem**. 27: 1-50.

Calzaferri, G., Huber, S., Devaux, A., Zabala Ruiz, A., Li, H., Bossart, O., and Dieu, L.-Q. (2006). Light harvesting host-guest antenna materials for photonic devices. **Proc. of SPIE, Organic Optoelectronics and Photonics II**. 619216-1 -619216-9.

Calzaferri, G., Li, H., and Brühwiler., D. (2008). Dye-modified nanochannel materials for photoelectronic and optical devices. **Chem. Eur. J**. 14: 7442-7449.

Calzaferri, G., and Devaux, A. (2010). Manipulation of energy transfer processes within the channels of zeolite L. **Int. J. Photoenergy**. ID 741834.

Calzaferri, G., Méallet-Renault, R., Brühwiler, D., Pansu, R., Dolamic, I., Dienel, T., Adler, P., Li, H,. and Kunzmann, A. (2011). Designing dye-nanochannel antenna hybrid materials for light harvesting, transport and trapping. **ChemPhysChem**. 12(3): 580-594.

Clegg, R. M. (1992). Fluorescence resonance energy transfer and nucleic acids. **Methods Enzymol**. 211: 353-388.

Ellis, D. W., and Solomon, B. S. (1967). Resonance energy transfer: Influence of heteroatoms on the donor's properties. **J. Chem. Phys**. 46: 3497-3501.

Gfeller, N., Megelski, S., and Calzaferri, G. (1999). Fast energy migration in pyronine- loaded zeolite L microcrystals. **J. Phys. Chem. B**. 103: 1250-1259.

Goetzberger, A., and Greubel, W. (1977). Solar energy conversion with fluorescent collectors. **Appl. Phys**. 14: 123-139.

Hameed, B. H., Ahmad, A. A., and Aziz, N. (2007). Isotherm, kinetics and thermodynamics of acid dye adsorption on activated plam ash. **Chem. Eng. J**. 133: 195-203.

Hashimoto, S. (2003). Zeolite photochemistry: impact of zeolites on photochemistry and feedback from photochemistry to zeolite science. **J. Photochem. Photobiol. C: Photochemistry Reviews**. 4: 19-49.

Hennessy, B., Megelski, S., Marcolli, C., Shklover, V., Bärlocher, C., and Calzaferri, G. (1999). Characterization of methyl viologen in the channels of zeolite L. **J. Phys. Chem. B**. 103: 3340-3351.

Hoffmann, K., Resch-Genger, K., and Marlow, F. (2003). Photosensitive optical properties of zeolitic nanocomposites. Host-Guest-Systems based on nanoporous crystals. 501-520.

Ibrahim, M. Sh., and Etaiw, S. El-din H. (2002). Supramolecular host–guest systems as frameworks for excitation energy transfer. **Spectrochimica Acta, Part A**. 58: 373-378.

Koeppea, R., Bossart, O., Calzaferri, G., and Sariciftci, N. S. (2007). Advanced Photon harvesting concepts for low-energy gap organic solar cells. **Solar Energy Materials & Solar Cells**. 91: 986-995.

Kortüm, G. (1969). Reflectance Spectroscopy, Principles, Methods, Applications, Springer, New York. pp. 335-336.

Lakowicz, J. R. (1999). Principles of fluorescence spectroscopy.2nd ed. Kluwer/ Plenum, New York. pp. 446-447.

Li, H., Devaux, A., Ruiz, A. Z., and Calzaferri, G. (2006). Electronic excitation energy transfer from dye-loaded zeolite L monolayers to a semiconductor. **Nanophotonics**. 6191-6195.

Lin, C., and Dienes, A. (1973). Study of excitation transfer in laser dye mixtures by direct measurement of fluorescence lifetime. **J. Appl. Phys**. 44: 5050-5052.

Megelski, S., and Calzaferri, G. (2001). Tuning the size and shape of zeolite L-based inorganic-organic host-guest composites for optical antenna systems. **Adv. Funct. Mater**. 11(4): 277-286.

Misra, V., Misra, H., Joshi, H. C., and Pant, T. C. (1999). Excitation energy transfer between acriflavine and rhodamine 6G as a pH sensor. **Sens. Actuators, A**. 63: 18-23.

Misra, V., Misra, H., Joshi, H. C., and Pant, T. C. (2002). An optical pH sensor based on excitation energy transfer in Nafion® film. **Sens. Actuators, A**. 82: 133-141.

Minkowski, C., Pansu , R., Takano, M., and Calzaferri, G. (2006). Energy collection, transport and trapping by a supramolecular organization of dyes in hexagonal zeolite nanocrystals. **Adv. Funct. Mater**. 16: 273-285.

Mohamed, E. El-Zaria., Safaa, El-din H. E., and Moustafa, Sh. I. (2005). Antenna behavior of donor–acceptor dye-loaded novel supramolecular framework hosts. **Appl. Organomet. Chem**. 19: 1114-1120.

Newsam, J. M. (1989). Structures of dehydrated potassium zeolite L at 298 and 78K and at 78K containing sorbed perdeuteriobenzene. **J. Phys. Chem. A**. 93: 7689-7694.

Ohgushi, T., Matsuo, T., Satoh, H., and Matsumoto, T. (2009). Cation distribution in K, H-L zeolite prepared through ion-exchange with TMA ion. **Micropor. Mesopor. Mater**. 117: 472-477.

Palomino, G. T., Area'n, C. O., Geobaldo, F., Ricchiardi, G., Bordiga, S., and Zecchina, A. (1997). FTIR study of CO adsorbed at low temperature on zeolite L. **J. Chem. Soc., Faraday Trans**. 93(1): 189-191.

Pauchard, M., Devaux, A., and Calzaferri, G. (2000). Dye loaded zeolite L sandwiches as artificial antenna systems for light transport. **Chem. Eur. J**. 6: 3456-3470.

Rytwo, G., and Ruiz-Hitzky, E. (2003). Enthalpies of adsorption of methylene blue and crystal violet to montmorillonite: Enthalpies of adsorption of dyes to montmorillonite. **J. Therm. Anal. Calorim**. 71: 751-759.

Selvin, P. R. (1995). Fluorescence resonance energy transfer. **Methods Enzymol**. 246: 300-334.

Silinsh, E. A. (1980). Organic Molecular Crystals, Springer-Verlag, Berlin. pp. 33-32.

Stryer, L. (1978). Fluorescence energy transfer as a spectroscopic ruler. **Annu. Rev. Biochem**. 47: 819-846.

Suib, S. L. (1993). Zeolitic and layered materials. **Chem. Rev**. 93: 803-826.

Veiga-Gutierrez, M., Woerdemann, M., Prasetyanto, E., Denz, C., and De Cola, L. (2012). Optical- Tweezers Assembly-Line for the Construction of Complex Functional Zeolite L Structures. **Adv. Mater**. 24: 5199-5204.

Xu, R., Pang, W., Yu, J., Huo, Q., and Chen, J. (2007). Chemistry of zeolites and related porous material-synthesis and structure. John Wiley & Sons, Inc. p. 51.

Yoon, K. B. (1993). Electron and charge transfer reactions within zeolites. **Chem. Rev**. 93: 321-339.

CHAPTER II

MORPHOLOGY CONTROLLED SYNTHESIS OF

ZEOLITE LTL AND PHYSICOCHEMICAL

PROPERTIES[1]

Abstract

Zeolite LTL is a crystalline aluminosilicate compound and a typical chemical composition of $K_9Al_9Si_{27}O_{72} \cdot nH_2O$ (n = 0–36). The structure and chemical properties, as well as their sizes and morphologies of zeolite LTL has led to various applications in different fields. The aim of this study is to investigate the effects of chemical compositions of the starting gel on the synthesis, size and morphology of zeolite LTL crystals. Zeolite LTL had been synthesized hydrothermally at 180 $^{\circ}$C for 2 days, from gels with the molar compositions of 2.62-3.78 K_2O: 0.8-1.4 Al_2O_3: 8-12 SiO_2: 80-200 H_2O. The variation of chemical compositions led to the differences in morphologies and crystal sizes. Their morphologies varied from ice hockey to cylindrical shapes and their crystal sizes varying from 1.50-7.53 μm. With an increase in H_2O and SiO_2, the crystal size was also increased but decreased with an increase in K_2O. In varying Al_2O_3, there was no effect on their shapes which were still cylindrical but with different crystal sizes. Moreover, the adsorption of ethylene on zeolite LTL samples depended significantly on crystal shapes and sizes.

2.1 Introduction

Zeolite LTL with well-defined size and morphology can be used in various applications. Zeolite LTL was first described in 1968 (Newsam, 1989). It is hexagonal with unit cell dimensions of a = 18.4 Å and c = 7.5 Å and with space group P6/mmm. The typical chemical composition of zeolite LTL is $K_9[(AlO_2)_9(SiO_2)_{27}] \cdot 22H_2O$ (Breck, 1974). Zeolite LTL is usually formed with the ratio of Si/Al between 3 and 6, but it is possible to make low-silica LTL phases with Si/Al equal 1 (Shane Carr and Shantz, 2005). Preparations of the zeolite LTL have been reported by various investigators. Most of the reports on the synthesis of zeolite LTL are involved with an increase in SiO_2 and H_2O and decrease in KOH and $Al(OH)_3$ leading to an increase in the size of zeolite LTL (Ko and Ahn, 2004).

Lee and co-workers (2005) found that when $Al_2(SO_4)_3$ was used as alumina source instead of $Al(OH)_3$, the size of crystals increased with an increase in $Al_2(SO_4)_3$. Moreover, Bhat and co-workers (2004) reported systematic studies of hydrothermal crystallization of K-LTL zeolite LTL at high temperature. The results showed that most of siliceous gel systems caused high rates of nucleation and crystallization. It resulted in the formation of more siliceous K-LTL zeolite with less yield and clam shape agglomerates. In more aluminous system, the particle size, Si/Al ratio and the yield of product were found to be increased with a decrease in molar K_2O/SiO_2 ratio. Moreover, zeolite LTL crystals that are clam and hockey-puck have been synthesized (Ruiz, Brühwiler, Ban, and Calzaferri, 2005). When alkanolamine was added into starting sols, it led to clam shape (Ban, Saito, Naito, Ohya, and Takahashi, 2007). In addition, the synthesis of columnar/cylindrical shape of zeolite LTL to observe optical properties of dye loaded LTL zeolite (Larlus and Valtchev,

2004). The structural and chemical properties of zeolite LTL, as well as their sizes and morphologies play a significant role in the applications. Large crystals (1-3 µm) with cylindrical shapes (Ban, Saito, Naito, Ohya, and Takahashi, 2007), are useful for studying the optical and photophysical properties of dye-composites on single crystals by means of optical microscopy method. A disc-shaped morphology is an important prerequisite for the preparation of oriented monolayer of zeolite LTL on the substrate use for optimizing the utilization of dye-zeolite composites as photonic antenna system. Small crystals (30-50 nm) are useful for photonic antenna materials (Calzaferri et al., 2006).

Trakarnroek et al. (2006) studied the effects of catalyst prepared by loading Pt on different morphologies and channel lengths of the K-LTL zeolite on the reaction of n-octane aromatization. They found that K-LTL zeolite with cylindrical shape was an effective catalyst and the effectiveness strongly depended on the channel length of the zeolite LTL crystals. Moreover, zeolites are used as adsorbent for adsorption of ethylene and other gases (Peiser and Suslow, 1998). The important role of ethylene is to control the growth process associated with aging of plants. Ethylene causes many physical changes in the appearance of fruits and vegetables such as colour change in fruits and stem wilting in flowers. Many researchers tried to search for appropriate adsorbents for ethylene removal. Zeolites have been reported for ethylene adsorption (Zhao, Vance, Ganjegunte, and Urynowicz, 2008; Miltenburg, Van, Zhu, Kapteijn, and Moulijn, 2006). The ethylene adsorption isotherm of zeolite Y and modified zeolite Y by cationic surfactant were studied. The results shown that zeolite Y modified by PTAB can enhance the ethylene adsorption capacity up to 111.19 cm^3g^{-1} (Patdhanagul, Srithanratana, Rangsriwatananon, and Hengrasmee, 2010). 13X zeolite

could be also separated ethylene from CO_2 (Costa, Calleja, Jimenez, and Pau, 1991). It was reported in many studies that there are two types of interaction between ethylene and zeolite framework. Firstly, the filled ethylene π- orbital donates electron density to an empty metal σ–orbital which is called σ -donation. Secondly, d–π* back-donation is interaction between the empty antibonding (π*) molecular orbital of ethylene accepts electron density from the filled metal d-orbital. Sometime all of interactions are called cation–π interaction (Patdhanagul et al., 2010; Sue-aok, Srithanratana, Rangsriwatananon, and Hengrasmee, 2010).

Although the amount of detail in the literature describing synthesis routes of LTL zeolite, no reports on extensive range to control the crystal morphology of LTL zeolite have been reported so far. The morphology of the zeolite LTL crystals synthesized in this study range from ice hockey to cylindrical morphologies. The optimum conditions for synthesis LTL zeolite with different shapes under variation of several synthesis parameters (alkalinity, dilution, Al_2O_3 and SiO_2 content) and some physicochemical properties were studies.

2.2 Experimental Section

2.2.1 Materials and Chemicals

Colloidal silica sol (Ludox HS–40 from Dupont, 40% SiO_2) and aluminium hydroxide (CARLO ERBA, 98%) were used as silica and alumina sources, respectively. Potassium hydroxide (CARLO ERBA, 85%) was used for alkali metal cations. Ethylene (C_2H_4) gas with 99% purity obtained from Mox (Malaysia) was selected as an adsorbate on LTL zeolite.

2.2.2 Synthesis (Cylindrical shape: 2.62 $K_2O:Al_2O_3:10SiO_2:160H_2O$)

LTL crystals was synthesized by a method modified from the literature (Johannes, 1993). A 0.59 g of aluminium hydroxide was dissolved in boiling potassium hydroxide solution (1.28 g of potassium hydroxide was added to 2.51 g of double distillated water until a clear solution). This solution was added to 5.52 g of Ludox HS-40 with 4.82 g of double distillated water in a mixer. The clear solution mixture was stirred for 3 minutes to obtain a gel with viscosity and turbidity. The starting gel was then transferred into a Teflon-lined autoclave for crystallization at 180 °C for 2 days without stirring. After crystallization, the Teflon-lined autoclave was cooled in cold water before opening. The product was washed with distilled water until the pH of liquid was close to 7. Finally, the crystalline solid was dried for overnight at 80 °C in an hot air oven. Another sample (19 samples) can be prepared by vary composition of starting materials.

2.2.3 Characterization

The products were analyzed by powder X-ray diffraction (XRD) using a Bruker, D5005 CuKα radiations scanning from 3-50° at a rate of 0.05 °/s with current 35 mV and 35 mA. The experimental XRD patterns of obtained products were compared with the simulated XRD patterns (Treacy, Higgins, and Von Ballmons, 2001). To calculate crystallinity of LTL zeolite, the areas of main peaks located at 2θ = 5.5, 19.4, 22.7, 28.0, 29.1 and 30.7 were integrated. The chemical compositions were analyzed by energy dispersive XRF (EDS Oxford Instrument ED 2000) with Rh X-ray tube with a vacuum medium. Scanning electron microscope (JSM6400, JEOL) at an acceleration voltage of 10-20 kV was used for the examination of LTL

morphology. The framework was also confirmed by XRF (Spectrum GX, Perkin-Elmer) with KBr pellet technique in the range between 4000 and 400 cm^{-1}. The particle size distribution was determined by DPSA (Malvern Instrument, Masterizer 2000) with the sample dispersed in distilled water and analyzed by He-Ne laser. The specific surface area was evaluated by the nitrogen gas adsorption at -196 °C using automated volumetric equipment (Autosorb 1-Quantachrome Instrument).

2.2.4 Ethylene adsorption

The determination of ethylene (C_2H_4) adsorption capability, the adsorption isotherm was carried out by NOVA 1200e instrument (Autosorb 1-Quantachrome Instrument) at adsorbate temperature of 0 °C.

2.3 Results and Discussion

2.3.1 XRD and FTIR

Figure 2.1 shows the XRD patterns of LTL zeolite with different morphologies. The patterns were compared to a standard pattern of commercial LTL zeolite (Union Carbide or UOP) (Treacy, Higgins, and Von Ballmons, 2001). The XRD pattern all of samples shows the same 2 theta (2θ) that the main peaks located at 2θ = 5.5, 19.4, 22.7, 28.0, 29.1 and 30.7.
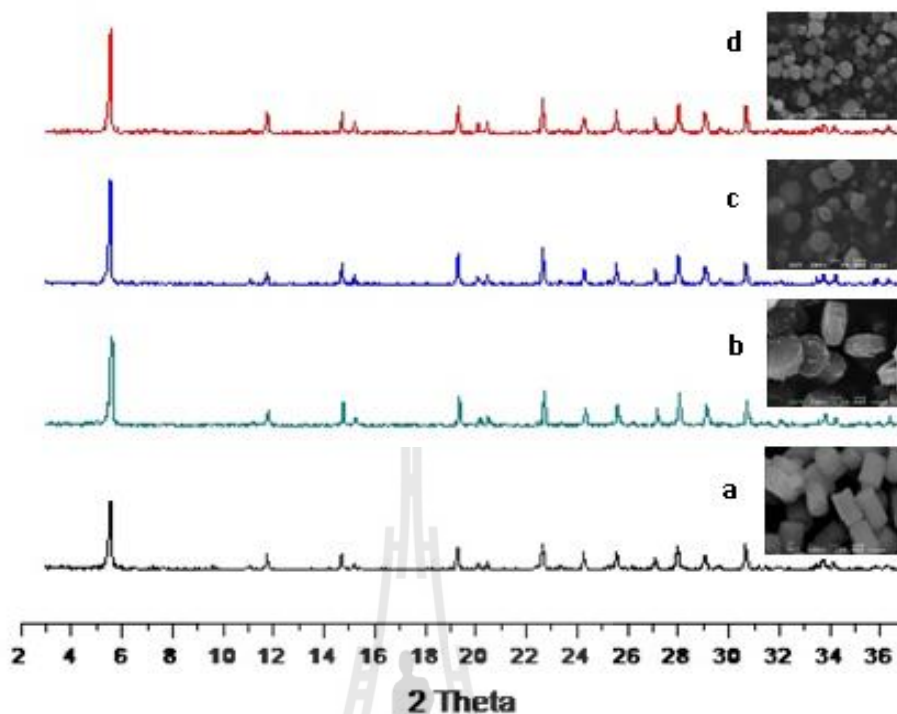
Figure 2.1 XRD patterns of crystalline LTL zeolite with different morphologies, where (a) cylindrical shape; (b) disk shape; (c) clam shape; (d) ice hockey shape.

IR spectra of LTL crystals with different morphologies were shown in Figure 2.2 The stretching vibration at 3480 - 3450 cm^{-1} which appeared in all the samples were attributed to the formation of H-bonds in water and one at 1641-1637 cm^{-1} was the bending vibration of water. The triplet band in the range 1098 - 1020 cm^{-1} corresponded to the previous report (Ko and Ahn, 1999) indicating the internal vibrations of T-O-T (T = Si, Al) tetrahedral. A sharp band around 767 - 772 cm^{-1} was the main band characteristics of external or internal symmetric stretching and the band around 608 - 611 cm^{-1} was the band characteristics of double-six-ring vibration. The bands at 478 - 482 cm^{-1} assigned to the T-O bending mode and a shoulder located at 432 cm^{-1} was the characteristics of a pore opening of external linkages. The band positions of internal and external T-O-T (T= Si, Al) tetrahedral vibration as well as

double-six-ring vibration were observed to shift to higher wave numbers with an increase in Si/Al ratio of LTL zeolite. The trends agreed well with the report of (Ali, Brisdon, and Thomas, 2003).
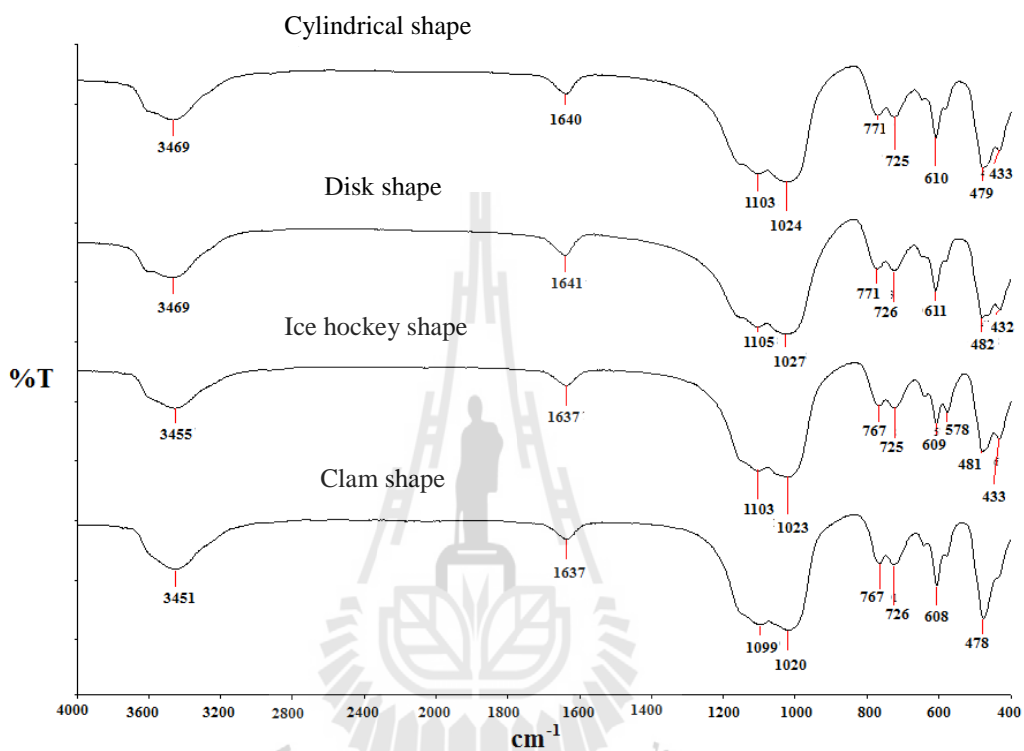
Figure 2.2 IR spectra of LTL zeolite crystals with different morphologies

2.3.2 Effects of KOH

Figure 2.3 shows the SEM photographs of the LTL zeolite samples. They were prepared from synthesis gels with the molar compositions of $aK_2O:Al_2O_3:10SiO_2:160H_2O$, where a = 2.62 (a), 2.78 (b), 3.04(c), 3.26(d), 3.54(e) and 3.78(f), to monitor the effects of KOH on the crystal morphology. K_2O had a high significant effect on the shape and crystal size of LTL zeolite (see Table 2.1). At low potassium oxide (2.62 mole), the shape of LTL crystal was cylindrical and the size

7.53 μm, while ice hockey shapes with 2.47-2.53 μm sizes occurred with K_2O varied from 2.78-3.26 moles. The clam-shape crystals with 2.17 and 1.58 μm sizes were observed at high concentration of KOH (3.54 and 3.78 moles of K_2O). It may arise from more dissolution of silica colloid according to more concentration of KOH. And also the polycondensation of hydroxoaluminate and silicate species was restricted (Bhat et al., 2004). Consequently, it provided a coin-like-shape crystals apparently for high concentration of KOH and cylindrical shape for low concentration. Similar results of crystal sizes of zeolite LTL depending on alkaline concentration have also been found from various zeolites such as FAU, MFI, MCM-22 zeolite (Kim, Jeong, Hwang, Kim, and Kim, 2009; Wu, Ren, Lu, and Wang, 2008).
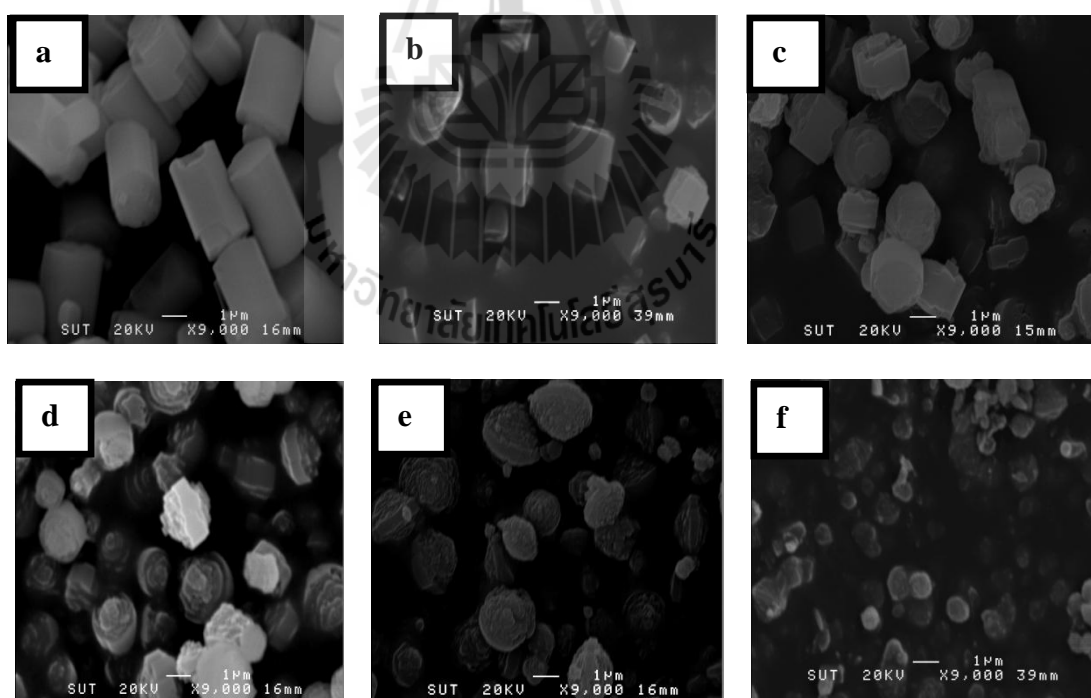
Figure 2.3 SEM images of LTL crystals synthesized from the gel compositions **a**K_2O: Al_2O_3:10SiO_2:160H_2O, where a = 2.62(a), 2.78(b), 3.04(c), 3.26(d), 3.54(e), 3.78(f).

2.3.3 Effects of Al$_2$O$_3$

Figure 2.4 shows the SEM images of the LTL samples prepared under variation of aluminum contents. The synthesis gels with the molar compositions of 2.62 K$_2$O: bAl$_2$O$_3$: 10SiO$_2$: 160H$_2$O, where b= 0.8(a), 1.0(b), 1.2(c) and 1.4(d), were monitored. Under these studied conditions, only cylindrical shape of all LTL morphologies was found. At 0.8 and 1.4 moles of Al$_2$O$_3$, the obtained solid contained only some crystalline phase but high amount of amorphous phase. (Two small additional pictures in Figure 2.4 (a) and (d) demonstrate crystalline phase of LTL). While at 1.0 and 1.2 moles, it was only a pure crystalline phase of LTL zeolite with a cylindrical shape 7.53 μm and 6.50 μm, respectively. The channel length was decreased with an increase in Al(OH)$_3$ (see Table 2.1).
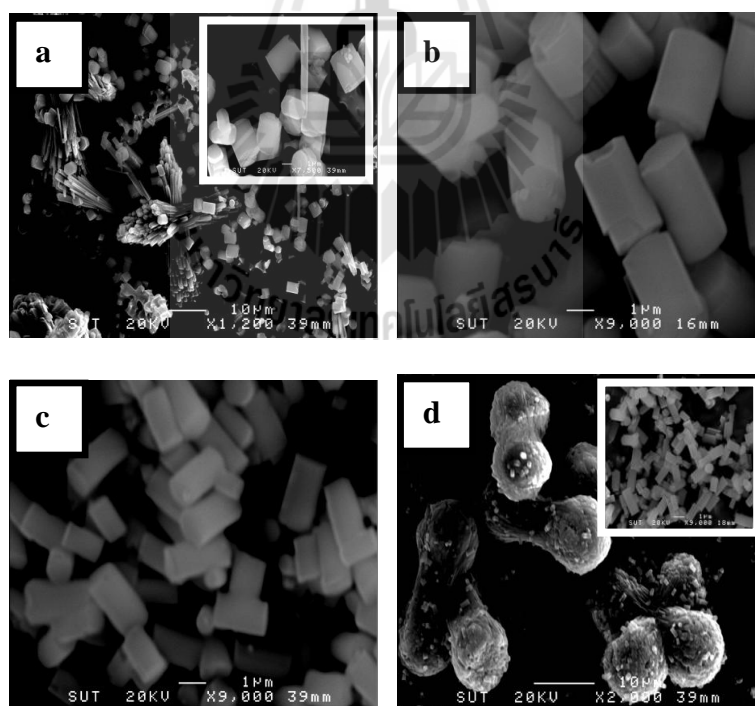
Figure 2.4 SEM images of LTL crystals synthesized from the gel compositions 2.62 K$_2$O :bAl$_2$O$_3$:10SiO$_2$:160H$_2$O, where b= 0.8(a), 1.0(b), 1.2(c), 1.4(d).

This result was consistent with the report of Kim et al (2009). As the Al_2O_3 increased, the crystal size was decreased. This implies that the nucleation was enhanced due to the increase of Al_2O_3 and the incorporation of Al into tetrahedrally coordinated silicate framework which should have been enhanced. Our result showed that there is no effect of Al_2O_3 content on the morphology of LTL zeolite. The crystals maintained the cylindrical morphology, regardless of the size. Contrary to some reports, Al_2O_3 content has a great effect on the morphology and crystal size of crystals. They found that as the Al_2O_3 content was increased the crystallization time increased and the crystal size decreased due to the disruptive effect of the Al on the structure. In addition at low Al content, the crystal shape was round and an increase in Al content the crystals were changed to an elliptical rice-like morphology (Lee, Yun-Jo, Lee, and Yoon,2005; Larlus and Valtche, 2004; Sagarzazu and González, 2005).

2.3.4 Effects of SiO_2

Figure 2.5 shows the SEM images of the LTL crystals from the synthesis gels with the molar compositions of 2.62 K_2O: Al_2O_3: $cSiO_2$: $160H_2O$, where c = 8(a), 9(b), 10(c) and 12(d). At 8, 9 and 10 moles of SiO_2, only pure phase of LTL crystals appeared in an ice hockey (1.50 μm) and cylindrical shapes with 7.53 and 6.50 μm. In case of 12 moles of SiO_2, the yield contained a quite small amount of crystalline LTL zeolite. When SiO_2 content was too high (more than 12 moles) or too low (less than 8 moles), the obtained solid appeared only in an amorphous phase. The average crystal size of LTL zeolite was increased from 1.50 to 7.53 μm with an increase in the concentration of SiO_2 from 8 to 10, respectively. It is consistent with the report of Ko and Ahn (Ko and Ahn, 2004). They found that the SiO_2/Al_2O_2 ratios of the synthesis

mixture affected the shapes and sizes of the LTL crystals. The crystals were clam-shaped whereas the siliceous gel produced crystals having basal planes of more flatness. And also the crystal size was increased with an increase in SiO_2 content (Ko and Ahn , 2004; Bajpai, Rao, and Gokhale, 1978).
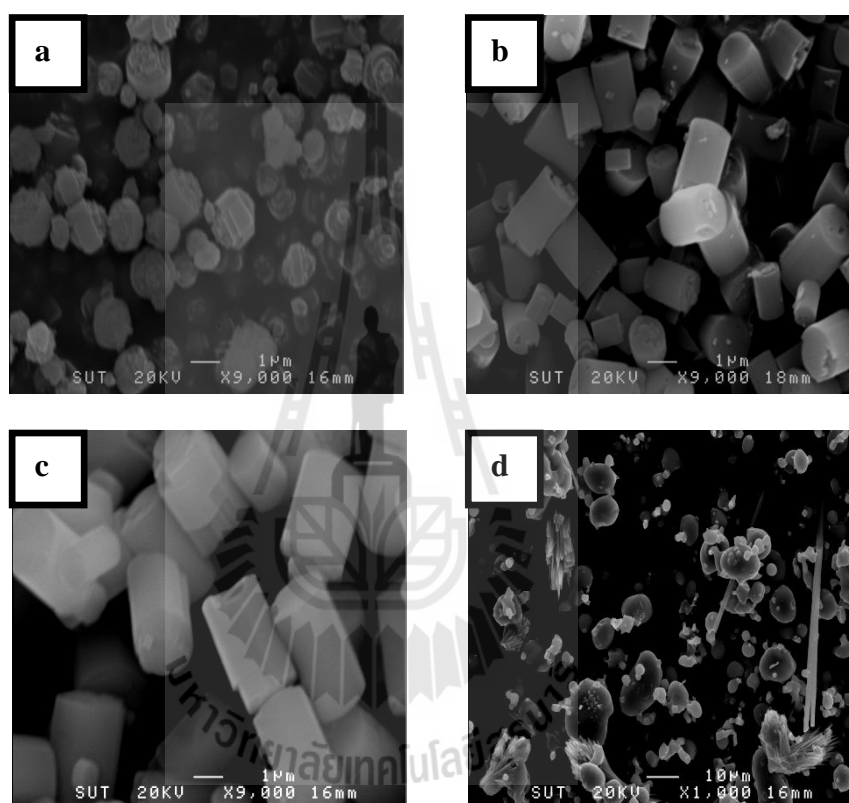
Figure 2.5 SEM images of LTL crystals synthesized from the gel compositions 2.62 K_2O:Al_2O_3:$cSiO_2$:$160H_2O$, where c = 8(a), 9(b), 10(c), 12(d).

2.3.5 Effects of H_2O

Figure 2.6 shows the SEM photographs of the synthesized LTL zeolite prepared from the synthesis gels with the molar compositions of 2.62 K_2O: Al_2O_3: $10SiO_2$: dH_2O, where d = 80(a), 100(b), 160(c), 180(d) and 200(e). At H_2O content of

80 and 100 moles, there were only pure LTL phases with a round and disk shape, respectively. Moreover, with H_2O of 160 mole the LTL crystal with a long cylindrical shape (7.53 µm) was observed. In case of H_2O contents varied from 180 to 200 moles, the mixed phases of LTL zeolite and zeolite W were appeared. (Two small additional pictures in Figure 2.6 (d) and (e) show the crystalline phase of LTL zeolite). Additionally, when the reaction time was extended to 3 days, in case of 180 and 200 moles of H_2O, at 180 moles, the obtained solid contained only single phase LTL. In contrast with 200 moles, mixed solid phases of LTL zeolite and zeolite W were still appeared. It was also found that the average crystal size of LTL zeolite increased as the H_2O increased. This may be attributed to the slowdown of nucleation and crystallization. The result agreed with the report of Kim et al (2009). If the water content in the optimum composition increased to 160 moles, the long cylindrical shape of LTL crystal was obtained. It indicated that in dilute systems a preferential growth along the c- direction was over the a-b plane. This was consistent with the report of Rhea Brent et al. (Brent and Anderson, 2008). The summary of the starting gel compositions in the synthesis of LTL zeolite and the products with some properties under the conditions studied was shown in Table 2.1.
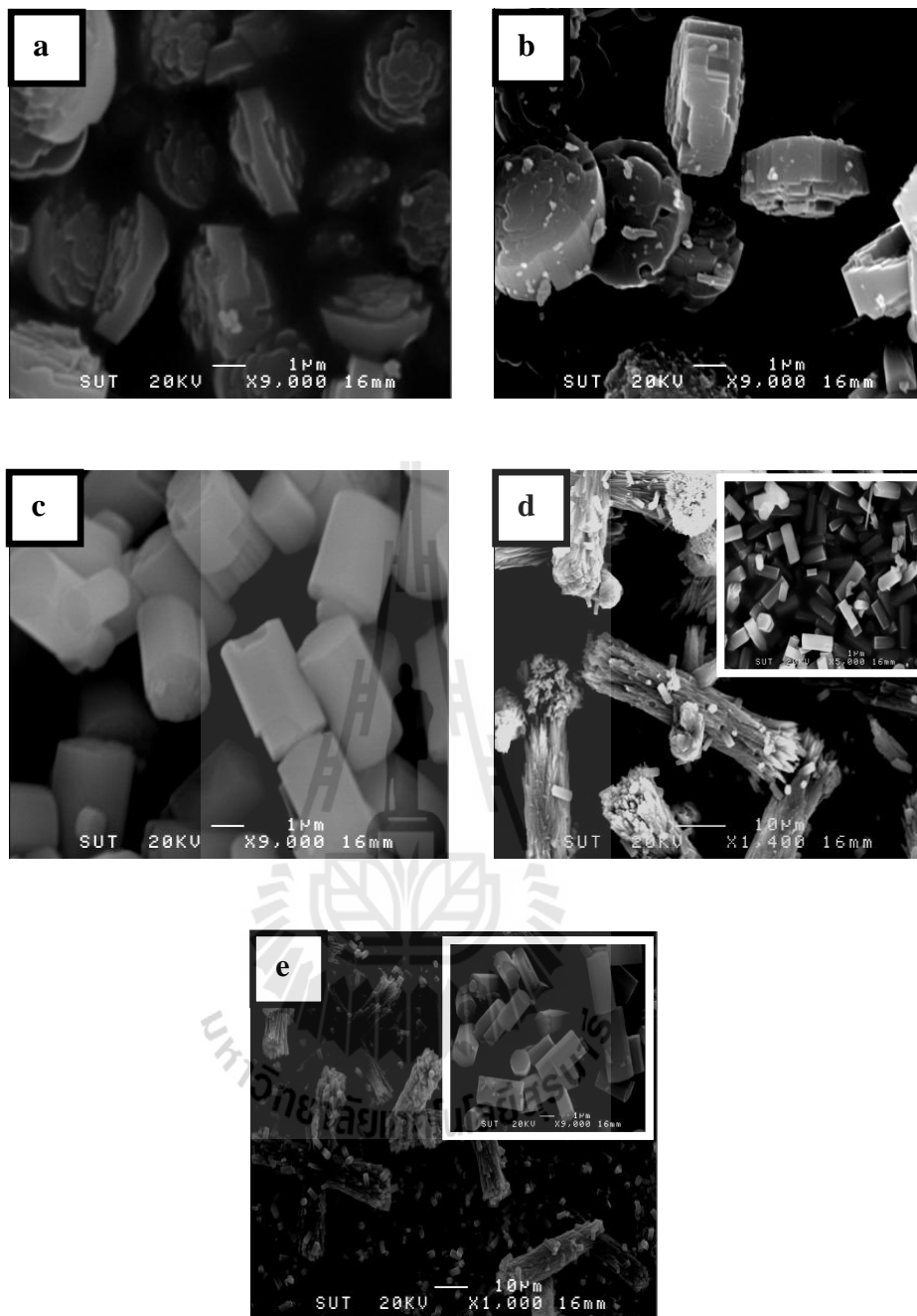
Figure 2.6 SEM images of LTL crystals synthesized from the gel compositions 2.62 K_2O:Al_2O_3:$10SiO_2$:dH_2O, where d = 80(a), 100(b), 160(c), 180(d), 200(e).

Table 2.1 Summary of the chemical compositions of starting gel for synthesis of LTL zeolite and obtained solid samples with their some properties under reaction time 2 days and at 180 ºC.

sample	Chemical composition $K_2O:Al_2O_3:SiO_2:H_2O$	% Crystallinity	Average particle size (µm)	Morphology
1	**2.62**:1.00:10.00:160.00	78.90	7.53	Long cylindrical
2	**2.78**:1.00:10.00:160.00	98.30	2.49	Ice hockey
3	**3.04**:1.00:10.00:160.00	100.00	2.47	Ice hockey
4	**3.26**:1.00:10.00:160.00	92.30	2.53	Ice hockey
5	**3.54**:1.00:10.00:160.00	98.20	2.17	Clam
6	**3.78**:1.00:10.00:160.00	76.00	1.58	Clam
7	2.62:**0.80**:10.00:160.00	45.30	15.04	Cylindrical
8	2.62:**1.00**:10.00:160.00	91.70	7.62	Long cylindrical
9	2.62:**1.20**:10.00:160.00	100.00	6.50	Short cylindrical
10	2.62:**1.40**:10.00:160.00	32.70	13.50	Cylindrical
11	2.62:1.00: **8.00**:160.00	100.00	1.50	Ice hockey
12	2.62:1.00: **9.00**:160.00	n.	3.39	Short cylindrical
13	2.62:1.00:**10.00**:160.00	87.40	7.62	Long cylindrical
14	2.62:1.00:10.00: **80.00**	100.00	4.25	Round
15	2.62:1.00:10.00:**100.00**	79.20	4.39	Disk
16	2.62:1.00:10.00:**160.00**	79.00	7.53	Long cylindrical
17	2.62:1.00:10.00:**180.00**	n.	20.97	Cylindrical
18	2.62:1.00:10.00:**180.00***	n.	1.56	Ice hockey
19	2.62:1.00:10.00:**200.00**	n.	22.28	Cylindrical
20	2.62:1.00:10.00:**200.00***	n.	11.26	Cylindrical

* = Reaction time for 3 days and n is not detected.

2.3.6 Particle size distribution

Figure 2.7(a) shows particle size distribution of highly crystalline phase of zeolite LTL zeolite. For clam, ice hockey and round shapes (samples 5, 11 and 15 in Table 2.1, respectively), monomodal narrow sized distributions having an average particle size 2.17, 1.50 and 4.39 µm, respectively, were displayed. For cylindrical shape (samples 9), it showed a broad band distribution an average particle size 7.53 µm. Figure 2.7(b) shows the particle size distribution of the yield from the gel composition of $2.62K_2O:Al_2O_3:10SiO_2:180H_2O$ (see Table 2.1) under 2 days reaction time (sample 17) and 3 days (sample 18). For the 2 days reaction time, the particle size distribution existed more than one mode and was very wide due to an inhomogeneous of large particle sizes (see also Figure. 2.4(d)), while the 3 days reaction time, a shape distribution curve was shown due to the high crystalline content of LTL zeolite.
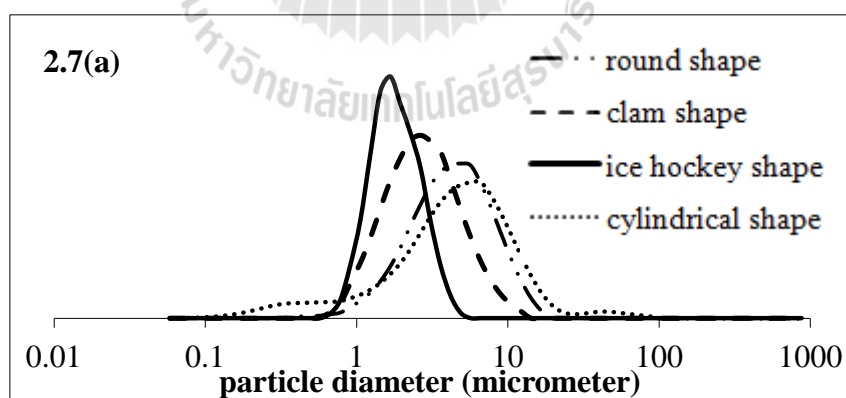
Figure 2.7(a) Particle size distribution of LTL zeolite with different crystal shapes.
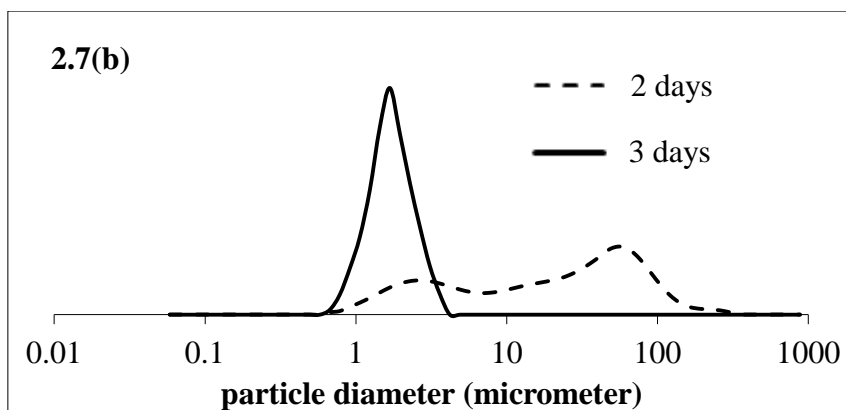
Figure 2.7(b) Particle size distribution of obtained solid from gel molar composition of $2.62K_2O:Al_2O_3:10SiO_2:180H_2O$ at reaction time 2 days and 3 days.

2.3.7 Adsorption of ethylene on zeolite LTL

The adsorption isotherms of ethylene on LTL zeolite with differences in sizes and shapes of the crystals were shown in Figure. 2.8
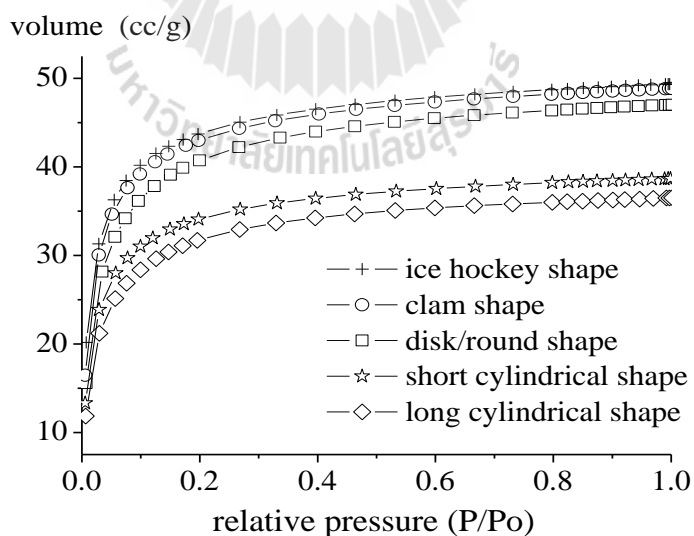
Figure 2.8 Adsorption of ethylene on LTL crystals with different morphologies.

All of the adsorption isotherms exhibited a type I adsorption isotherm based on the IUPAC classification. The adsorption isotherms of the samples were divided into two groups. The first group (ice hockey, clam and disk shape with crystal sizes: 1.50, 2.17, and 4.39 μm, respectively) had a relatively higher adsorptive capability than that of the other group (cylindrical with 6.50 μm and 7.53 μm). It could be attributed to the fact that the smaller the crystal size was, the more the surface areas became (see Table 2.2). When considered the effect of Si/Al ratio, it was found that at lower Si/Al ratio of LTL zeolite, the adsorption capacity was enhance due to more compensated by K^+ ions, so that there are more sites for ethylene adsorption (Yates, 1966; Calleja, Pau, and Calles, 1998). Based on this reason, it was anticipated that the first group could better adsorb ethylene than the other one.

Table 2.2 Textural properties of different morphologies of LTL crystals.

Gel composition $K_2O:Al_2O_3:SiO_2:H_2O$	Morphology	Surface Area (m^2/g)	Micropore surface area (m^2/g)	Si/Al ratio
2.62 : 1 : 8 : 160	Ice hockey	327.3	293.8	3.30
3.54 : 1 : 10 : 160	Clam	320.1	297.7	3.40
2.62 : 1 : 10 : 100	Disk	324.9	309.7	3.70
2.62 : 1.2 : 10 : 160	Short cylindrical	247.9	231.1	3.80
2.62 : 1 :10 : 160	Long cylindrical	232.3	218.1	3.70

2.4 Conclusions

The crystalline LTL zeolite could be synthesized with different mole ratios of aK_2O: bAl_2O_3: $cSiO_2$: dH_2O and it appeared with different morphologies and crystal sizes. The optimal molar compositions to yield a pure phase of highly crystalline LTL zeolite in different shapes were $2.62K_2O$: Al_2O_3: $10SiO_2$: $160H_2O$ for a long cylindrical shape, $2.62K_2O$: $1.2 Al_2O_3$: $10SiO_2$: $160H_2O$ for a short cylindrical shape, $2.62K_2O$: Al_2O_3: $10SiO_2$: $80H_2O$ for a round shape, $3.54K_2O$: Al_2O_3: $10SiO_2$: $160H_2O$ for a clam shape and $2.62K_2O$: Al_2O_3: $8SiO_2$: $160 H_2O$ or $3.04K_2O$: Al_2O_3: $10SiO_2$: $160 H_2O$ for an ice hockey shape. The differences in crystal sizes and shapes of the resulting LTL zeolite caused by nucleation and crystal growth which depended strongly on starting gel compositions and crystallization condition. The change in morphology seemed related to the crystal sizes. The faster the nucleation/crystallization occurred, the smaller crystal sizes were achieved. The results of characterization as well as the adsorption of ethylene indicated that the crystal morphologies and also the crystal sizes affected the physicochemical properties of LTL zeolite.

2.5 References

Ali, M. A., Brisdon, B., and Thomas, W. J. (2003). Synthesis, characterization and catalytic activity of ZSM-5 zeolites having variable silicon-to-aluminum ratios. **Appl Catal A Gen**. 252: 149-162.

Ban, T., Saito, H., Naito, M., Ohya, Y., and Takahashi, Y. (2007). Synthesis of zeolite L crystals with different shapes. **J. Porous Mater**. 14: 119-126.

Bajpai, P. K., Rao, M. S., and Gokhale, K. V. G. K. (1978). Synthesis of mordenite type zeolites. **Ind. Eng. Chem. Prod. Res. Dev**. 17: 223-227.

Bhat, S. D., Niphadkar, P. S., Gaydhankar, T. R., Awate, S.V., Belhekar, A. A., and Joshi, P. N. (2004). High temperature hydrothermal crystallization, morphology and yield control of zeolite type K-LTL. **Micropor. Mesopor. Mater.** 76: 81-89.

Breck, D. W. (1974). Zeolite Molecular Sieves: Structure, Chemistry and Use. Wiley, New York, pp. 113:156.

Brent, R., and Anderson, M. W. (2008). Fundamental crystal growth mechanism in zeolite L revealed by atomic force microscopy. **Angew. Chem. Int. Ed**. 47: 5327-5330.

Calleja, G., Pau, J., and Calles, J. A. (1998). Pure and multicomponent adsorption equilibrium of carbon dioxide, ethylene, and propane on ZSM-5 zeolites with different Si/Al ratios. **J. Chem. Eng. Data**. 43: 994-1003.

Calzaferri, G., Bossart, O., Brühwiler, D., Huber, S., Leiggener, C., van Veen, K. M., and Ruiz, A. Z. (2006). Light-harvesting host–guest antenna materials for quantum solar energy conversion devices. **Comptes Rendus Chimie**. 9: 214-225.

Costa, E., Calleja, G., Jimenez, A., and Pau, J. (1991). Adsorption equilibrium of ethylene, propane, propylene, carbon dioxide, and their mixtures on 13X zeolite. **J. Chem. Eng. Data**. 36(2): 218-224.

Johannes. (1993). Exxon Research & Engineering Company, Linden, N. J., Zeolite L, U. S. Pat 5,242,675.

Kim, Y. C., Jeong, J.Y., Hwang, J. Y., Kim, S. D., and Kim, W. J. (2009). Influencing factors on rapid crystallization of high silica nano-sized zeolite Y without organic template under atmospheric pressure. **J. Porous Mater**. 16: 299-306.

Ko, Y.S. and Ahn, W.S. (1999). Synthesis and characterization of zeolite L. **Bull. Korean Chem. Soc**. 20: 1-6.

Ko, Y. S., and Ahn, W. S. (2004). Crystallization of zeolite L from $Na_2O–K_2O–Al_2O_3–SiO_2–H_2O$ system. **Powder Technol**. 145: 10-19.

Ko, Y. S., and Ahn, W. S. (2004). Influence of synthesis parameters on the morphology and particle size distribution of zeolite L. **J. Ind. Eng. Chem**. 10: 636-644.

Larlus, O., and Valtchev, V. P. (2004). Crystal morphology control of LTL-type zeolite crystals. **Chem. Mater**.16: 3381-3389.

Lee, Y-J., Lee, J. S., and Yoon, K. B. (2005). Synthesis of long zeolite- L crystals with flat facets. **Micropor. Mesopor. Mater**. 80: 237-246**.**

Miltenburg, A. Van., Zhu, W., Kapteijn, F., and Moulijn, J. A. (2006). Adsorptive separation of light olefin/paraffin mixture. **Chem. Eng. Res. Des**. 84: 350-354.

Newsam, J. M. (1989). Structures of dehydrated potassium zeolite L at 298 and 78K containing sorbed perdeuteriobenzene. J. Phys Chem. A. 93: 7689-7694.

Patdhanagul, N., Srithanratana, T., Rangsriwatananon, K., and Hengrasmee, S. (2010). Ethylene adsorption on cationic surfactant modified zeolite NaY. **Micropor. Mesopor. Mater**. 131: 97-102.

Peiser, G., and Suslow, T. V. (1998). Factors affecting ethylene adsorption by zeolite: The last word (from us). **Perishables Handling Quart**. 95: 17-19.

Ruiz, A. Z., Brühwiler, D., Ban, T., and Calzaferri, G. (2005). Synthesis of zeolite L. tuning size and morphology. **Monatsh. Chem**. 136: 77-89.

Sagarzazu, A., and González, G. (2005). Aluminum content on the crystallization of zeolite Beta. **Microsc. Microanal**. 11: 1560-1561.

Shane Carr, C., and Shantz, D. F. (2005). Synthesis of high aspect ratio low silica zeolite L rods in oil/water/surfactant mixtures. **Chem. Mater**. 17: 6192- 6197.

Sue-aok, N., Srithanratana, T., Rangsriwatananon, K., and Hengrasmee, S. (2010). Study of ethylene adsorption on zeolite NaY modified with group I metal ions. **Appl. Surf. Sci**. 256: 3997-4002.

Trakarnroek, S., Jongpatiwut, S., Rirksomboon, T., Osuwan, S., and Resasco, D.E. (2006). n- Octane aromatization over Pt/KL of varying morphology and channel lengths. **Appl Catal A Gen**. 313: 189-199.

Treacy, M. M. J., Higgins, J. B., and Von Ballmons, R. (2001). Collection of simulated XRD power diffraction pattern of zeolites. Elsevier. pp. 497-498.

Wu, Y. J., Ren, X. Q., Lu, Y. D., and Wang, J. (2008). Crystallization and morphology of zeolite MCM-22 influenced by various conditions in the static hydrothermal synthesis. **Micropor. Mesopor. Mater**. 112: 138-146.

Yates, D. J. C. (1966). On the location of adsorbed ethylene in a zeolite. **J. Phys. Chem**. 70: 3693-3697.

Zhao, H., Vance, G. F., Ganjegunte, G. K., and Urynowicz, M. A. (2008). Use of zeolite for treating natural gas co-produced waters in Wyoming, USA. **Desalination**. 228: 263-276.

CHAPTER III

PHOTOPHYSICAL PROPERTIES OF CATIONIC DYES CONFINED IN ZEOLITE LTL: EXPERIMENTAL AND THEORETICAL STUDIES

Abstract

Experimental and theoretical studies of the photophysical properties of acridine hydrochloride (Ac) and acriflavine hydrochloride (AF) were performed. The structural and spectral properties of Ac and AF loaded on ice hockey and round shape zeolite LTL (K-LTL and H-LTL) were investigated by the absorption and emission spectroscopy. The observed spectroscopic properties of the two dyes were in line with the theoretical calculations in which a density function theory (DFT) and a time dependent density function theory (TD-DFT) were used. Results from our studies suggested that the photophysical properties of Ac and AF are sensitive to the form of zeolite LTL regardless of morphology. The energy transfered from donor to acceptors of Ac and AF loaded on zeolite LTL were also demonstrated. The geometrical constraint of the host allowed the cationic dye molecules encapsulated within the parallel channels to form host–guest systems of artificial antenna materials. The excitation energy transfer occured from Ac as a donor to AF as an acceptor by fluorescence resonance energy transfer (FRET) within supramolecular systems filled with a mixture of both dyes.

3.1 Introduction

Zeolite LTL has attracted increasing attention during the years to come because they can act as a host for accommodation of organic dyes (Megelski and Calzaferri, 2001; Barrer and Villiger, 1969). The pore structure of zeolite LTL consists of one-dimensional channels running across the whole crystal axis. The performance of zeolite LTL in the aforementioned applications relies upon their physical properties such as crystal size and morphology. For example, disc-like LTL crystals can be used in photonic devices to produce higher trapping efficiency. Disk-like shapes can also facilitate c-oriented layering for the preparation of thin-film technologies (Veiga-Gutierrez et al., 2012).

Excited state processes of dyes in host materials fined novel applications in various systems (Koeppe, Bossart, Calzaferri, and Sariciftci, 2007; Clazaferri et al., 2006). It can be used as an artificial antenna and potential use of these compounds as microlaser are well reported (Maas and Calzaferri, 2003; Maeda, 1984). Furthermore, the FRET between cationic dyes from pyronine (donor) to oxonine (accepter) in the channels was studied by Calzaferri's group which proceeded very efficiently (Calzaferri et al., 2011). The energy transfer can be happened by spontaneous emission. The necessary condition of the arrangement is that energy transfer from an excited molecule to an unexcited neighbor is much faster than any other processes (Huber and Calzaferri, 2004). In the meantime, the aggregation at low concentration of the dyes in solution caused fast thermal relaxation of electronic excitation energy. If the dye molecules are dispersed in the zeolite pores, the aggregation of molecules can be avoided, and as a result, the dye molecules may exhibit excellent optical activities. Thus, many reports proposed that the dye-loaded zeolite LTL has opened

up new possibilities for antenna application. Overall, zeolite LTL is well suited for photophysical and photochemical applications utilizing cationic dyes. Cationic dyes (Calzaferri and Gfeller, 1992), such as thionine (TH^+) can be incorporated in the monomer form even at a high loading whereas methylene blue (MB^+) which is larger than the channel diameters, cannot enter the channels but remains on the outer surface, forming dimer and aggregated. Moreover, the association of the methyl viologen radical cation ($MV^{\bullet+}$) was investigated in the reviews of (Park, Lee, Lee, and Yoon, 2000; Hennessy et al., 1999). They observed the dimerization of $MV^{\bullet+}$ from the measurement of absorption spectra.

Acridine hydrochloride (Ac) and acriflavine hydrochloride (AF) are cationic dyes, small enough to fit into the main channel (Scheme 3.1). They have been widely applied for organic light-emitting diode (OLED) materials, photovoltaic cell (PVC), pH sensor and fluorescent probe (Chunxiang, Peipei, Lijun, Yi, and Chien-Hong, 2008 ; Kaewsuya, Miller, Danielson, Sanjeevi, and James, 2008 ; Kazima, Zulfequar, Mazharul Haq, Bhatnagar, and Husain, 2007 ; Misra, Mishra, Joshi, and Pant, 2000). Based on the FRET both of them can be used in antenna application. However, no previous studies have been explored in the use of Ac as donor and AF as acceptor. In this report, spectroscopic and computational techniques were applied to investigate the photophysical properties and the behavior of electronic excitation energy of these cationic guest species intercalated in ice hockey and round shape of zeolite LTL (K-LTL and H-LTL.
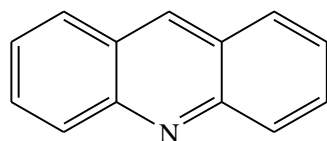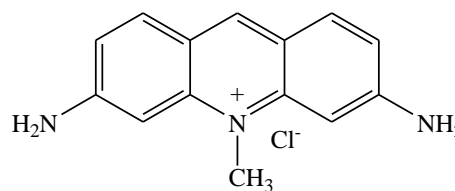
Acridine hydrochloride (Ac)   Acriflavine hydrochloride (AF)

Scheme 3.1 Structure formula of cationic dyes.

3.2 Materials and method

3.2.1 Experimental Details

Synthesis of zeolite LTL

All materials used in this study were of reagent grade. The typical procedure for the preparation of synthesis gel of K-LTL zeolite was modified according to a Chapter II in page 41.

NH$_4$LTL was prepared by ion-exchanging the K-LTL with 1M NH$_4$NO$_3$ solution. Ion exchange was carried out at 80 °C for 12 hours. After that the zeolite samples were washed with distillated water and dried at 100 °C for 12 hours. NH$_4$LTL was calcined at 450 °C for 4 hours to decompose NH$_4^+$ ions to NH$_3$, then NH$_4$LTL was transformed to H-LTL.

Dyes-loaded on zeolite LTL

Acridine hydrochloride (Ac) and acriflavine hydrochloride (AF) were purchased from Sigma-Aldrich and used without further purification. Incorporation of dyes onto ice hockey and round shape of K-LTL, and H-LTL zeolite were performed at 30 °C using accurately weighed dehydrated zeolite LTL 0.5 g in a 125 mL conical flask. Then 50 mL of the two dyes solution with concentration 0.1 mM and 0.01 mM were added to a flask. The flask was sealed and transferred to a shaker bath for 24

hours to equilibrate the system. The dyes loaded zeolite LTL were collected by separation of solid from solution by centrifugation and dried at 100 °C overnight. To remove the dyes molecules on the zeolite surface, the following washing procedure was used. The suspension was transferred into a 125 mL conical flask with 50 mL n-butanol, sonicated for 10 minutes then stirred at room temperature for 24 hours. The n-butanol washing were repeated until the supernatant did not show dyes luminescence.

Loading zeolite LTL with Ac and AF

The dye-loaded zeolite LTL crystals, used for the investigation of energy transfer, were prepared as follows: zeolite LTL 1 g was added to 50 mL of 0.01 mM of Ac. This suspension was treated in an ultrasonic bath for at least 10 minutes in order to avoid aggregation of the crystals before stirring for typically 12 hours. The suspension was then centrifuged and the remaining dye concentration in the supernatant was analyzed. To modify the crystals at each end with AF, the Ac loaded sample was added to 0.01 mM of AF and stirred for 12 hours. To remove the dyes molecules on the zeolite surface, the same washing procedure was used.

Physical Measurements

UV/vis spectra were recorded on a Varian cary 1E UV/vis Spectrophotometer. Dye molecules were dissolved in various solvents and quartz cuvette was used in the measurement. Diffuse reflectance spectra of dyes loaded on zeolite LTL was recorded using a Shimadzu UV-2550 UV-Visible spectrometer with the condition of slit width (5 nm), sampling interval (0.1 nm) and wavelength range of 200-800 nm. Fluorescence spectra were recorded on a luminescence spectrometer LS 50B (Perkin-Elmer). Dye molecules were measured either in various solvents in

quartz cuvette, or incorporated in zeolite LTL by suspending dyes/zeolite LTL in chloroform (~1 mg in 100 mL).

3.2.2 Computational Details

Model

The topology of the crystal lattice of zeolite LTL had been refined assuming space group P6/mmm with unit cell parameters a = 18.4 Å and c = 7.5 Å. It had the framework structure designated zeolite LTL and consisted of a main straight twelve ring channel with a pore diameter 7.1 Å with co-linear side channels of six and eight rings (Figure 3.1).
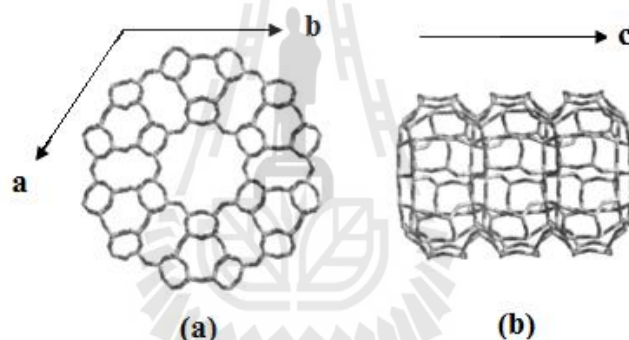
Figure 3.1 (a) View of pore along c-direction of the LTL framework topology P6/mmm and (b) view perpendicular to c-direction showing the chains of four-rings and eight-rings that line the pore of zeolite LTL from Calzaferri and Devaux, 2010.

The structure of H-LTL and K-LTL were modeled by the 324T cluster (323 tetrahedral atoms of Si and 1 tetrahedral atoms of Al) that show in Figure 3.2 and 3.3. To increase the computational efficiency, the 324T cluster was subdivided to two layers of calculation methods according to the two-layer ONIOM (ONIOM2 scheme). The inner layer was a fourteen-tetrahedral represented by ball and stick (14T) cluster consisting of the 12-membered ring (MR) and a silicon atom was

substituted by an aluminum atom. This layer and the reacting molecules were treated with the B3LYP/6-31G(d,p) method. The rest of the model was treated with the Universal Force Field (UFF) to represent the confinement effect of the zeolite pore structure and to reduce the required computational time. Geometry optimizations of all structures were performed at the ONIOM(B3LYP/6- 31G(d,p):UFF) level of theory where only the active site region 5T, ($\equiv$Si$_3$O$_3$AlO(H/K)Si$\equiv$) and the adsorbate were allowed to relax.

Method

The system was treated with the two-layer ONIOM approach. The outer layer consists of zeolite LTL part and is treated with Universal Force Field (UFF). Its structure was fixed during the calculation. The inner layer is the AF and Ac. Density functional methods was applied to the high layer. All structures were optimized with the B3LYP functional, the basis set was 6-31g (d,p). After optimization, an excited-state was calculated by time-dependent DFT method (TD-B3LYP/6-31g (d,p). The solvent (water) effect was calculated by using the CPCM (UAKS) salvation method. Dye-zeolite system was calculated in the gas phase by using the ONIOM(B3LYP/6-31g(d,p):UFF method. For dye-zeolite system, the adsorbed dye molecule and the adjacent 14T atoms of LTL zeolite were cut-off to simulate the frontier molecular orbitals.

3.3 Results and discussion (Acriflavine hydrochloride, AF)

3.3.1 Ground state geometry optimization

The structure and properties of H-LTL and K-LTL

This work the acidic cluster (H-LTL) and potassium (K-LTL) were modeled by 324 T cluster that consists of five tetrahedral; 5T ($\equiv Si_3O_3AlO(H/K)Si\equiv$). There are two non-equivalent tetrahedral silicon atoms in siliceous LTL zeolite. T1 and T2 are located at the 12 membered ring window and 6-memberd ring connecting the nonplanar 8-membered rings, respectively. These results correspond to report of (Meeprasert, Jungsuttiwong, and Namuangruk, 2013) which T1 is the most stable site for Al atom substitution. This generates a negative charge on the framework oxygens, which is compensated by extraframework cations. When the negative charge is compensated by potassium ion (K^+) and proton (H^+) is called K-LTL and H-LTL, respectively. During the optimization all atoms were allowed to relax. Figure 3.2 the proton (H_Z) is placed at the 12 membered ring window or at the narrowest of main channel. The H_Z-O_Z distance of bare H-LTL is 0.967 Å. For the potassium ion (K_Z) is placed at the connection of 12 membered ring and 8 membered ring windows or at the widest of the main channel. The K_Z-O_Z distances of bare K-LTL are 2.779 and 2.577 Å (Figure 3.3). The H_Z and K_Z act as the active sites for adsorption of dye molecules, which will be discussed in the next section.

(a) **(b)** **(c)**
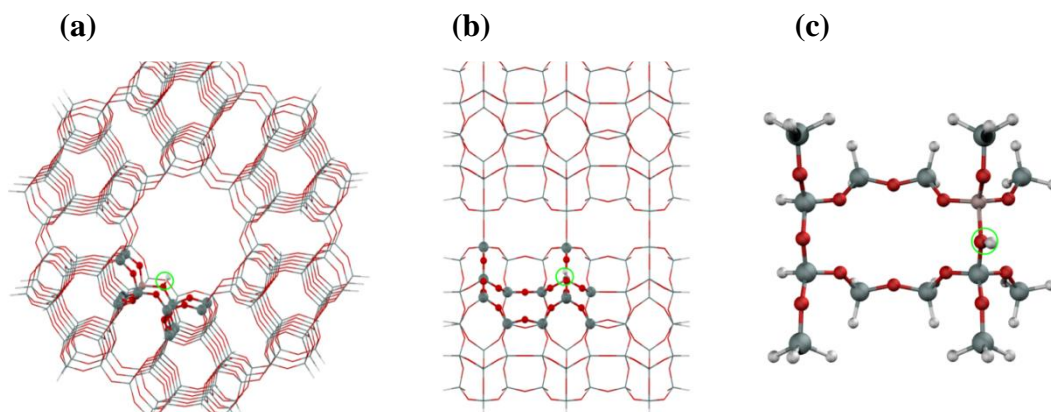
Figure 3.2 The ONIOM model of the 324T cluster of the H-LTL. Atoms belonging to the quantum region are drawn as balls and sticks while the lines represent universal force field (UFF): (a) front view, (b) show side view of 12 MR and (c) 14T cluster of the H-LTL.

(b) **(b)** **(c)**
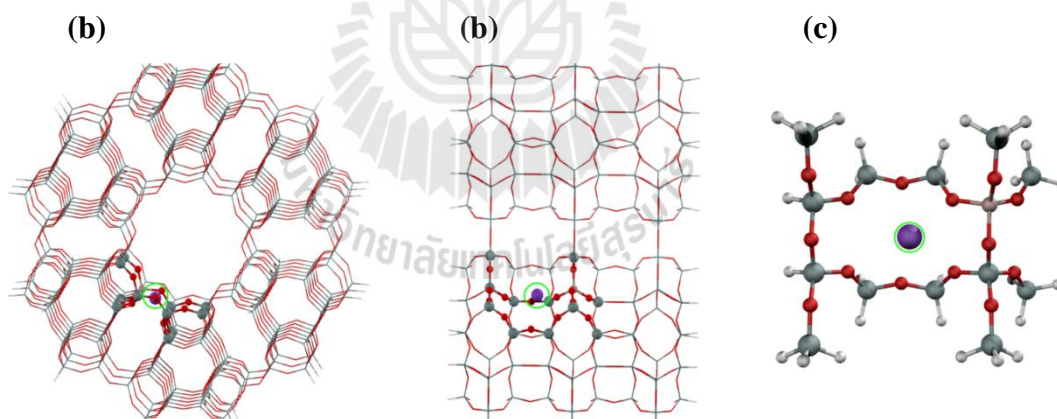
Figure 3.3 The ONIOM model of the 324T cluster of the K-LTL. Atoms belonging to the quantum region are drawn as balls and sticks while the lines represent universal force field (UFF): (a) front view, (b) show side view of 12 MR and (c) 14T cluster of the K-LTL.

3.3.2 The structure and properties of bare AF and confined in zeolite channels

Ground state geometry optimization

Figure 3.4 shows the optimized geometries of bare AF was planar geometry. Once absorbed AF in K-LTL were found to be slightly bent because of the interaction between N atom of AF and K^+ ion of K-LTL and the distance between N atom of AF and K^+ ion of K-LTL are 5.662 and 5.106 Å when confined in K-LTL zeolite. Moreover, AF molecule can be interacted with oxygen framework as well.

The optimized structure of bare AF and AF in H-LTL was shown in Figure 3.5a to 3.5d. Acriflavine molecule did not protonated but only interacted with BrØnsted acid site of H-LTL. This result can be seen from the calculated the O-H distance of bare H-LTL which are extend from 0.967 Å to 1.002 Å when adsorbed with AF molecule. In addition, protonated acriflavine (AFH^+) adsorbs H-LTL zeolite, dye molecule interacts through its NH_3- group with the oxygen atom in zeolite framework not directly interacts with BrØnsted acid site of zeolite (see Figure 3.6).

(a)

(b)

(c)

(d)
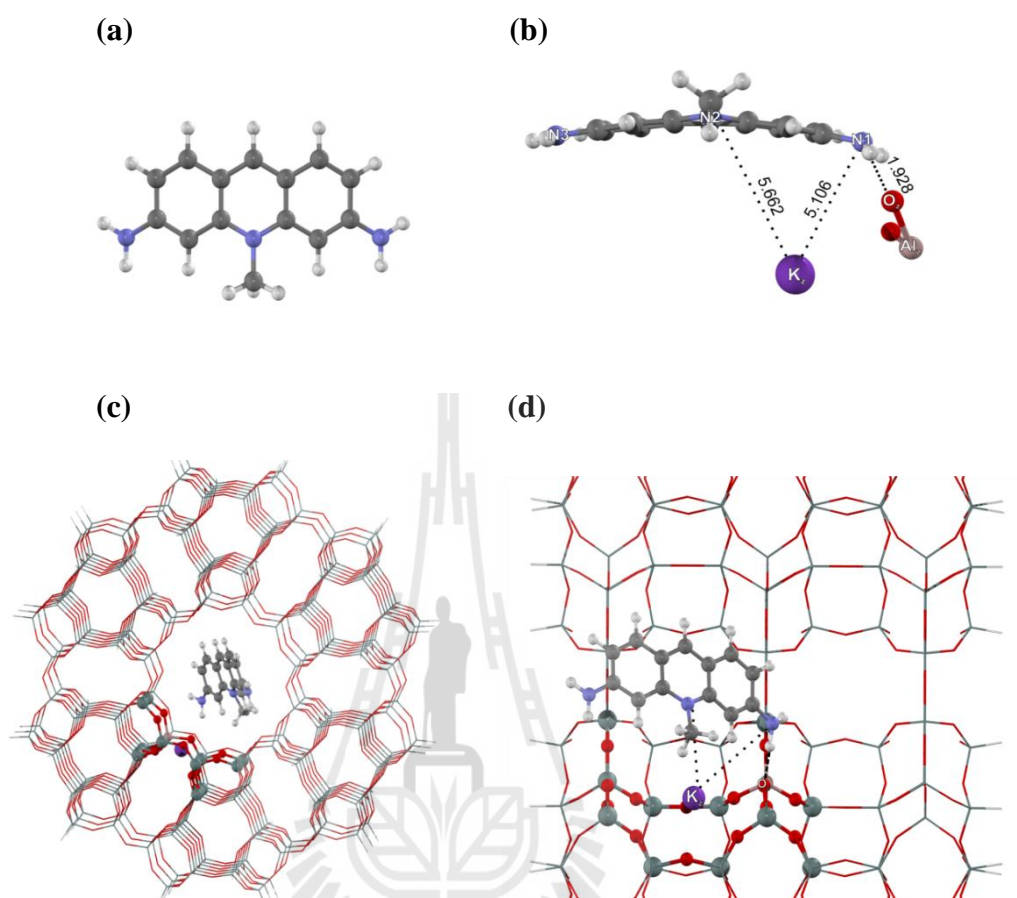
Figure 3.4 (a) Optimized structures of bare acriflavine (AF), (b) AF interacted with K$^+$ ion of K-LTL, and acriflavine in K-LTL (AF-K-LTL), (c) Front view and (d) side view of the channel.

(a)   **(b)**

(c)   **(d)**
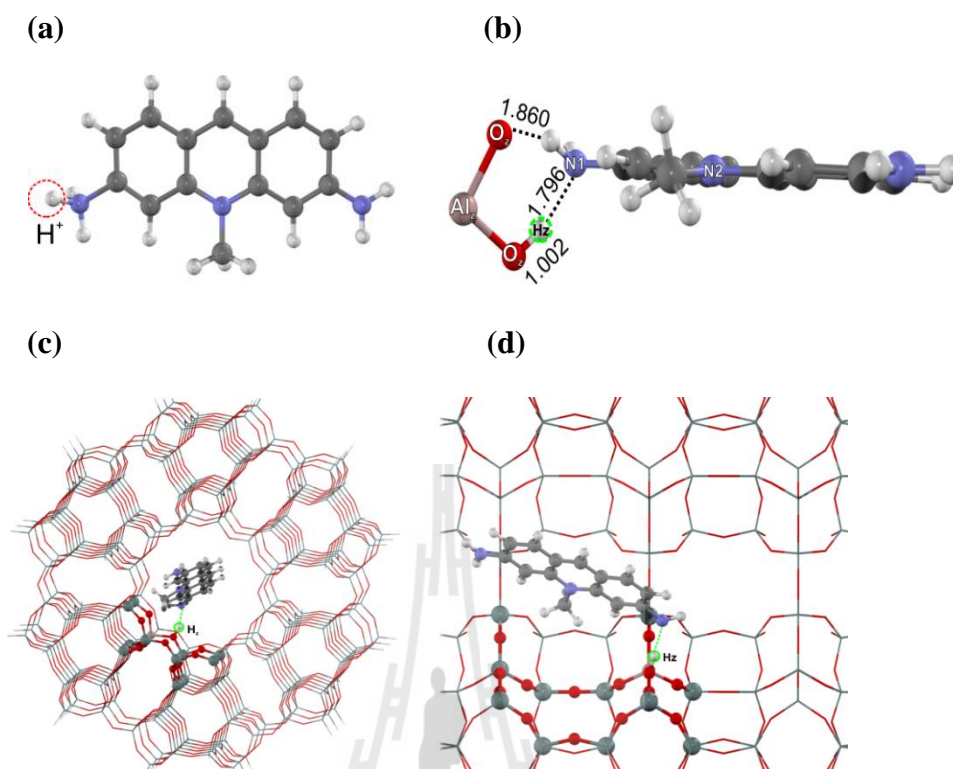
Figure 3.5 (a) Optimized structures of protonated acriflavine (AFH$^+$), (b) AF interacted with H$^+$ of H-LTL, and acriflavine in H-LTL (AF-H-LTL), (c) Front view and (d) side view of the channel.

(a)   **(b)**
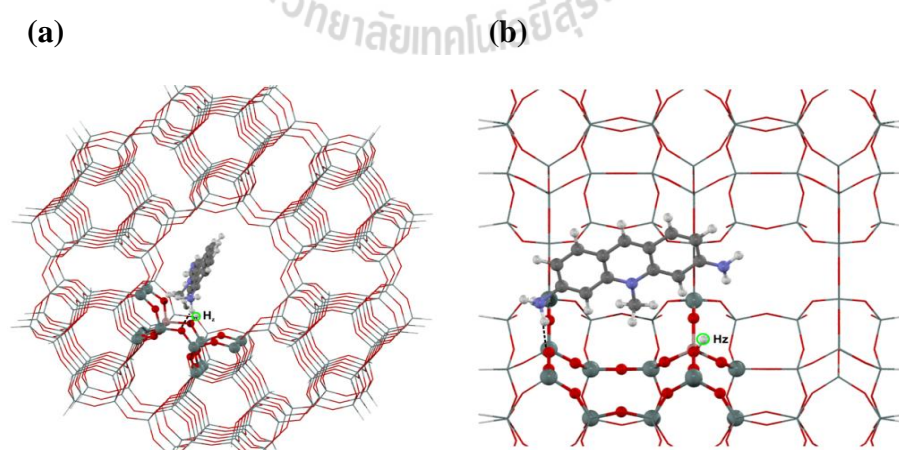
Figure 3.6 Optimized structures of protonated acriflavine in H-LTL (AFH$^+$-H-LTL), (a) Front view and (b) side view of the channel.

3.3.3 UV-Vis absorption spectra: Experimental and Theoretical studies.

Acriflavine hydrochloride (AF) in solution

UV-visible absorption of AF in various solvents are given in Table 3.1 The band maximum varies from 448 to 462 nm depending on the solvent polarity. An increase in the polarity/dielectric constant results in the shift of the CT-band to blue shift, which is characteristic of charge transfer transition. In a protic solvent non-bonding electrons of nitrogen atom (amine groups) interact with the solvents to form hydrogen bonds. Hydrogen bonding can stabilize the ground state of n-π* transition, leading to an increases in transition energy. This behavior is similar to that reported earlier (Kumar, Selvaraju, Malar, and Natarajan, 2012).

Table 3.1 Photophysical characteristics of AF in different of solvents (excitation at 440 nm)

solvent	λ_{abs} (nm)	λ_{emis} (nm)	dielectric constant
AFH$^+$	458	540	None
n-butanol	462	515	17.51**
methanol	460	510	32.70**
acetonitrile	453	510	37.50*
water	448	518	80.10*

* measured at 20 °C and ** measured at 25 °C
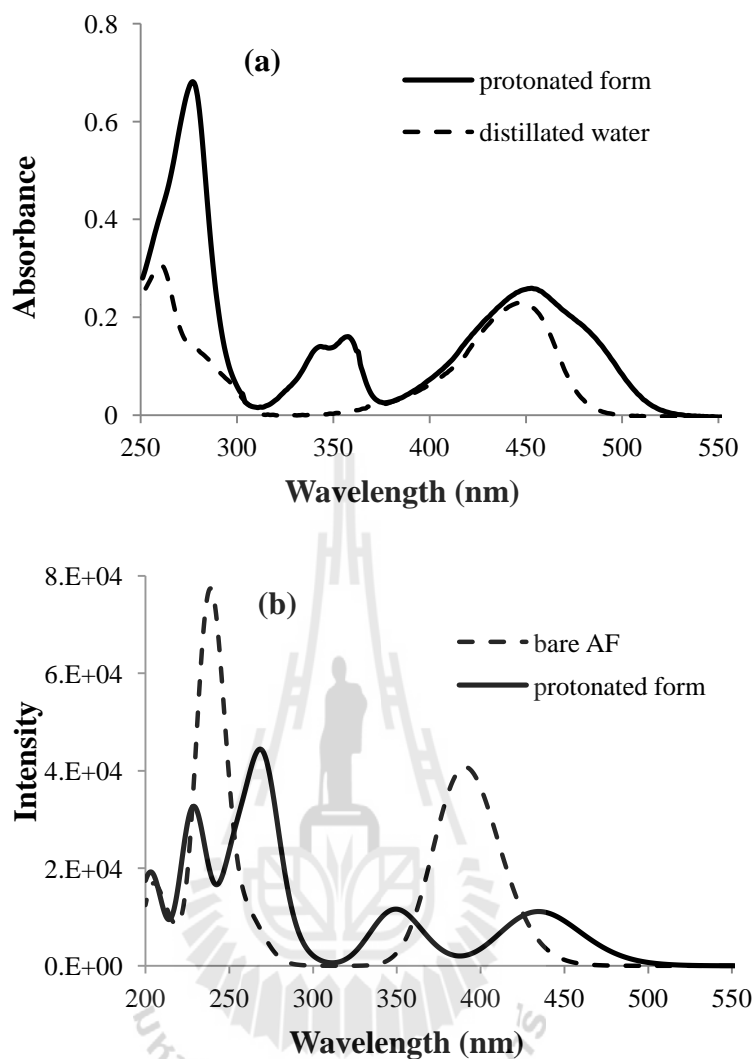
Figure 3.7 (a) Experimental absorption spectra of AF and (b) calculated absorption spectra in gas phase.

To further understand the properties of ground and excited states and also in order to predict the maximum of absorption band of AF molecule, we performed quantum chemistry computation for comparison with experimental data. Figure 3.7b was shown the calculated absorption spectra of bare AF and protonated AF (AFH$^+$) in gas phase. The blue shifted (~58-68 nm) have been observed when compared to those experimental absorption spectra (see figure 3.7a). However, it is quite similar with

experimental results. The excitation energy calculation shows that the first absorption peak for the bare AF was appeared at 390 nm that corresponds to the lowest excited singlet (S_0- S_1) transition from the highest occupied MO (HOMO) to the lowest unoccupied MO (LUMO) while that the most intense peak (243 nm) corresponds to the excitation of electron from the (HOMO-1) to the (LUMO+1) that assign to π-π* of AF molecule (see figure 3.8a and Table 3.3). In case of calculated absorption spectrum of protonated AF (AFH$^+$) compared with the experimental absorption spectrum. The first peak at 434 and 458 nm for calculated and experimental absorption spectrum of protonated AF (AFH$^+$), respectively assigned to the excitation of electron from HOMO to the LUMO. The second peak at 349 and 350 nm for calculated and experimental absorption spectrum of protonated AF (AFH$^+$), respectively suggests the present of protonated form of AF which assigned to the excitation of electron from HOMO-1 to the LUMO. While the most intense peak (270, 252 and 227 nm) corresponds to many different characters (see figure 3.8b and Table 3.3).

(a)

LUMO LUMO+1

HOMO HOMO-1

(b)   LUMO   LUMO+1

HOMO   HOMO-1
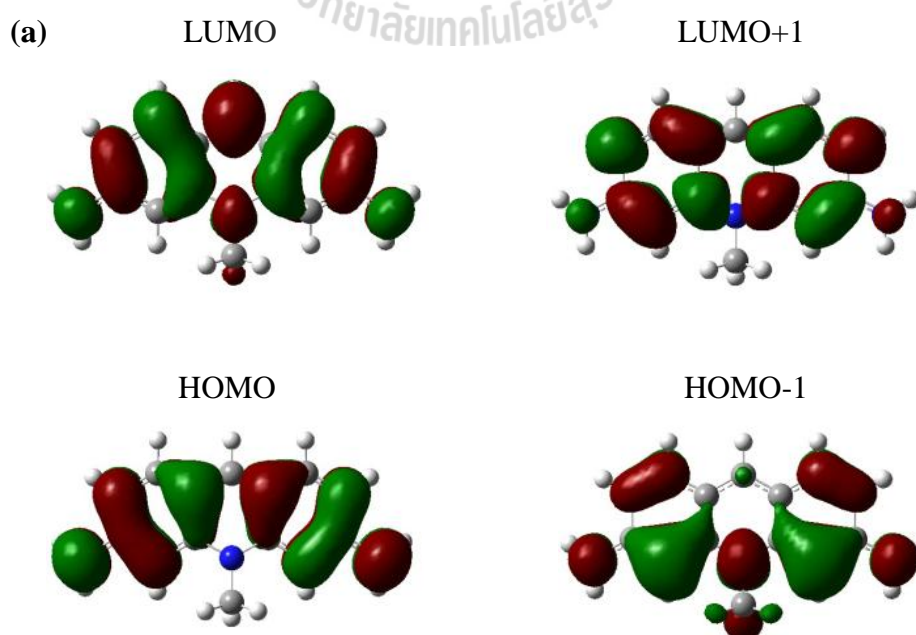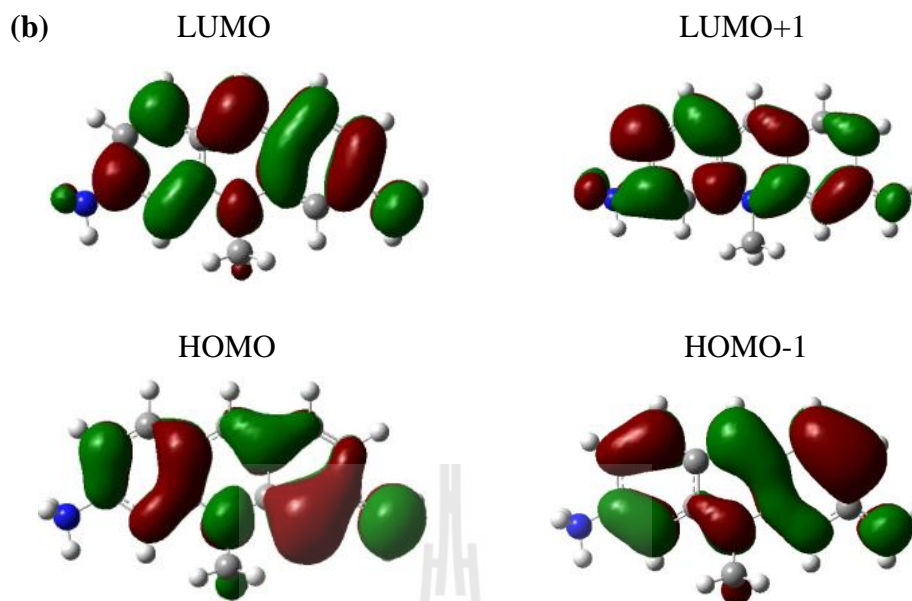
Figure 3.8 (a) Frontier molecular orbital of acriflavine and (b) protonated in acriflavine gas phase calculated by BTLYP 6-31G(d,p).

Acriflavine hydrochloride (AF) in K-LTL zeolite

Table 3.2 Spectral data of AF in aqueous solution and in zeolite LTL.

Dye	Absorption maxima (nm)	Emission maxima (nm)
AF	448, 260	518 (in water)
AFH$^+$	458, 363 (w), 348 (w), 282,	540 (in 0.2 M HCl)
AF_K-LTL	460, 265	496
AF_H-LTL	465, 350 (w), 290, 235	538

w: weak,

The absorption and emission spectral band maxima for AF measured in K-LTL, H-LTL and aqueous solution are given in Table 3.2. In aqueous solution AF shows an absorption band at 448 nm and emission band at 518 nm. AF in 2M HCl solution can be monoprotonated /diprotonated AFH$^+$/AFH$_2^{2+}$ which shows an absorption band at 458, 363, 348, 282, 235 nm and an emission band at 540 nm that

consistent with the previous reports (Matsuoka and Yamaoka, 1979; Yamaoka and Shimadzu, 1983). The absorption and emission bands of AF at different concentrations in K-LTL (ice hockey and round shape), are given in Figures 3.9 and 3.13a. AF exchanged K-LTL samples exhibit the characteristic absorption band at 460 nm and emission band at 496 nm, that shifted to longer wavelength compared to AF in water (448 to 460 nm) and shorter wavelength (518 to 496 nm), respectively. This behavior is due to the channels of K-LTL less polar than that in the aqueous environment.
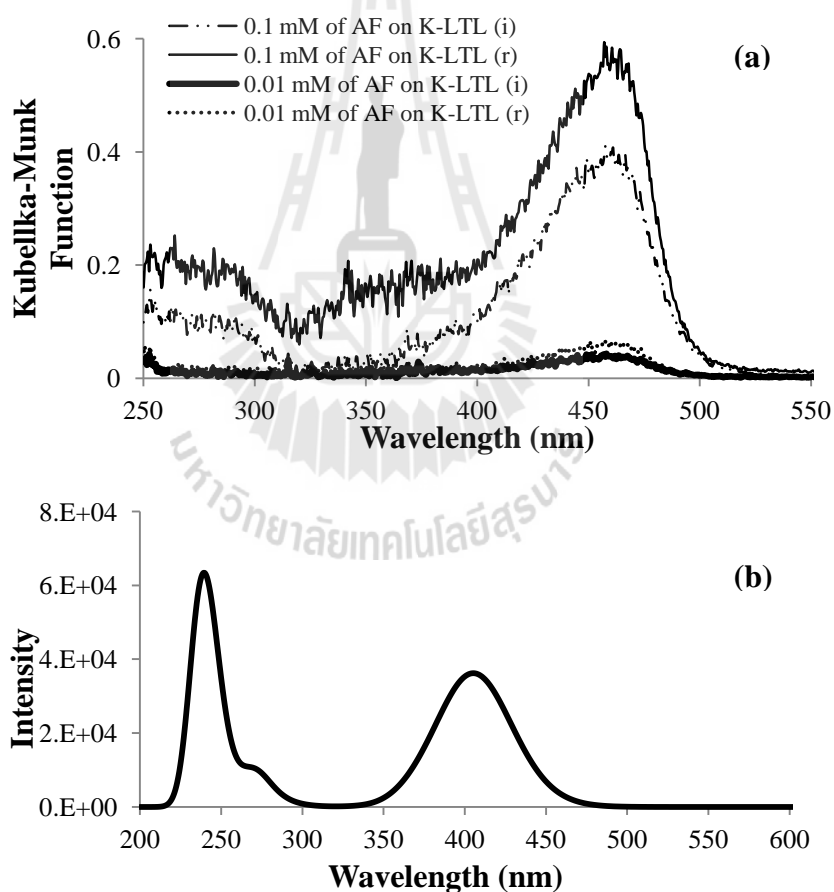
Figure 3.9 (a) Experimental diffuse reflectance spectra of AF on ice hockey (i) and round (r) shape of K-LTL at different loading levels of the dye and (b) calculated absorption spectra.

(a)   LUMO   LUMO+1

HOMO   HOMO-2
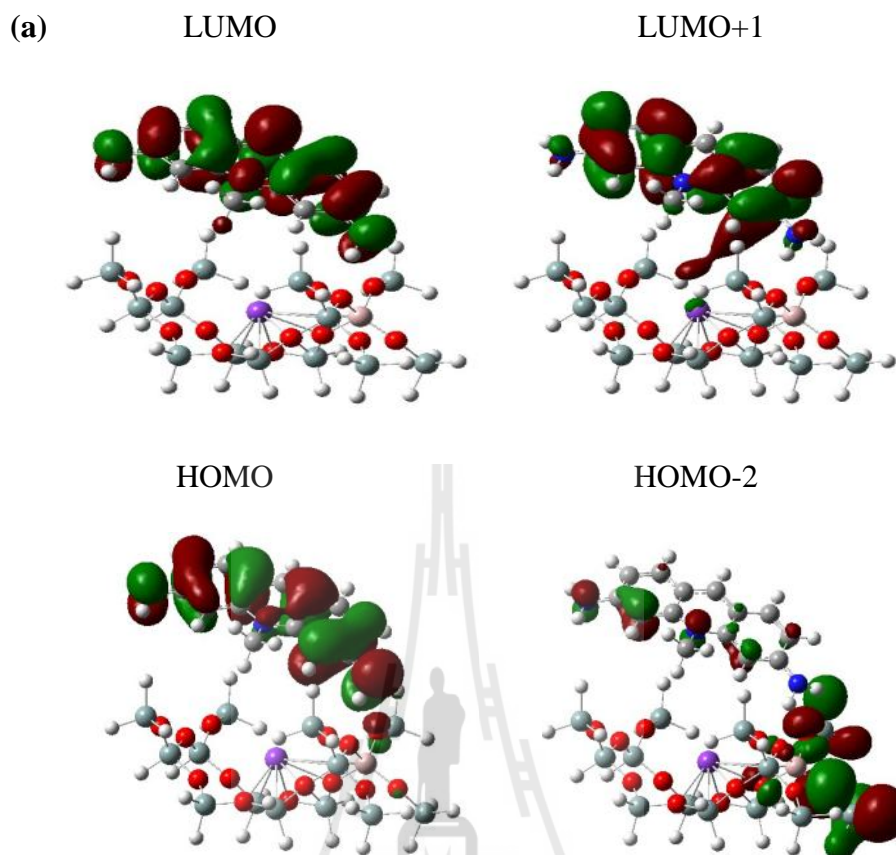
Figure 3.10 Frontier molecular orbital of AF in K-LTL in gas phase calculated by TD-BTLYP 6-31G(d,p).

Figure 3.9b shown the calculated absorption spectra of AF in K-LTL compared with the experimental spectra (see Figure 3.9a) and that found to be consistented, although slightly the blue shift. However, the calculation result can be also supported the experimental results very well. The calculated absorption spectra show that there are two main peaks. The first peak of at 405 nm and 460 nm for calculated and experimental absorption spectra, respectively are to be assigned to the excitation of electron from the highest occupied MO (HOMO) to the lowest unoccupied MO (LUMO), corresponds to π-π* of AF. In addition the most intense

peak (239 nm) in calculated spectrum assigned to charge transfer from zeolite to the

AF molecule (HOMO-2 to LUMO+1) that shown in Figure 10 and Table 3.3.

Acriflavine hydrochloride (AF) in H-LTL

Considering AF adsorbed on ice hockey (i) and round (r) shape of H-LTL

the absorption bands appeared at 465, 350, 290, and 235 nm (see Figure 3.11b) and

the emission band at around 538 nm (see Figure 3.13b). It seems to be that behavior

of AF in H-LTL is similar to AF in 0.2 M HCl solution indicating that AF in H-LTL

exhibits as protonated forms (AFH^+/AFH_2^{2+}). AF exists as cationic and protonated

species depending upon the pH of the aqueous medium as written as Scheme 3.2.
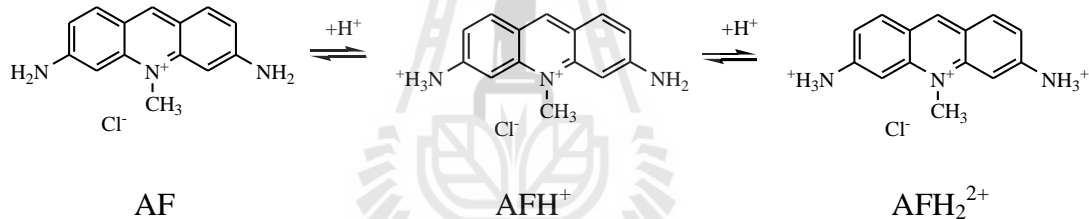
Scheme 3.2 Protolytic equilibria AF in the aqueous solution.

This phenomenon has been previously reported in proflavine (PF) which

is similar to AF when referring to protonation and deprotonation of the species (Pileni

and Grätzel, 1980). In solution found that the PF can be in diprotonated,

monoprotonated, or neutral form with pKa about 0.2 for doubly protonated form and

pKa about 9.5 for monoprotonated form (Misra, Mishra, Joshi, and Pant, 2001;

Ganesan and Ramaraj, 2000). Therefore, AF molecule in H-LTL assumed to be

protonated form of AFH^+/AFH_2^{2+} because H-LTL contains high amount of strong

brønsted acid site corresponding to the result of TPD-NH$_3$ results. The presence of a

shoulder band around 350 nm in diffuse reflectance spectra (see Figure 3.11a) and the absorption spectrum of protonated AF (see Figure 3.4a) strongly suggests the present of AFH^+/AFH_2^{2+}. From these results, it implies that the dominant species in H-LTL is AFH^+/AFH_2^{2+}.
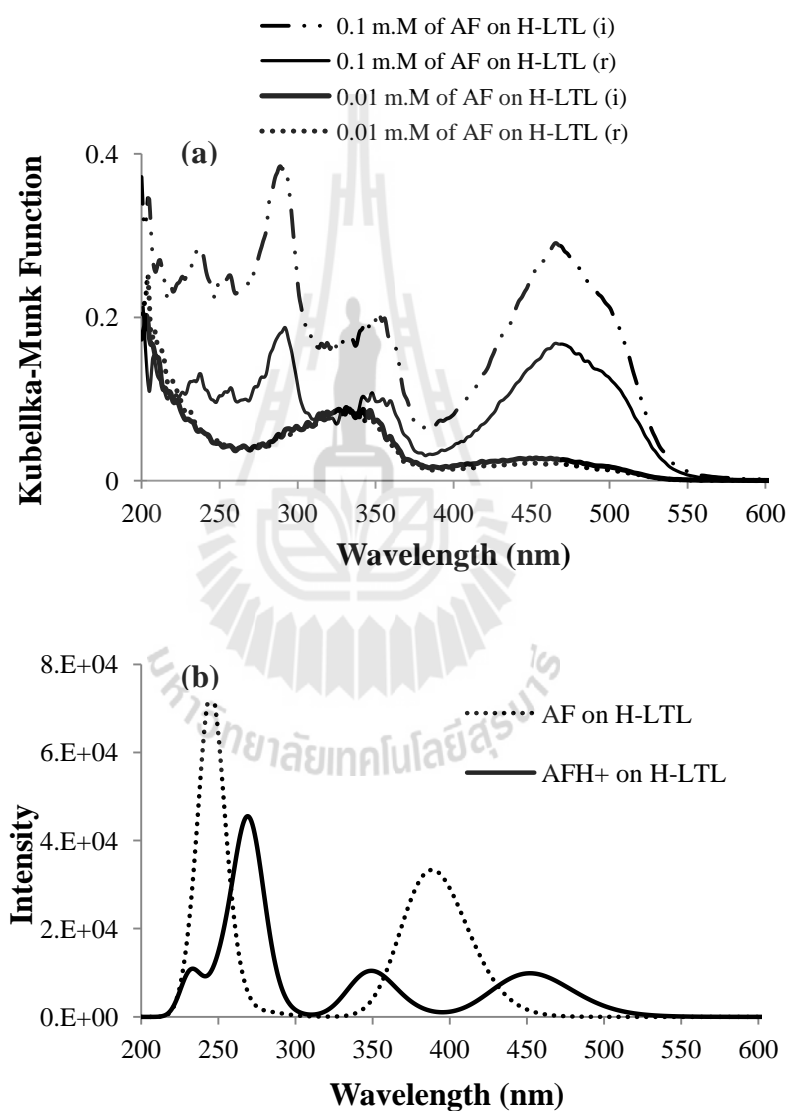
Figure 3.11 (a) Experimental diffuse reflectance spectra of AF in ice hockey (i) and round (r) shape of H-LTL at different loading levels of the dye and (b) calculated absorption spectra.

(a) LUMO LUMO+1 LUMO+2

HOMO HOMO-2

(b) LUMO HOMO-3

HOMO-8 HOMO-9
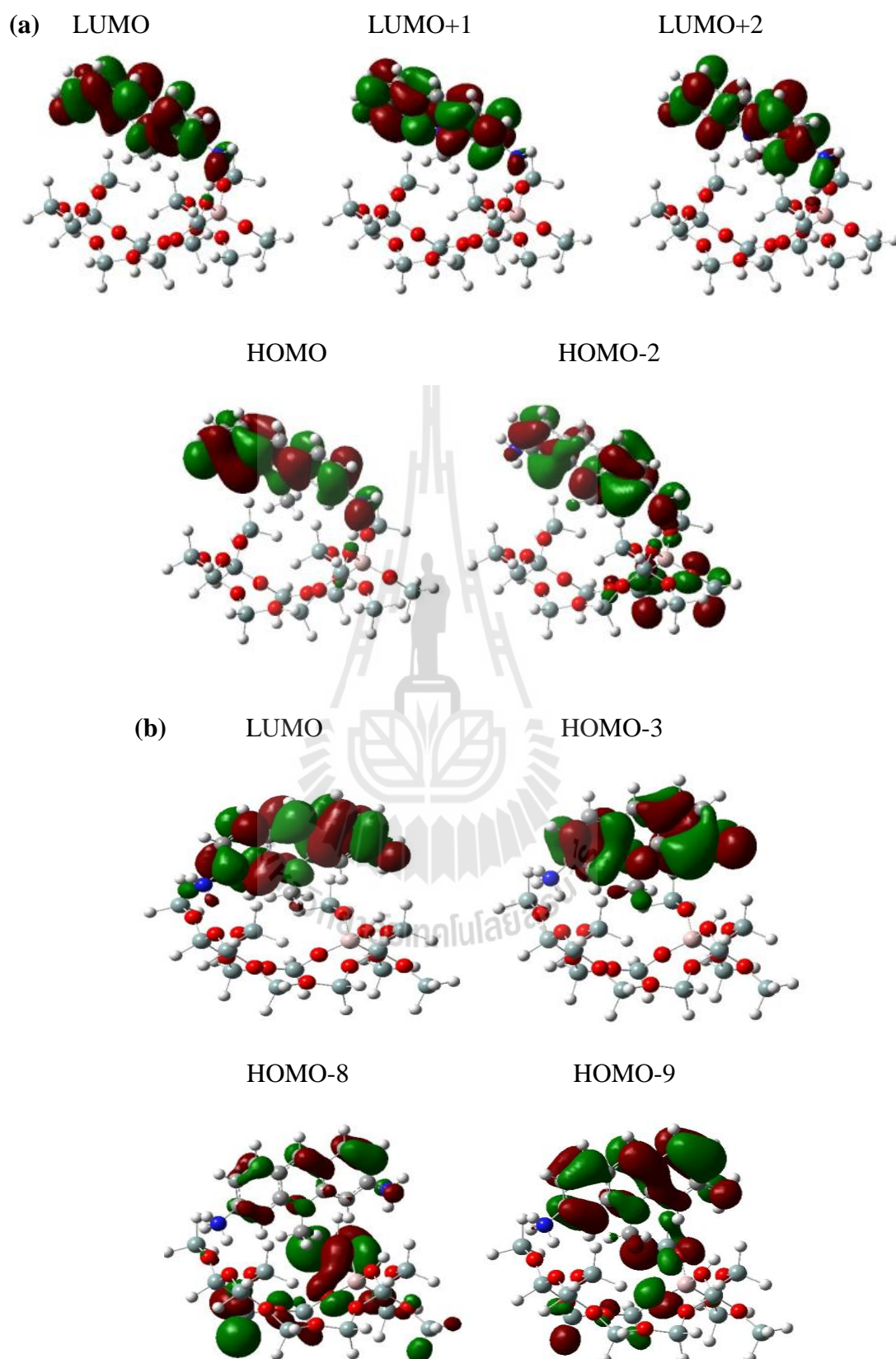
Figure 3.12 (a) Frontier molecular orbital of AF and (b) AFH$^+$ in H-LTL in gas phase calculated by TD-BTLYP 6-31G(d,p).

Figure 3.11b was shown the calculated absorption spectra of AF and protonated AF (AFH$^+$) in H-LTL for confirm the experimental result. It was found that AF in H-LTL was not protonated by BrØnsted acid site of H-LTL zeolite. Moreover, the absorption spectrum around 350 nm of AF in H-LTL cannot be observed. The first peak at 403 nm and 465 nm for calculated and experimental absorption spectra were observed. This bands are to be assigned to the excitation of electron from the highest occupied MO (HOMO) to the lowest unoccupied MO (LUMO) combination with HOMO-2 to LUMO, corresponds to π-π* of AF and charge transfer from zeolite framework to the dye molecule. In addition the peak at 257 nm (experimental is 250 nm) assigned to excitation of electron from the HOMO to the LUMO+1 and HOMO to LUMO+2 (see Figure 3.12a and Table 3.3). However, the complex of protonated acriflavine (AFH$^+$) confined in H-LTL zeolite was also calculated. It was found that its absorption spectrum is similar to that of experimental results that peak at around 350 nm was appeared. This peak is the excitation of electron from the HOMO-8 to the LUMO and HOMO-9 to LUMO. Furthermore, the peak of calculated AFH$^+$-H-LTL spectrum at 451 nm (experiment value, 465 nm) corresponds to the combination of HOMO-3 to LUMO and HOMO-8 to LUMO (see Figure 3.12b and Table 3.3) that assign to π-π* of dye and charge transfer from zeolite framework to the dye, respectively.

Table 3.3 Summary the photophysical properties of AF and AF confined in K-LTL and AF confined in H-LTL.

Structure	λ(nm) (cal.)	Oscillator strength (f)	λ(nm) (Ex.)	Assignment
AF (g)	390	0.5522	448	HOMO to LUMO(74%)
				HOMO-1 to LUMO+1 (9%)
	243	0.5549	250	HOMO-1 to LUMO+1 (38%)
				HOMO-0 to LUMO+3 (33%)
AFH$^+$ (g)	434	0.1537	458	HOMO to LUMO (73%)
				HOMO-1 to LUMO (10%)
	349	0.1604	348	HOMO-1 to LUMO (65%)
				HOMO to LUMO+1 (19%)
	252	0.2796	275	HOMO-1 to LUMO+1 (44%)
				HOMO-3 to LUMO (30%)
AF$^-$ K-LTL	405	0.4281	460	HOMO to LUMO (66%)
	240	0.1381	-	HOMO-2 to LUMO+1 (44%)
				HOMO-3 to LUMO+1 (24%)
AF$^-$ H-LTL	403	0.1482	465	HOMO to LUMO (42%)
				HOMO-2 to LUMO (33%)
	-	-	350	-
	256	0.1393	290	HOMO to LUMO+1 (47%)
				HOMO to LUMO+2 (20%)
AFH$^+$-H-LTL	452	0.1358	-	HOMO-3 to LUMO (76%)
				HOMO-8 to LUMO (5%)
	349	0.0839	-	HOMO-8 to LUMO (29%)
				HOMO to LUMO+2 (20%)
	270	0.4951	-	HOMO-3 to LUMO+1 (53%)
				HOMO-3 to LUMO+2 (12%)

(*more detail in Appendix A: Table A.1 and A.2)
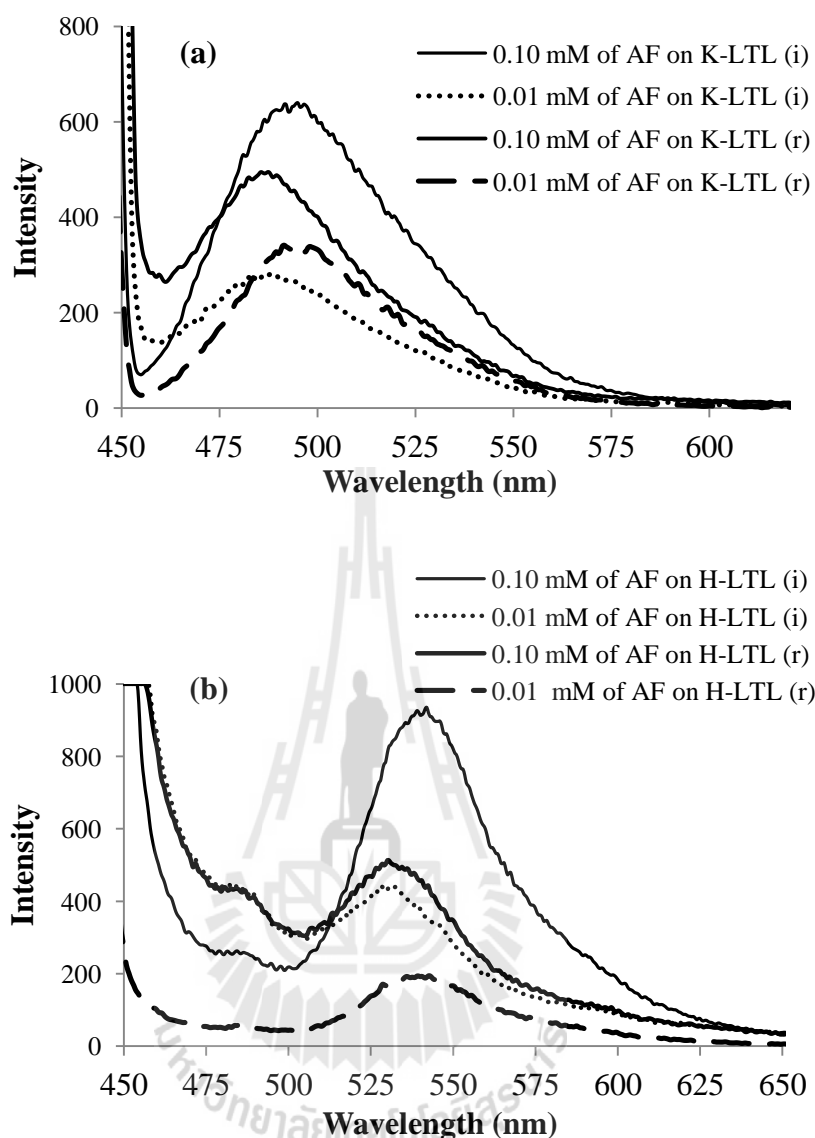
Figure 3.13 (a) Emission spectrum of AF on round shape of K-LTL and (b) H-LTL at different loading levels of the dye.

Considering the effect of concentrations, Figure 3.13, the red shift of the emission spectra of AF in K-LTL and H-LH was observed upon increased the concentrations of the dye. This shift is probably due to self-absorption and reemission of AF molecules that agreed with report (Gfeller, Megelski, and Calzaferri, 1999). Moreover, this work presence that microenvironment of zeolite LTL (K-LTL and

H-LTL) has influenced on the spectral properties of AF molecule whereas the morphology of the crystals did not influence on the spectral properties of AF molecule.

3.4 Results and discussion (Acridine hydrochloride, Ac)

3.4.1 The structure and properties of bare acridine hydrochloride and confined in zeolite channels

Ground state geometry optimization

Figure 3.14a and 3.14d illustrated the optimized geometries of bare Ac and protonated Ac (AcH$^+$) which were planar geometry. The interaction of absorbed Ac in K-LTL was occurred between N atom of Ac molecule and K$^+$ ion of K-LTL and the calculated distance of N atom of Ac molecule and K$^+$ ion of K-LTL is 3.198 Å. Moreover, benzene ring of Ac molecule can interact with the K$^+$ ion via cation-π interaction according to Figure 3.14b and 3.14c. While the optimized structure of Ac in H-LTL was also shown in Figure 3.14e and 3.14f. Acridine molecule is protonated by BrØnsted acid site of H-LTL. This result can be seen in the calculated the Oz-Hz distance of bare H-LTL which was extended from 0.968 Å to 1.690 Å when it was adsorbed with Ac molecule.

(a)   **(b)**   **(c)**

(d)   **(e)**   **(f)**
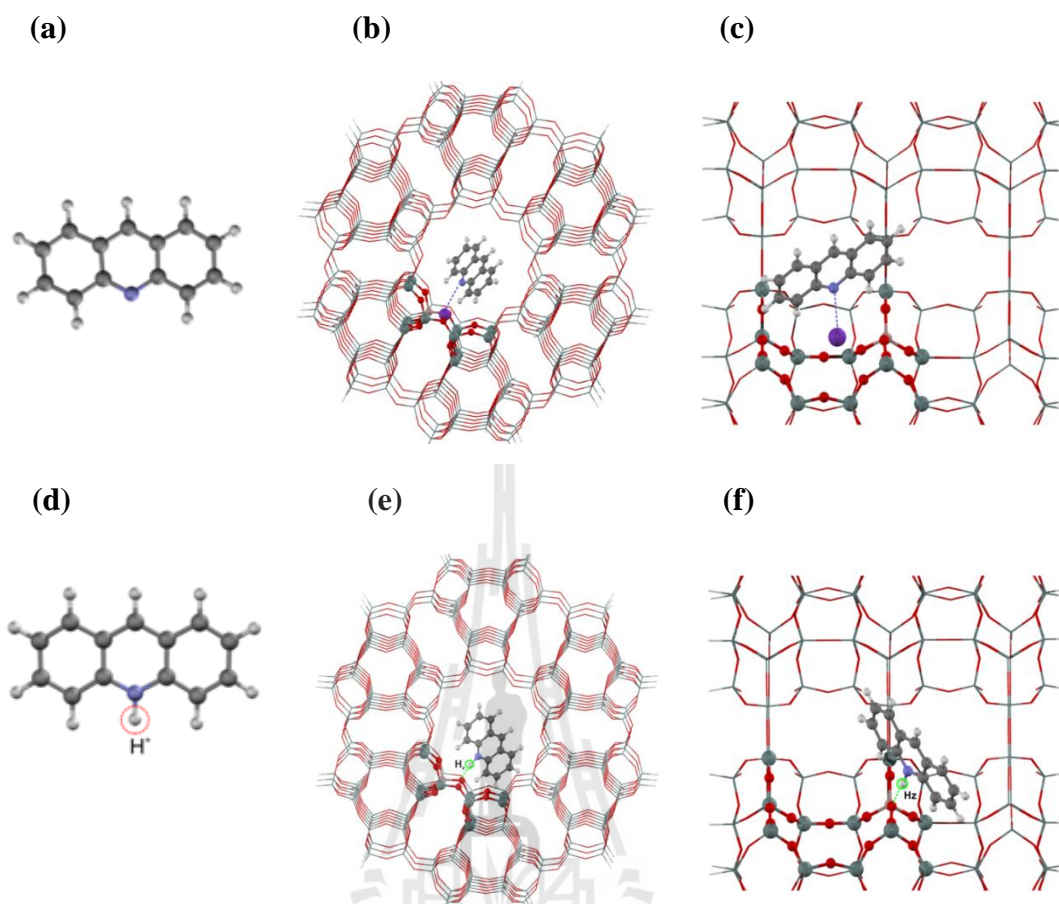
Figure 3.14 (a) Optimized structures of acridine, acrinine in K-LTL, (b) front view and (c) side view of the channel, (d) protonated acridine, and acridine in H-LTL (e) front view, (f) side view of the channel.

3.4.2 UV-Vis absorption spectra: Experimental and Theoretical studies

Acridine hydrochloride (Ac) in solution

Figure 3.15a illustrated the experiment absorption spectra of Ac in various solvents that show the absorption peak at 355 nm suggesting that the band was a π-π* character while the band around 375-430 nm could be n-π* or π-π*, depending on polar nature of the solvent and the Ac species present (Ito, Ito, Yoshikawa, Watanabe,

and Kokubun, 1996; Ryan, Xiang, Johnston, and Fox, 1997). Acridine molecule exist as protonated form when it was dissolved in water and acidic solution (0.2 M HCl) and shows a broad band around 400-450 nm. This band was a π-π* character that agreed with the report of Tomasz and coworker (Tomasz, Bronislaw, and Gordon, 2002). Some researchers reported absorption maxima of Ac in neutral, hydrogen-bonded and protonated species appeared at 355 nm, only the spectrum of protonated species (AcH$^+$) has a broad shoulder within 370-430 nm range. The broad shoulder is the characteristic of the protonated form but not for aggregated Ac form (Ito, Ito, Yoshikawa, Watanabe, and Kokubun, 1996; Ryan, Xiang, Johnston, and Fox, 1997).
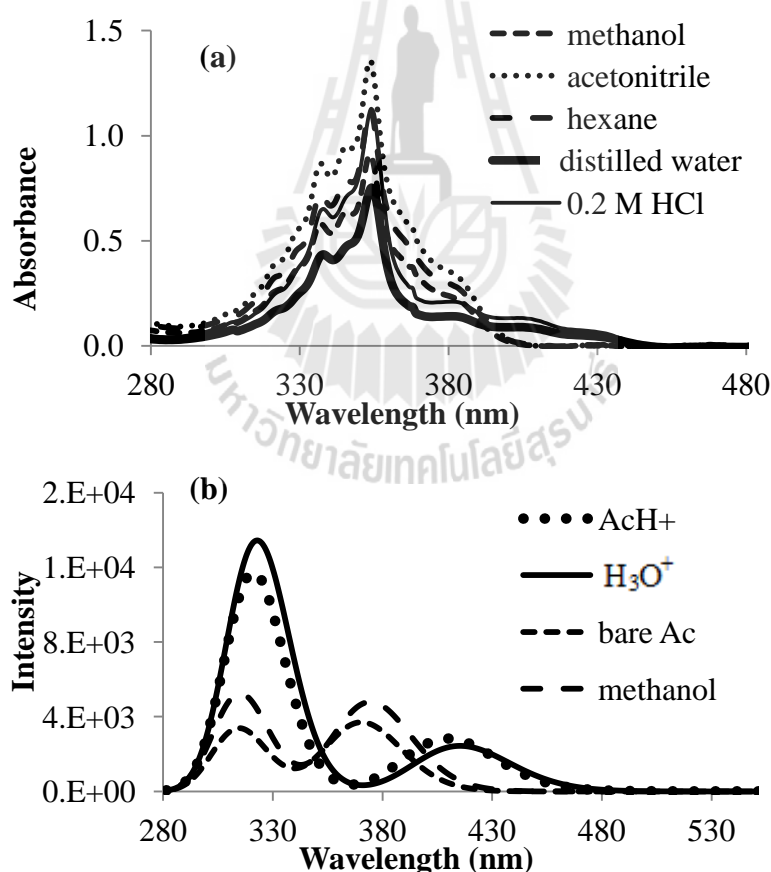
Figure 3.15 (a) Experimental and (b) computational absorption spectra of Ac in various solvents.

The solvent effect was studied by using the CPCM method. Figure 3.15b illustrated the results of the calculated absorption spectra in different solvents which are not significantly different, except Ac in protonated form (AcH$^+$) and H$_3$O$^+$. Acridine in acetonitrile, methanol, butanol and bare acridine exist as neutral form that showed two peaks at around 370 and 315 nm, while the experiment was observed one broad band around at 355 nm. The calculated absorption peak separate into 2 peaks, because the peak around 350 nm is the electronic transition from HOMO-2 to LUMO (n-π*) which oscillator strength is nearly zero resulting in low intensity. Therefore, the broad peak in the experiment is likely due to a combination of the 370 nm and 315 nm. While n-π* transition of the protonated form cannot observed, because its lone pair electrons is used for N-H bond formation. Therefore, 2 peaks are clearly separated from each other as well. The calculated absorption peaks of neutral Ac at 370 nm and 315 nm, corresponded to the electronic transition from HOMO to LUMO (n-π*) and HOMO-1 to LUMO combined with HOMO to LUMO+1(π-π*), (Figure 3.16a and Table 3.4). The experiment absorption spectra of Ac in water, acidic solution (0.2 M HCl) and calculated absorption spectra of Ac in H$_3$O$^+$ exist as the protonated form. The calculated absorption peak at 410 nm corresponds to the electronic transitions from HOMO to LUMO (π-π*) and the peak at 325 nm was assigned to the combination between the HOMO-1 to LUMO (π-π*) and HOMO-2 to LUMO (Figure 3.16b and Table 3.4).

(a) bare acridine, methanol, butanol, and acetonitrile

LUMO   LUMO+1

HOMO   HOMO-1   HOMO-2

(b) protonated form

LUMO   HOMO   HOMO-1   HOMO-2
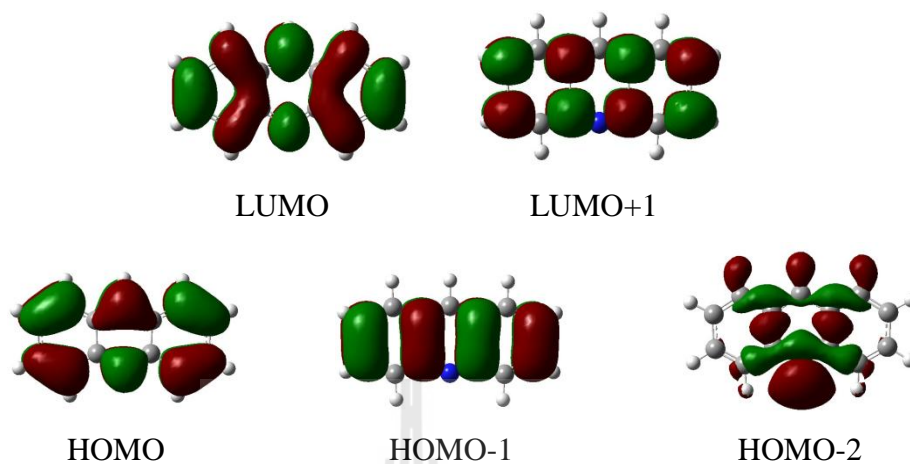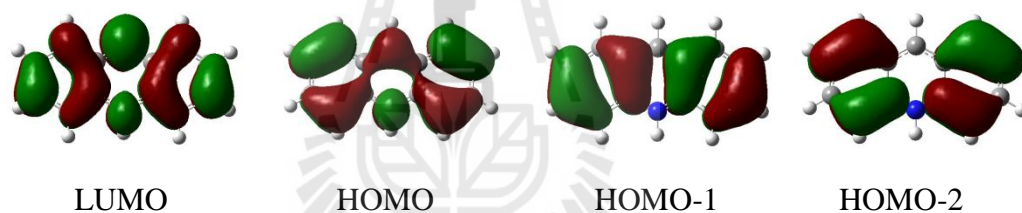
Figure 3.16 (a) Frontier molecular orbital of bare acridine in the gas phase, methanol,acetonitrile, butanol and (b) protonated form calculated by TD-B3LYP 6-31G(d,p).

Acridine hydrochloride (Ac) in zeolite K-LTL

The properties of the Ac in the channels of zeolite LTL depend upon the microenvironment of the channels of zeolite LTL (K-LTL and H-LTL) regardless of morphology and loading of the dye. The diffuse reflectance spectra of Ac adsorbed on ice hockey (i) and round (r) shape of K-LTL were shown in Figure 3.17. The spectra were quietly similar to the neutral form of Ac in hexane with the band at 355 nm.

While Figure 3.17 (inset) the calculated absorption spectrum of Ac confined in K-LTL has two peaks (381 and 317 nm) while the experiment observed one peak at 355 nm. This result is show the same trend with the experiment and calculated absorption spectra of Ac in solution. The first absorption peak of dye-zeolite system (381 nm) corresponds to the first excited singlet state which is the electronic transitions from HOMO to LUMO (see Figure 3.19a and Table 3.4), assigned to π-π* of dye molecule. The second absorption peak (317 nm) corresponds to S_2 excited state that assign to be the electronic transitions from π-π* of dye molecule (HOMO to LUMO) and also the small amount of electron transfer from zeolite to Ac molecule (HOMO-3 to LUMO (see Figure 3.19a and Table 3.4).
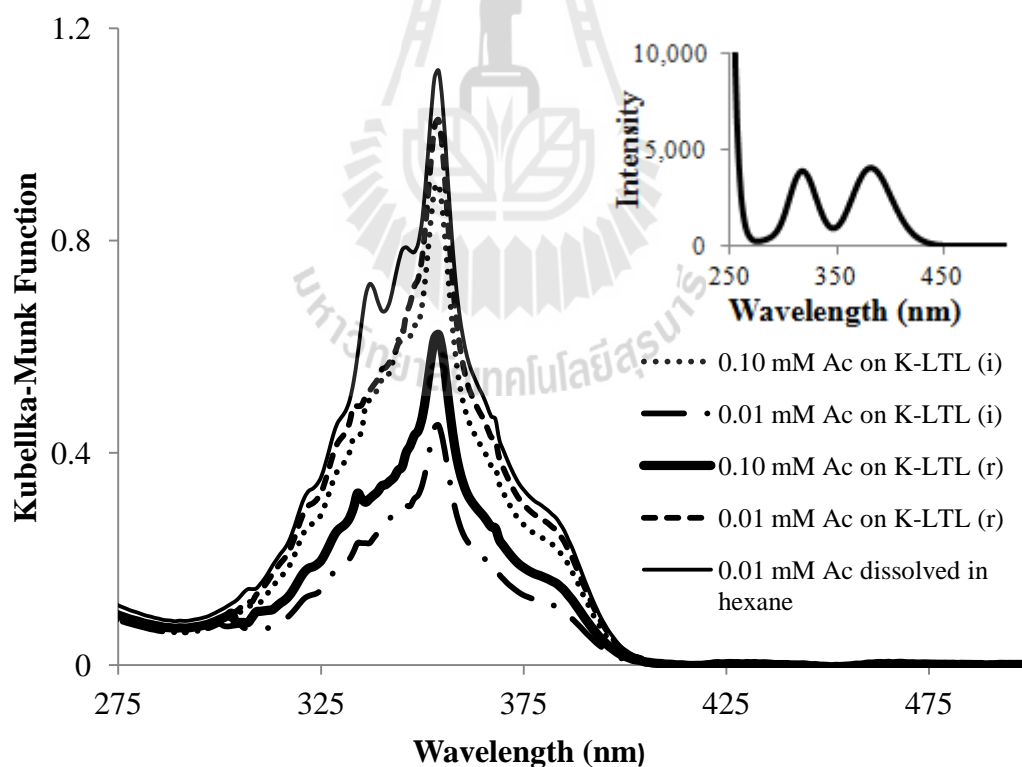
Figure 3.17 Diffuse reflectance spectra of Ac in round shape of K-LTL. Inset is calculated absorption spectrum of Ac in K-LTL.

Acridine hydrochloride (Ac) in zeolite H-LTL

Figure 3.18 the diffuse reflectance spectra of Ac confined in ice hockey (i) and round (r) shape of zeolite H-LTL are similar to the Ac in acidic solution (0.2 M HCl) and water (see Figure 3.15a). The first band was observed at 355 nm and the second band is a broad band around 375-450 nm. This band is strong evidence of the presence of acridine protonated species (AcH$^+$). The result was agreed with the calculation method.
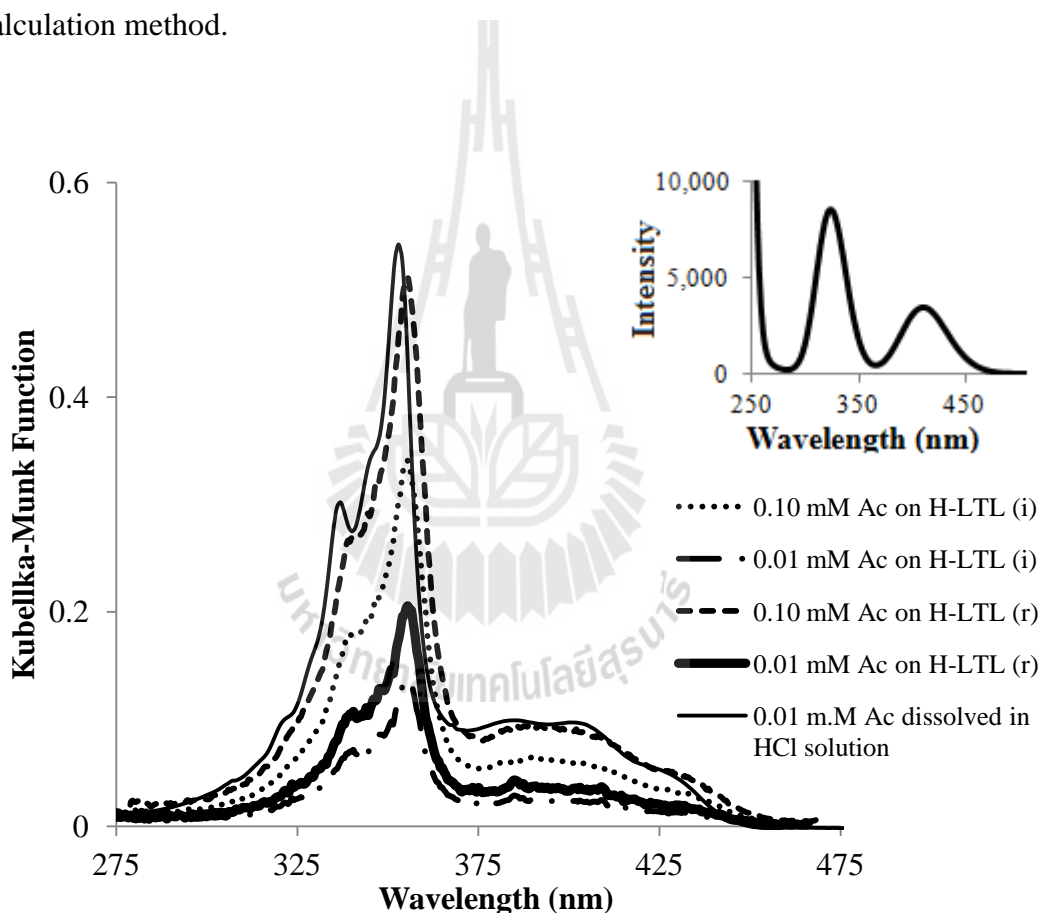
Figure 3.18 Diffuse reflectance spectra of Ac in round shape of H-LTL. Inset is calculated absorption spectrum of Ac in H-LTL.

The first absorption peak of dye-zeolite system (see Figure 3.18, inset) appeared at 410 nm (experimental at 375-450 nm). The first peak results from the

electronic transitions from HOMO-3 to LUMO (π- π*) of dye molecule and small amount of electron transfer from zeolite to Ac (HOMO-4 to LUMO) that was shown in Figure 3.19b and Table 3.4. The second absorption peak at 324 nm (experimental at 356 nm) corresponds to the electronic transition from HOMO-9 to LUMO combined with HOMO-4 to LUMO+1 was assigned to π-π* transition and charge transfer form zeolite to Ac molecule.

(a)   LUMO   HOMO   HOMO-3

(b)   LUMO   LUMO+1

HOMO-3   HOMO-4   HOMO-9
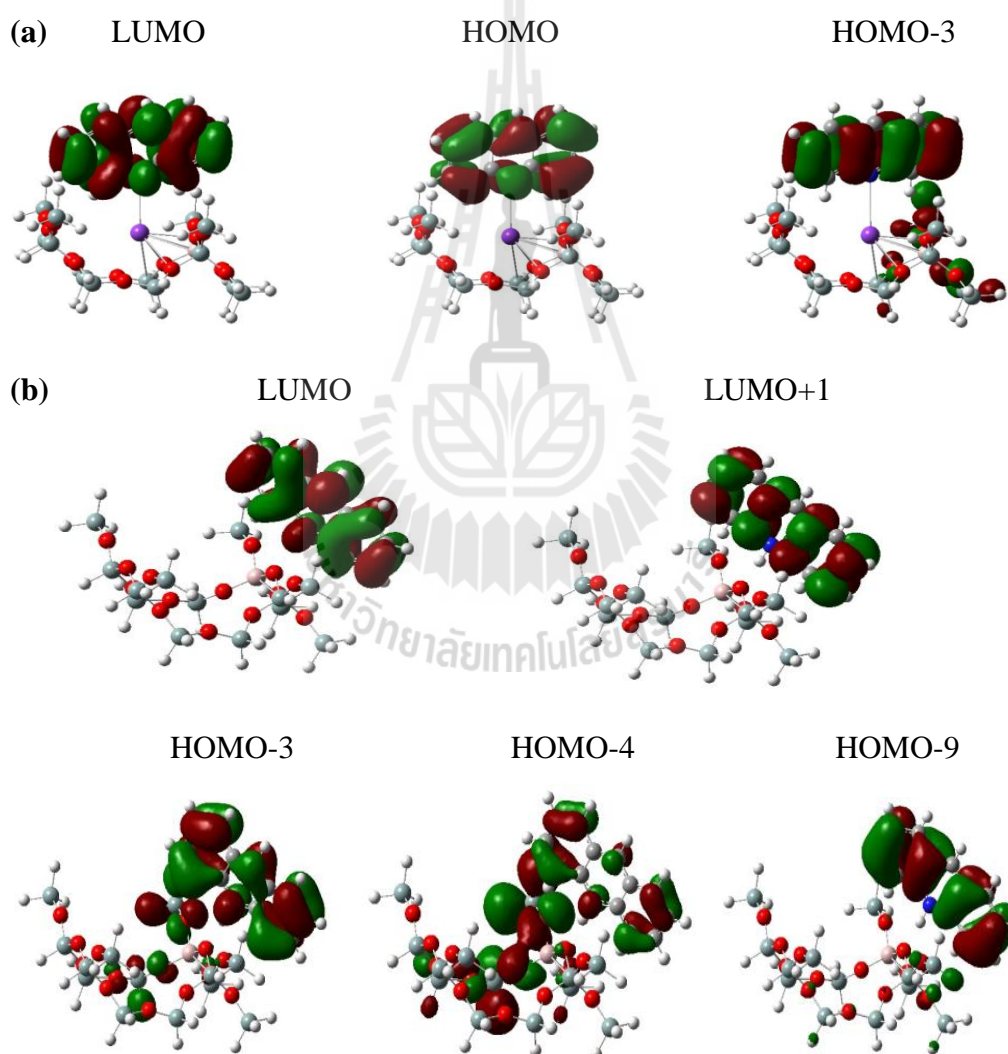
Figure 3.19 (a) Frontier molecular orbital of acridine in K-LTL and (b) H-LTL calculated by TD-B3LYP 6-31G(d,p).

Table 3.4 Summary the photophysical properties of Ac in the solvents and in K-LTL and H-LTL.

Structure	λ(nm) (cal.)	Oscillator strength (f)	λ(nm) (Ex.)	Assignment
Ac	370	0.0511	355	HOMO to LUMO (82%)
	315	0.0464	-	HOMO-1 to LUMO (63%)
				HOMO to LUMO+1 (39%)
Ac-methanol Ac-acetonitrile	~ 370	~0.0700	355	HOMO to LUMO (83%)
Ac-butanol	~315	~0.0012	-	HOMO-2 to LUMO+0 (96%)
AcH$^+$	410	0.0390	400-450	HOMO to LUMO (98%)
	325	0.1368	355	HOMO-1 to LUMO (64%)
				HOMO-2 to LUMO (21%)
Ac-K-LTL	381	0.0561	355	HOMO to LUMO (97%)
	317	0.0524	-	HOMO-3 to LUMO (54%)
				HOMO to LUMO+1 (30%)
Ac-H-LTL	410	0.0185	375-450	HOMO-3 to LUMO (92%)
				HOMO-4 to LUMO (88%)
	324	0.0941	356	HOMO-9 to LUMO (59%)
				HOMO-4 to LUMO+1 (12%)

(*more detail in Appendix A: Table A.3 and A.4)

3.4.3 Emission spectra of Acridine hydrochloride (Ac) in solution

The emission spectra of Ac were also used to establish the nature of the excited-state species on each solvent. According to the diffuse reflectance spectra, the adsorbed ground-state Ac exists as neutral, hydrogen-bonded and protonated species. The emission spectra in different solvents were divided into three types (see Figure 3.20). Firstly, when Ac was dissolved in chloroform and hexane, neutral species were presented the emission band with maximum at 425-430 nm. Secondly, the hydrogen-bonded species showed the emission maximum at 412 nm when Ac was dissolved in methanol. Some reports demonstrated that in methanol hydrogen-bonded species showed the emission band at 414 nm (Negrón-Encarnación, Arce, and Jiménez, 2005; Samsonova et al., 2009). Finally, the emission maximum around 465 nm was shown by the protonated species. (Diverdi and Topp, 1984; Ryan, Xiang, Johnston, and Fox, 1997). Moreover, the spectroscopic measurements of excited state pKa of Ac indicate that, the singlet states of Ac are stronger bases than the ground state due to a large increase in the electron density over the N-atom (pKa 5.4, pKa* 9.2) (Ryan, Xiang, Johnston, and Fox, 1997). Hence at suitable pH, it abstracts proton from the surrounding solvent and become protonated species. (Ryan, Xiang, Johnston, and Fox, 1997; Negrón-Encarnación, Arce, and Jiménez, 2005).
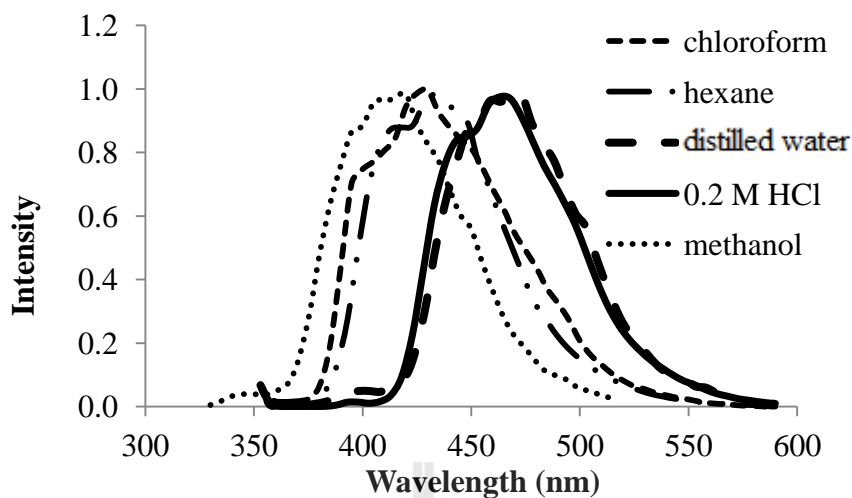
Figure 3.20 Emission spectra of Ac in different solvents, the samples were excited at 355 nm.

3.4.4 Emission spectra of Acridine hydrochloride (Ac) in zeolite LTL

Emission spectra of Ac in K-LTL

Figure 3.21 illustrated Ac adsorbed on ice hockey (i) and round (r) shape of K-LTL. The emission maximum spectra of all the samples appeared at 408 and 438 nm. It was consistent with the emission spectrum of Ac in methanol which showed the emission maximum spectrum at 412 nm. It suggests that hydrogen-bonded are presence on zeolite K-LTL. Some researchers reported that Ac adsorbed on MgO surface showed the hydrogen-bonded and neutral acridine species are present on MgO (Negrón-Encarnación, Arce, and Jiménez, 2005). Thus, K-LTL can be considered as a basic surface character.
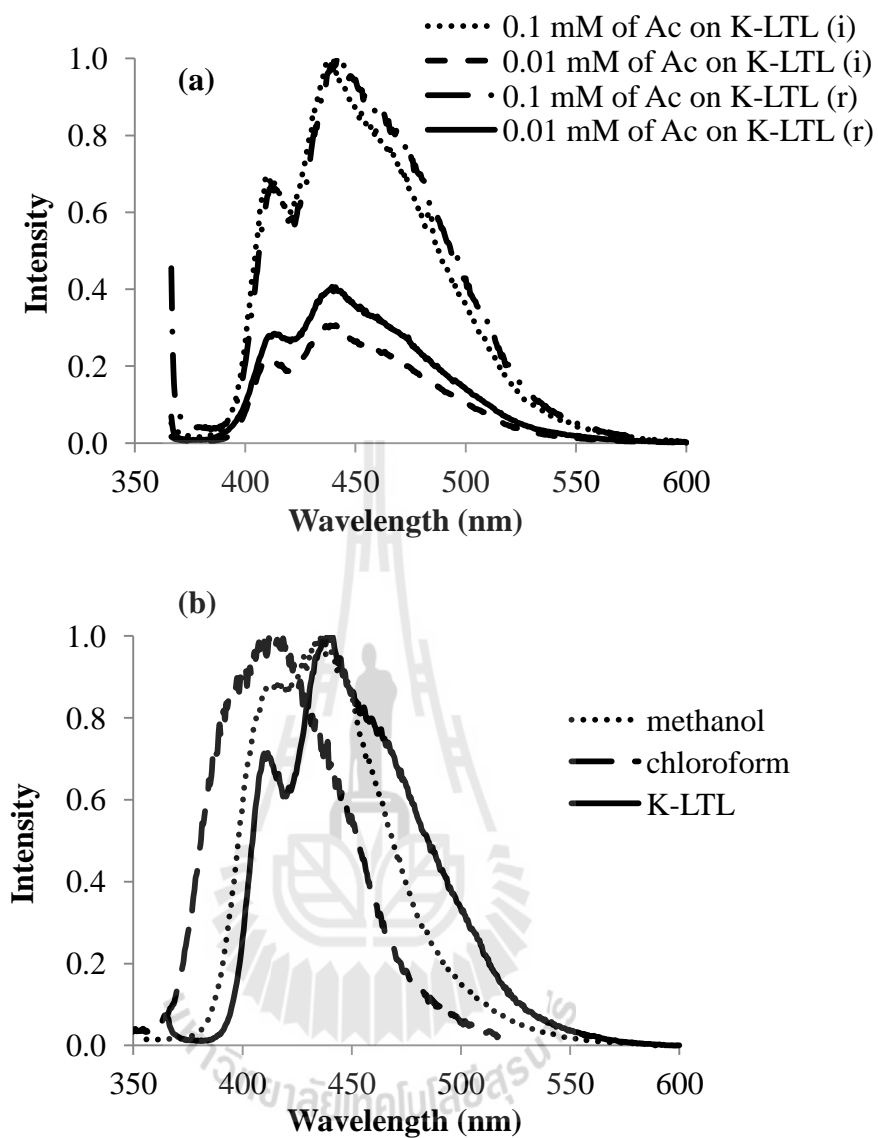
Figure 3.21 (a) Emission spectra of Ac on ice hockey and round shape of K-LTL and

(b) emission spectra of Ac in solution, samples were excited at 355 nm.
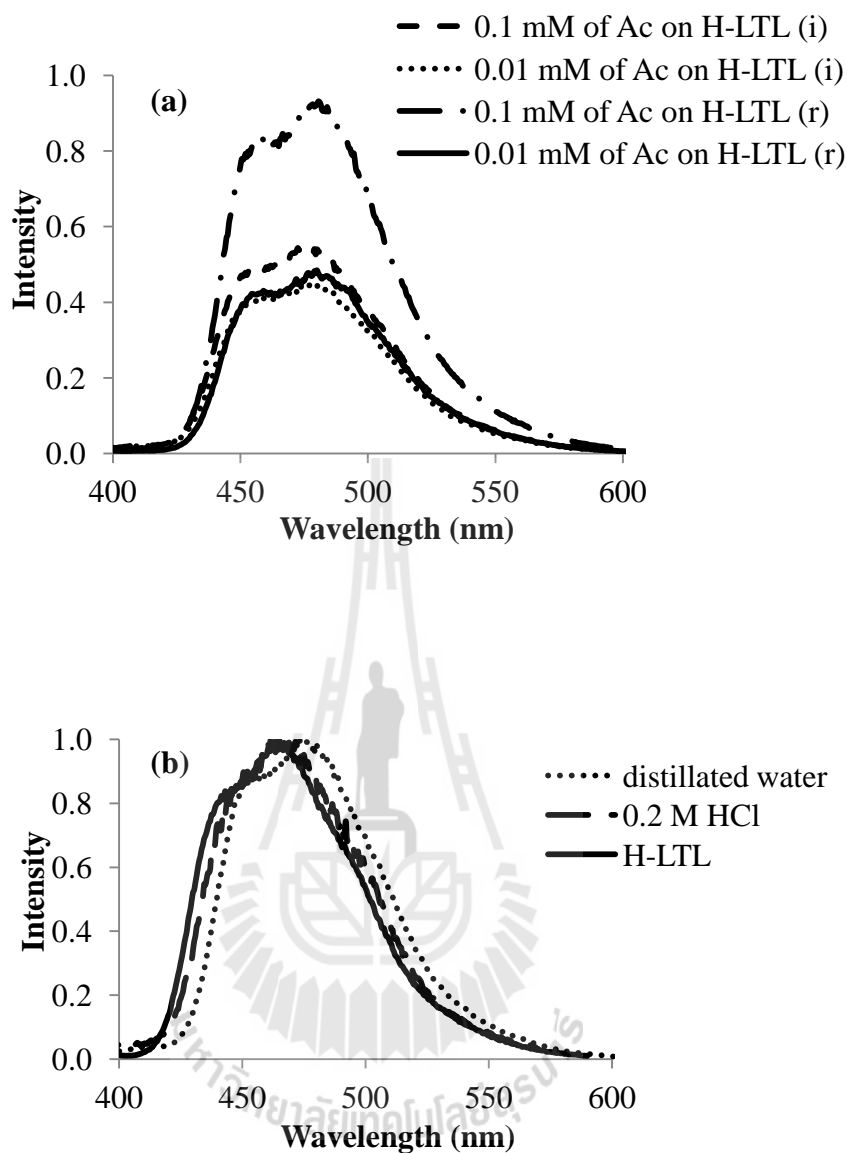
Figure 3.22 (a) Emission spectra of Ac on ice hockey and round shape of H-LTL and (b) emission spectra of Ac in solution, samples were excited at 355 nm.

Emission spectra of Ac in H-LTL

In the case of Ac adsorbed on ice hockey (i) and round (r) shape of H-LTL, the emission maximum spectra of all the samples appeared at 475 nm (see Figure 3.22a). This result are similar to the results of Ac dissolved in 0.2 M HCl and

water that showed the emission maximum spectra at 469 nm (see Figure 3.22a). It suggests that Ac undergoes an excited state proton transfer reaction on H-LTL. The pKa of the excited state of Ac is 9.2 which is much larger than for its ground state (pKa 5.4). This change suggests that the nitrogen atom becomes more negative in the excited state facilitating adding proton (Bowen, Holder, and Woodger, 1962). Thus, it is possible that on H-LTL, the protonated form is produced through a proton abstraction reaction by excited Ac. The difference between the maximum emission of protonated species in H-LTL and neutral species in K-LTL is about 38 nm. Based on this result, H-LTL form can be considered as an acidic surface. From the above mention Ac can also used as fluorescent probe for estimation the pH of surface as well.

3.5 Fluorescence resonance energy transfer (FRET) experiments

The objective of the present work is to investigate the possibilities of energy transfer within antenna material. This material was prepared by loaded Ac (donor) and AF (acceptor) molecules onto zeolite LTL. The energy transfer can take long-rang dipole-dipole energy transfer from the donor to the acceptor that has been developed by Förster mechanism (Calzaferri and Devaux, 2010). Energy transfer processes occur when the separation distance between donor and acceptor species at least 10 Å. Figure 3.23 illustrates the absorption and emission spectra of both dyes (Ac and AF) in the aqueous solution. The emission spectra of Ac and AF were measured upon excitation at 355 and 440 nm, respectively. The spectral overlap of two dyes is marked as gray region. The energy transfer between the two dyes is more efficient due to the large of spectral overlaps between the absorption of AF and

emission of Ac, so that energy transfer can occur upon selective excitation of the donor molecule.
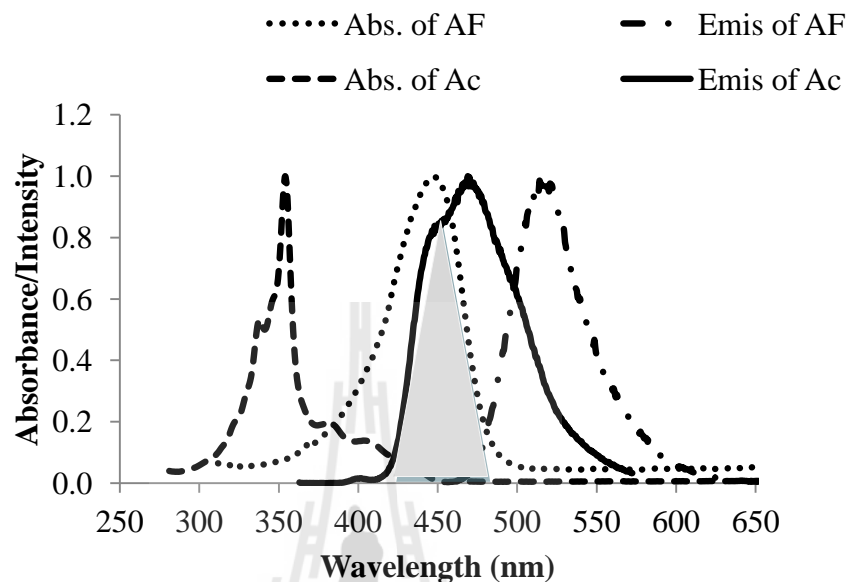
Figure 3.23 Energy transfer experiment, absorption and emission spectra of Ac and AF dissolved in aqueous solution.

The emission spectra of K-LTL and H-LTL loaded with 0.01 mM of Ac and AF are showed in Figure 3.24a and 3.24b, respectively. The excitation wavelength of the dyes loaded on zeolite LTL was fixed at 355 nm that only Ac (donor) absorbed. The maximum emission band of the dyes loaded on K-LTL was observed at 450 nm and 492 nm which assigned to the emission of Ac in neutral from and AF in cationic form, respectively. Whereas, the dyes loaded on H-LTL exhibits the emission band at 450, 475 and 540 nm which assigned to the emission of Ac in neutral form, Ac in protonated form and AF in protonated form, respectively. However, the position of the emission band does not change when varied excitation wavelength, but the decrease in intensity with increasing excitation wavelength from 355 to 375 nm. From

the spectral properties of dyes, we expect an efficient resonance energy transfer from

Ac to AF.
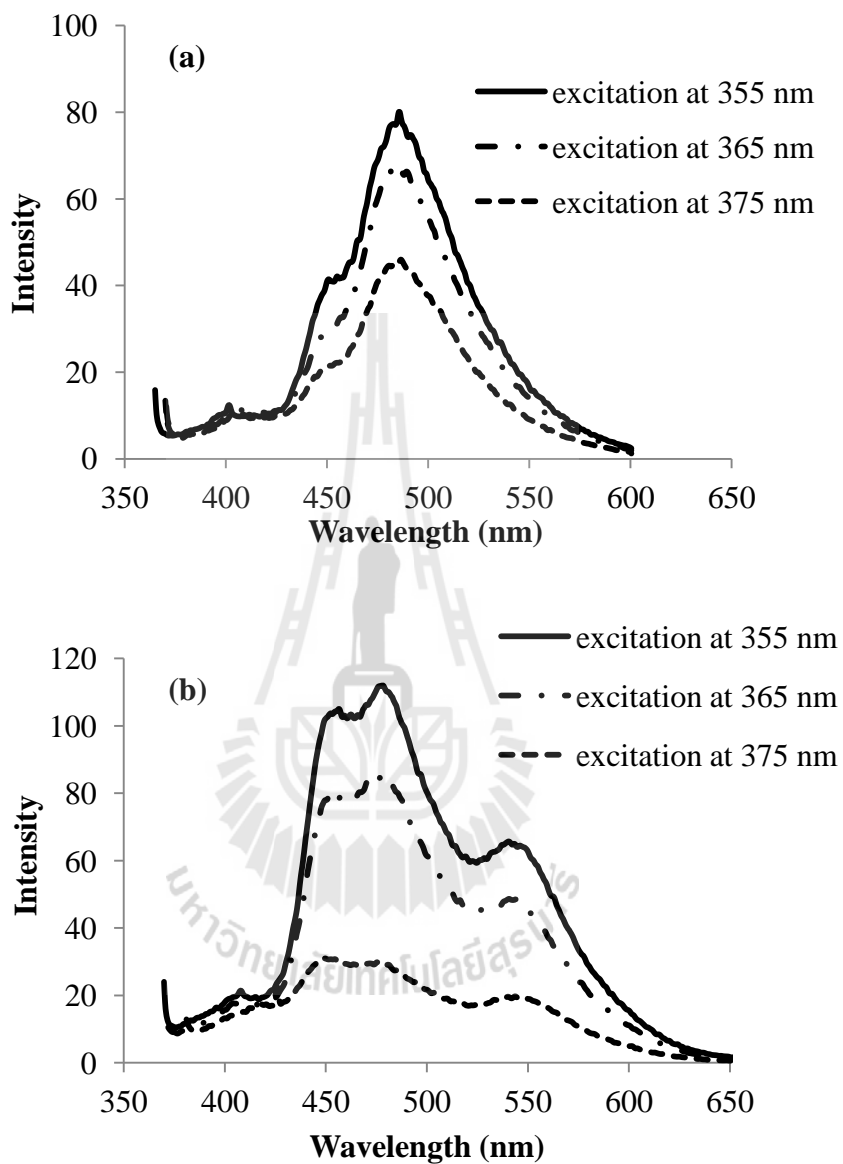
Figure 3.24 (a) Energy transfer experiment, excitation and emission spectra of Ac and AF on round shape of K-LTL and (b) H-LTL.

The fluorescence intensity of the AF within the zeolite LTL framework indicates that the following steps occur.

1. A ground state Ac molecule encapsulated within the channels of zeolite LTL absorbs light and is converted to its first excited singlet state Ac*.

$$Ac + h\nu \longrightarrow Ac* \qquad \text{absorption within host frameworks}$$
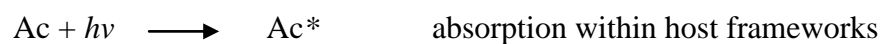
2. The rapid fluorescence resonance energy transfer occurs to a neighbor Ac that is excited.

$$Ac* + Ac \longrightarrow Ac + Ac* \quad \text{energy transfer within channels of zeolite LTL.}$$
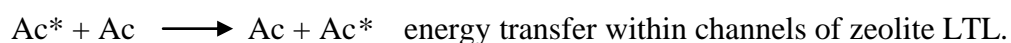
3. After this, if the excited Ac* reaches AF molecules, the energy transfer becomes very probable and hence quenching occurs. But if the internal conversion is very fast compared with the quenching process, emission from AF can be observed (see Scheme 3.3) (Binder, Galzaferri, and Gefeller, 1995; Binder, Galzaferri, and Gefeller, 1995).

$$Ac* + AF \longrightarrow Ac + AF* \quad \text{quenching within channels of zeolite LTL.}$$

$$AF* \longrightarrow AF + \text{fluorescence emission.}$$
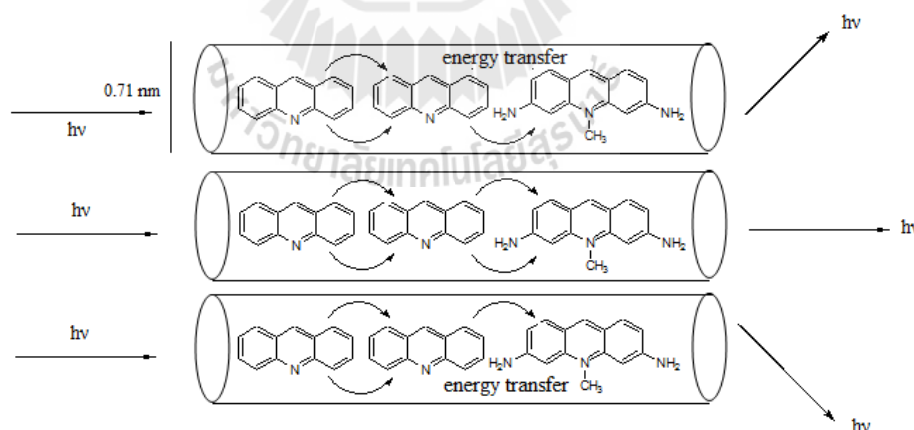
Scheme 3.3 The light absorbed by Ac molecule encapsulated in the host channels, then energy transfer to AF at the end of the hosts.

3.6 Conclusions

The host-guest materials containing fluorescent donor (Ac) and acceptor (AF) molecules were inserted into the zeolite LTL (K-LTL and H-LTL including ice hockey and round shape) by ion exchange process. The structural and spectral properties of Ac and AF loaded on zeolite LTL were examined experimentally by the diffuse reflectance UV−visible absorption and fluorescence emission. In the comparison of the experimental and the calculation result, the density functional theory (DFT) calculations at B3LYP/6-31G(d,p) level was employed. The 324T cluster model and the ONIOM(B3LYP/6-31G(d,p):UFF) method were performed for the calculations of dyes in the zeolite system. The study clearly indicates that the microenvironment of zeolite LTL (K-LTL and H-LTL) remarkably influences the photophysical process of Ac and AF molecules regardless of morphology of the crystals. Moreover, the energy transfer in dye-loaded zeolite LTL can be established. The light absorbed by Ac molecule encapsulated in the channels and is eventually trapped by AF. The present work illustrates that both Ac (donor) and AF (acceptor) loaded on zeolite LTL can be used as an artificial antenna material.

3.7 References

Barrer, R. M., and Villiger, H. (1969). The crystal structure of the synthetic zeolite L. **Z. Kristallogr**. 128: 352-370.

Binder, F., Galzaferri, G., and Gefeller, N. (1995). Cationic dye molecules in zeolite L as artificial antenna. **Proc. Indian Acad. Sci. (Chem. Sci.)**. 107: 753-767.

Binder, F., Galzaferri, G., and Gfeller, N. (1995). Dye molecules in zeolites as artificial antenna. **Solar Energy Mater. Solar Cells**. 38: 175-186.

Bowen, E. J., Holder, N. J., and Woodger, G. B. (1962). Hydrogen bonding of excited states. **J. Phys. Chem**. 66: 2491-2492.

Calzaferri, G., and Gfeller, N. (1992). Thionine in the cage of zeolite L. **J. Phys. Chem. A**. 96: 3428.

Clazaferri, G., Bossart, O., Brühwiler, D., Huber, S., Leiggener, C., Van Veen, M. K., and Ruiz, A. Z. (2006). Light-harvesting host-guest antenna materials for quantum solar energy conversion devices. **C. R. Chimie**. 9: 214-225.

Calzaferri, G., and Devaux, A. (2010). Manipulation of energy transfer processes within the channels of zeolite L. **Int. J. Photoenergy**. ID 741834.

Calzaferri, G., Meallet-Renault, R., Bruhwiler, D., Pansu, R., Dolamic, I., Dienel, T., Adler, P., Li, H. R., and Kunzmann, A. (2011). Designing dye nanochannel antenna hybrid materials for light harvesting, transport and trapping. **Chem. Phys.Chem**. 12: 580-594.

Chunxiang, L., Peipei, S., Lijun, Y., Yi, P., and Chien-Hong, C. (2008). Synthesis and electroluminescent properties of Ir complexes with benzo[c]acridine or 5,6-dihydro-benzo[c]acridine ligands. **Thin Solid Films**. 516: 6186-6190.

Diverdi, L. A., and Topp, M. R. (1984). Subnanosecond time-resolved fluorescence of acridine in solution. **J. Phys. Chem**. 88: 3447-3451.

Ganesan, V., and Ramaraj, R. (2000). Spectral properties of proflavin in zeolite L and zeolite-Y. **J. Lumin**. 92: 167-173.

Gfeller, N., Megelski, S., and Calzaferri, G. (1999). Fast energy migration in pyronine loaded zeolite L microcrystals, **J. Phys. Chem. B**. 103: 1250-1257.

Hennessy, B., Megelski, S., Marcolli, C., Shklover, V., Bärlocher, C., and Calzaferri,

G. (1999). Characterization of methyl viologen in the channels of zeolite L. **J. Phys. Chem. B**. 103: 3340-3351.

Huber, S., and Calzaferri, G. (2004). Energy transfer from dye-zeolite L antenna crystals to bulk silicon. **Chem Phys Chem**. 5: 239-242.

Insuwan, W. and Rangsriwatananon, K. (2012). Morphology-controlled synthesis of zeolite and physicochemical properties. **Engineering Journal**. 16(3): 1-12.

Ito, O., Ito, E., Yoshikawa, Y., Watanabe, A., and Kokubun, H. (1996). Preferential solvation studied by the fluorescence lifetime of acridine in water–alcohol mixtures. **J. Chem. Soc., Faraday Trans**. 92: 227-230.

Kaewsuya, P., Miller, J. D., Danielson, N. D., Sanjeevi, J., and James, P. F. (2008). Comparison of N-alkyl acridine orange dyes as fluorescence probes for the determination of cardiolipin. **Anal. Chim. Acta**. 626: 111-118.

Kazima, S., Zulfequar, M., Mazharul Haq, M., Bhatnagar, P. K., and Husain, M. (2007). Electrical and optical properties of thin films based on poly [2-methoxy-5(20-ethyl hexyloxy)-1,4-phenylene vinylene] doped with acridine orange dye with possible photovoltaic applications. **Sol. Energ. Mat. Sol. C**. 9: 1462-1466.

Koeppe, R., Bossart, O., Calzaferri, G., and Sariciftci, N. S. (2007). Advanced photon-harvesting concepts for low- energy gap organic solar cells. **Sol. Energy Mater. Sol. C**. 91: 986-995.

Kumar, K. S., Selvaraju, C., Malar, E. J. P., and Natarajan, P. (2012). Existence of a new emitting singlet state of proflavine: Femtosecond dynamics of the excited state processes and quantum chemical studies in different solvents. **J. Phys. Chem. A**. 116: 37-45.

Maas, H., and Calzaferri, G. (2003). Constructing dye-zeolite photonic nanodevices. **The spectrum**. 16(3): 18-24.

Maeda, M. (1984). Laser Dyes. Academic Press, New York. pp. 161-167.

Matsuoka, Y., and Yamaoka, K. (1979). Film Dichroism. II. Linearly-polarized absorption spectra of acridine dye in the stretched poly(vinyl alcohol) film). **Bull. Chem. Soc. Jpn**. 52(11): 3163-3170.

Meeprasert, J., Jungsuttiwong, S., and Namuangruk, S. (2013). Location and acidity of BrØnsted acid sites in isomorphously substituted LTL zeolite: a periodic density functional study. **Micropor. Mesopor. Mater**. 175(15): 99-106.

Megelski, S., and Calzaferri, G. (2001). Tuning the size and shape of zeolite L-based inorganic-organic host-guest composites for optical antenna systems. **Adv. Funct. Mater**. 11: 277-286.

Misra, V., Mishra, H., Joshi, H. C., and Pant, T. C. (2000). Excitation energy transfer between acriflavine and rhodamine 6G as a pH sensor. **Sensor Actuat B**: **Chem**. 63: 18-23.

Misra, V., Mishra, H., Joshi, H. C., and Pant, T. C. (2001). An optical pH sensor based on excitation energy transfer in Nafion® flim. **Sensor Actuat B: Chem**. 82: 133-141.

Negrón-Encarnación, I., Arce, R., and Jiménez, M. (2005). Characterization of acridine species adsorbed on $(NH_4)_2SO_4$, SiO_2, Al_2O_3, and MgO by steady-state and time-resolved fluorescence and diffuse reflectance techniques. **J. Phys. Chem. A**. 109: 787-797.

Pileni, M., and Grätzel, M. (1980). Light-induced redox reactions of proflavine in

aqueous and micellar solution. **J. Phys. Chem**. 84: 2402-2406.

Park, Y. S., Lee, K., Lee, C., Yoon, K. B. (2000). Facile Reduction of zeolite-encapsulated viologens with solvated electrons and selective dispersion of inter- and intramolecular dimers of propylene-bridged bisviologen radical cation. **Langmuir**. 16(10): 4470-4477.

Ryan, E. T., Xiang, T., Johnston, K. P. and Fox, M. A. (1997). Absorption and fluorescence studies of acridine in subcritical and supercritical water. **J. Phys. Chem. A**. 101: 1827-1835.

Samsonova, L. G., Selivanov, N. I., Kopylova, T. N., Artyukhov, V. Ya., Maier, G. V., Plotnikov, V. G., Sazhnikov, V. A., Khlebunov, A. A., and Alfimov, M. V. (2009). Experimental and theoretical investigation of the spectral and luminescent properties of some acridine compounds. **Khimiya Vysokikh Energii (Khim. Vys. Energ)**. 43(2): 149-159.

Tomasz, P., Bronislaw, M., and Gordon, L. H. (2002). Quenching of the excited singlet state of acridine and 10-methylacridinium cation by thio-organic compounds in aqueous solution. **J. Photochem. Photobiol. A: Chem**. 150: 21-30.

Veiga-Gutierrez, M., Woerdemann, M., Prasetyanto, E., Denz, C., and De Cola, L. (2012). Optical-tweezers assembly-line for the construction of complex functional zeolite L structures. **Adv. Mater**. 24: 5199-5204.

Yamaoka, K., and Shimadzu, M. (1983). Film Dichroism VI. Linearly- polarized absorption spectra of neutral and divalent 3,6-diainoacridine dyes in the stretched poly(vinyl alcohol) film. **Bull. Chem. Soc. Jpn**. 56: 55-59.

CHAPTER IV

PHOTOPHYSICAL PROPERTIES OF *t*-AZOBENZENE CONFINED IN ZEOLITE LTL: EXPERIMENTAL AND THEORETICAL STUDIES

Abstract

The spectroscopic methods and molecular modeling were employed to study the photophysical properties of *t*-azobenzene in solution and in the channel of zeolite LTL. The effects of the interactions between the dye molecules and zeolite framework on the electronic states are examined experimentally by the diffuse reflectance UV−visible absorption and fluorescence emission. The changes observed in the spectra are found to depend on the forms of zeolite LTL (K-LTL and H-LTL). The structural properties of the dye in the different environments were deeply investigated by density functional theory (DFT) calculations with B3LYP/6-31G(d,p) level of theory. The experimental data are consistent with the calculations results. The dye in solution can be relaxed into the planar structure, while in LTL zeotite is constrained by the framework and is therefore twisted due to the confinement effects in zeolite. Moreover, the emission spectra were detected only from protonated *t*-azobenzene incorporated into H-LTL while no emission was detected from *t*-azobenzene confined in K-LTL framework.

4.1 Introduction

Zeolite crystals provide well-defined internal structure and controllable voids and photochemical studies is a growing interest in the field of material chemistry. Especially, zeolite LTL served as a host for modifying the photophysics and photochemistry of a guest species (Calzaferri et al., 2006). Controlling chemistry in the zeolite cavities may lead to electronic and optical materials. Gfeller and co-worker incorporated chromophores within zeolite LTL channels which a good example to study exhibit energy transfer process (Gfeller, Megelski, and Calzaferri, 1999). Because of these attractive properties, zeolite LTL has been utilized as a medium for photophysical and photochemical studies of various chromophores (Calzaferri et al., 2002; Devaux, Minkowski, and Calzaferri, 2004; Vohra et al., 2009; Megelski and Calzaferri, 2001; Calzaferri and Devaux, 2010). Cationic dyes, thionine (TH^+) (Calzaferri and Gfeller, 1992), pyronine (Gfeller, Megelski, and Calzaferri 1999); Calzaferri et al., 2006) and oxonine (Maas and Calzaferri, 2003), can be incorporated in the monomer form even at high loading. The association of the methyl viologen radical cation ($MV^{\bullet+}$) was also investigated by Park et al., 2000. However, there are a few studies and a less of information on the photophysical properties of *t*- azobenzene incorprated within zeolite LTL.

Azobenzene, sometimes referred to as diazobenzenes in which two phenyl rings separated by an azo bond (N=N), serves as the parent molecule for a broad class of aromatic azo compound. Moreover, it is versatile molecule and it is very interesting in research areas for various applications such as dyes and pigments (El Halabieh, Mermut, and Barrett, 2004). Besides its applicability as pigment, Hartley studied its photochemical *trans* and *cis* isomerization. There are two mechanisms of

photoisomerization process which depends on the excitation wavelength. In n-π*(S$_1$) excitation the isomerization proceeds with the in-plane inversion at one N atom while under π-π* (S$_2$) excitation it takes place by rotation around the N=N double bond (Rao, 1990; Zimmermann, Chow, and Park, 1958). Moreover, many studies dealing with photochemistry of *t*-azobenzene on a large pore zeolite Y or zeolite β with strong BrØnsted acidity were found that the photolysis of *t*-azobenzene led to the cyclization forming benzo[c]cinnoline and benzidine. However, the cyclization was not observed in a narrow pore ZSM-5 zeolite, even in the presence of acidic functionality because of the tight fit of the molecule in the channels prohibiting isomerization of azobenzene (Hoffman, Marlow, and Caro, 1997).

Generally, azobenzene does not exhibit fluorescence in a solution at room temperature, because the nature n-π* (S1) state of *t*-azobenzene is forbidden transition. However, a few exceptions were reported in some literatures. Bo and Zha, (2007) could not observed fluorescence from an azobenzene-containing diblock copolymer dissolved in DMF solution, excepted additional of water which confines azobenzene groups that can be observed fluorescence due to the micellization of the polymer in solution. Tung and Guan, (1996) studied photophysical behavior of azobenzene incorporated into solvent-swollen Nafion, in water-swollen Nafion-H$^+$, azobenzene molecules are located in the fluorocarbon/water interface and as protonated form leading to strong fluorescence. But no fluorescence was detected in methanol-swollen Nafion because azobenzene molecules are solubilized into methanol pool and cannot be protonated. From the literatures the behaviors of *t*-azobenzene are very sensitive to environment of the mediums. Therefore, in this research we determined the zeolite LTL framework affecting the arrangement and the

photophysical properties of *t*-azobenzene by the experimental and the theoretical studies.

4.2 Materials and method

4.2.1 Experimental Details

Synthesis of zeolite LTL

All materials used in this study were of reagent grade. The typical procedure for the preparation of synthesis gel of K-LTL and H-LTL zeolite were modified according to a Chapter II in page 41.

Dyes-loaded on zeolite LTL (gas phase method)

A weighed amount 0.1 g of zeolite sample was introduced to an ampoule. The sample was dehydrated in vacuum oven at 200 °C for 1 day and it was then cooled to room temperature in a desciscator. The amounts of azobenzene corresponding to occupation probability (p = 0.01, 0.05, 0.1, 0.25, 0.50 and 0.75) were introduced into the ampoule, then the powder mixture was added with 1 mL of chloroform and then ampoule was sonicated for 15 minutes to provide a homogeneous dispersion of the dye molecules and zeolite LTL crystals. After evaporation of chloroform, the ampoule was sealed. All dyes-zeolite samples were heated at the insertion temperature (melting point of *t*-azobenzene; 69 °C) for 24 hours. After cooling, the sealed ampoule was broken and the dye-zeolite LTL was obtained. After the insertion step, it was followed by the washing procedure of dye-loaded zeolite crystals to eliminate dye molecules adsorbed on the outer surface of the crystals by adding 10 mL of n-butanol to the sample, sonicated for 5 minutes and centrifuged.

The procedure was repeated until the absorption of the dye in the solvent was negligible. At that point the remaining dye is assumed to be located inside the channels of zeolite LTL. Finally, the sample was then dried at 80 °C for 12 hours.

The loading, or occupation probability (ρ) of a *t*-azobenzene loaded on zeolite LTL is defined as follows (Hennessy et al., 1999);

$$\rho = \frac{\text{number of occupied sites}}{\text{total amount of sites}} \tag{1}$$

From (Eq. 1) one gets the following expression to calculate the loading or occupation probability (Calzaferri and Devaux, 2010);

$$\rho = \frac{m_D}{M_D}(\frac{M_Z n_s}{m_z}) \tag{2}$$

Where M_D is the molar mass of *t*-azobenzene (182.22 g/mol), M_z is the molar mass of zeolite LTL per one unit cell (2883 g/mol), m_D and m_z are weight of dye and zeolite LTL in grams, respectively, n_s represents the number of unit cells occupied by one *t*-azobenzene molecule that determined by the length of the dye molecule (*t*-azobenzene; 1).

Physical Measurements

UV/vis spectra were recorded on a Varian cary 1E UV/vis Spectrophotometer. The dye molecules were dissolved in various solvents and quartz cuvette was used. Diffuse reflectance spectra of the dyes loaded on zeolite LTL was recorded using a Shimadzu UV-2550 UV-Visible spectrometer with the condition of slid width (5 nm), sampling interval (0.1 nm) and wavelength range 200-800 nm. Fluorescence spectra were recorded on a Luminescence Spectrometer LS 50B (Perkin-Elmer). Dye molecules were measured either in various solvents in quartz

cuvette, or incorporated into zeolite LTL by suspending dyes/zeolite LTL in chloroform (~1 mg in 100 mL).

4.2.2 Computational Details

Model and method for theoretical study are also explained in Chapter III, pp. 64-65.

4.3 Results and discussion

4.3.1 Ground state geometry optimization

The structure and properties of H-LTL and K-LTL

This work the acidic cluster (H-LTL) and potassium (K-LTL) are also explained in the Chapter III, p. 62.

The structure and properties of bare *t*-azobenzene and confined in zeolite channels

The structure of *t*-azobenzene has been a subject of argument for several years. The X-ray diffraction (XRD) result suggests a planar structure (Bouwstra, Schouten, and Kroon, 1983). On the other hand, gas-phase electron diffraction (ED) (Traetteberg, Hilmo, and Hagen, 1977) studies suggest a nonplanar structure. ED results showed that the phenyl ring is twisted by 30° (C_i symmetry) around the C-N=N-C plane. This distorted structure is also found to be present in solution and has been supported by the Raman measurements on *t*-azobenzene (Kellerer, Hacker, and Brandmuller, 1971).

Table 4.1 Selected structural parameters of *t*-azobenzene confined in solvent and zeolite LTL.

	Distance (Å)					Dihedral angle
	C-N	**N=N**	**N-H**	**N-K**	**N-H(m)**	**(C-N=N-C)**
t-azobenzene (g)	1.419	1.261	-	-	-	180
t-azobenzene-H$^+$ (g)	1.409	1.268	1.026	-	-	180
t-azobenzene-1CH$_3$OH	1.422	1.26	-	-	1.959	174
t-azobenzene-2CH$_3$OH	1.422	1.261	-	-	1.924	160
t-azobenzene-K$^+$ (g)	1.413	1.264	-	2.880,3.304	-	140
t-azobenzene-H-LTL	1.411	1.263	1.086			158
t-azobenzene-K-LTL	1.419	1.261	-	6.755,7.672	-	164

The optimized parameters, *i.e.* the bond lengths and bond angles, of *t*-azobenzene are computed by DFT: BTLYP/6-31G(d,p). The bond length of N=N bond of bare *t*-azobenzene has come out to be 1.261 Å and 1.268 Å for protonated *t*-azobenzene (*t*-azobenzene - H$^+$) and others in range 1.261-1264 Å under B3LYP method. These are in good agreement with that obtained from the crystal structure, 1.268 Å (Park, Lee, Lee, and Yoon, 2005). Moreover, the structure of *t*-azobenzene observed to be planar. For protonated *t*-azobenzene (*t*-azobenzene - H$^+$) is also planar where the proton is attracted to azo nitrogen that shown the dihedral angle (C-N=N-C) are about 180° (see Table 4.1 and Figure 4.1a and 4.1c). In case of *t*-azobenzene-K$^+$, the distance between azo group and K$^+$ ion are 2.880 Å and 3.304 Å (Figure 4.1d). Because of the larger atom size of K$^+$ ion and stronger interaction between K$^+$ ion with azo groups and benzene ring of dye resulting in the twist of C-N=N-C bond angle (140°) than methanol that O atom of methanol molecule interacted with *t*-azobenzene (C-N=N-C bond angle is 174°) (Figure 4.1b). In addition, increasing the

number of methanol of 2 molecules, the interaction was stronger than the former that illustrated in Table 4.1.
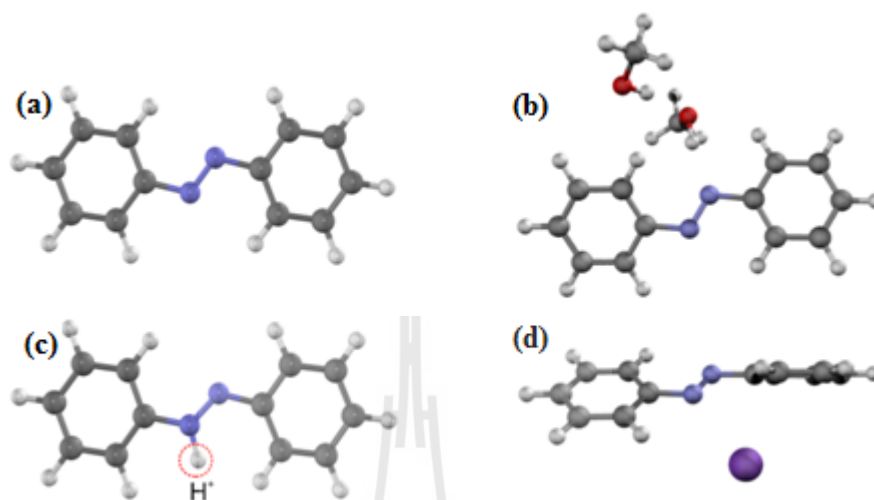
Figure 4.1 Optimized structure of *t*-azobenzene (a), *t*-azobenzene-2CH$_3$OH (b), *t*-azobenzene-H$^+$ (c), and *t*-azobenzene-K$^+$ (d).

In dye-zeolite system, *t*-azobenzene can be absorbed in H-LTL and was protonated by BrØnsted acid site of zeolite according to the calculated the H$_z$-O$_z$ distances of bare H-LTL and *t*-azobenzene adsorbed on H-LTL extend to 0.967 from 1.533 Å (Figure 4.2a). It is confirmed that the *t*-azobenzene was protonated in H-LTL and the zeolite framework induced the twist the C-N=N-C bond angle (158°) of azobenzene molecule. For *t*-azobenzene adsorbed on K-LTL, the distances between K$^+$ and N=N bond are 6.775 and 7.672 Å. Figure 4.2b illustrated that *t*-azobenzene in K-LTL only interacted directly with framework resulting in the twist of the C-N=N-C bond angle (164°) less than that *t*-azobenzene adsorbed on H-LTL. From above mention the *t*-azobenzene in zeolite LTL is constrained by the framework and is therefore twisted while in bare *t*-azobenzene and protonated form are planar. The

twisting angle of *t*-azobenzene confined in zeolite LTL has affect on the unusual

photophysical properties dye molecule which will be discussed in the next section.
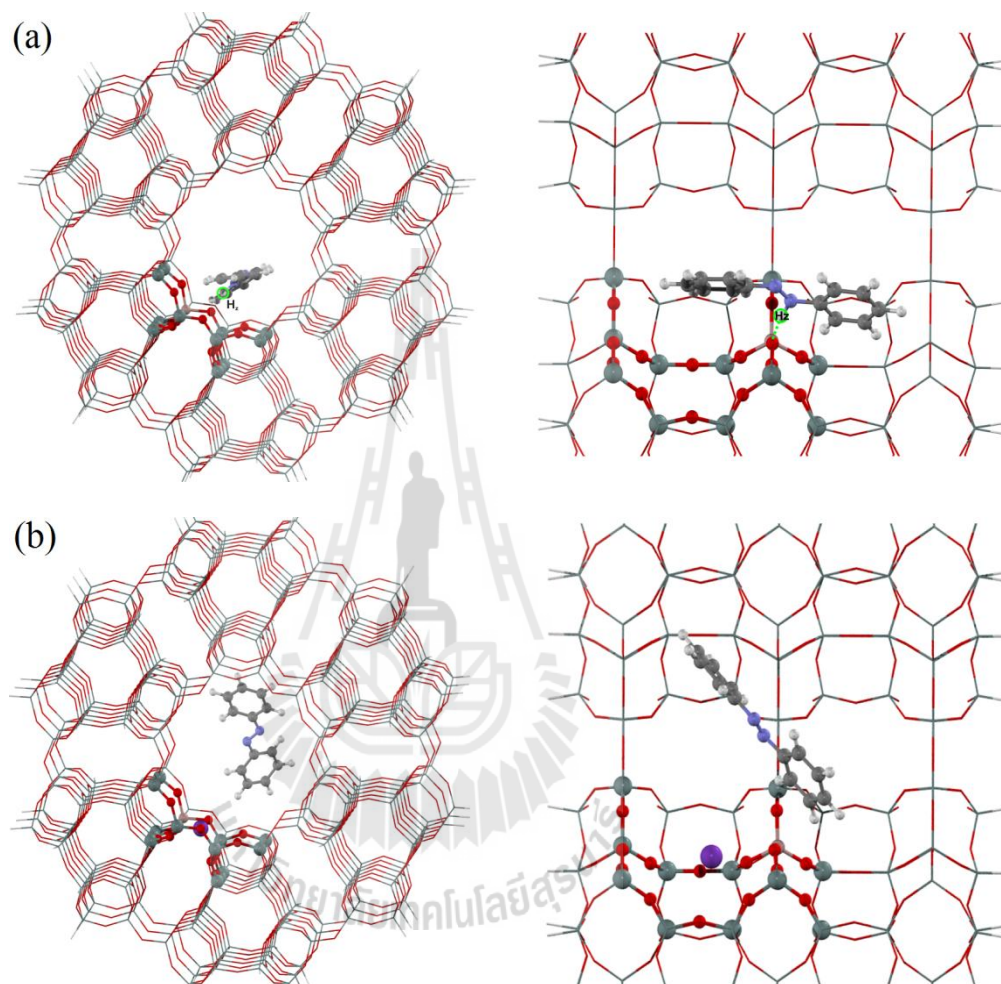
Figure 4.2 Optimized structure of *t*-azobenzene in H-LTL (a) and K-LTL (b).

4.3.2 UV-Vis absorption spectra: experimental and theoretical studies

t-azobenzene in solution

The experimental absorption spectrum of *t*-azobenzene dissolved in methanol was showed in Figure 4.3a. The band corresponding to the very intense π-π* transition and was appeared at 320 nm. The much weaker band at 445 nm is n-π* transition which is not allowed by the symmetry rules, however, this small peak can be described as the interaction between methanol and *t*-azobenzene, which is the isomerization of trans-form to the cis-form can be occurred. When a solution of *t*-azobenzene in methanol was exposed to UV light, the cis isomer was form. We found that the intensity of n-π* transition band at 430 nm is increased while π-π* transition shifted to shorter wavelength at 280-300 nm and decreasing significantly in intensity when compare to *t*-azobenzene. The difference between the two isomers is due to the non-planar configuration of the cis isomer in solution (Robin and Simpson, 1962). In trans-form the two benzene rings are pointing away from each other, spanning an angle of about 180°. The trans-isomer can be photoisomerize to the cis-isomer with ultraviolet light (360 nm). During this process the geometry of the molecule is changed which is two benzene rings moieties approach each other and span an angle of around 64°. This situation lead to decrease in length into 5.5 Å (see Figure 4.4).
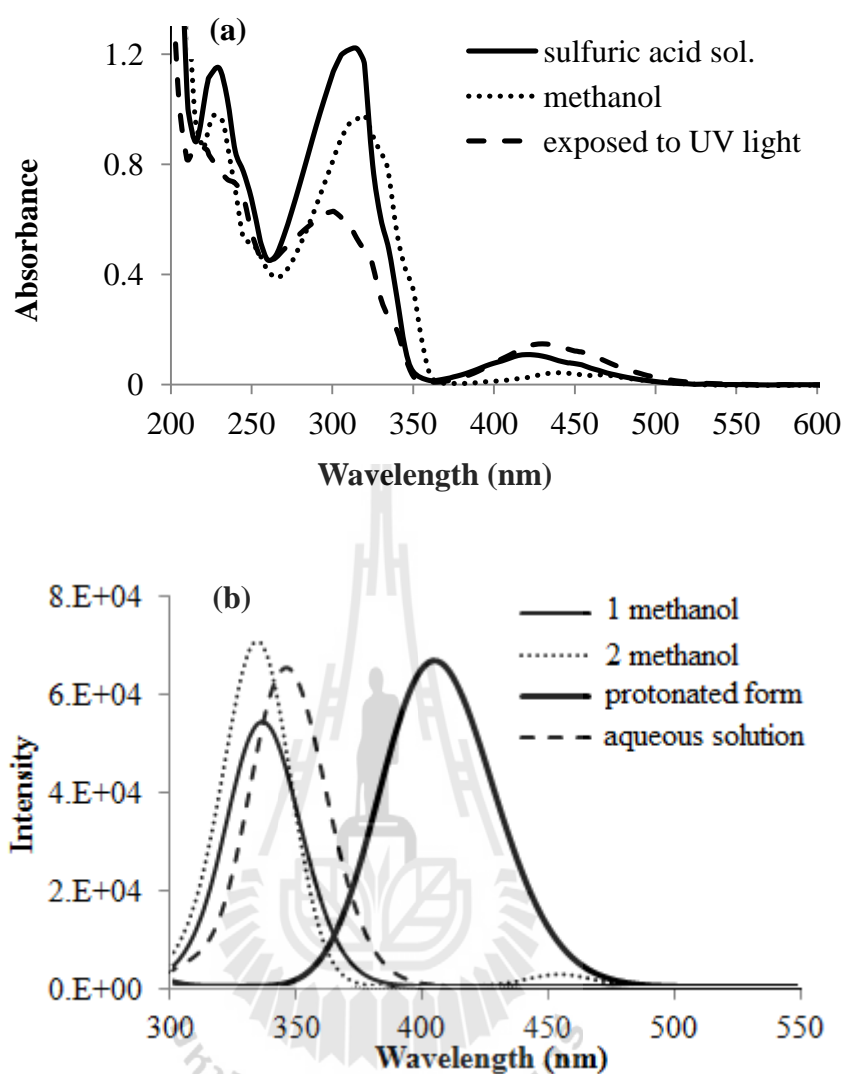
Figure 4.3 (a) Experimental absorption spectra and (b) computational of *t*-azobenzene in different conditions.
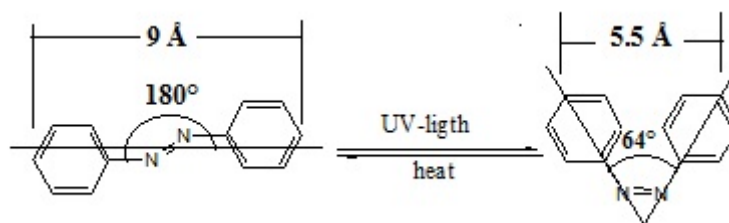
Figure 4.4 Reversible isomerization of azobenzene.

In sulfuric acid solution two absorption bands at 323 nm and 420 nm were observed. This result indicated that nitrogen atom of *t*-azobenzene was protonated in strong acid media, leaded to the shift in absorption band around at 445 nm to 420 nm. This result was in agreement with the report of Goncharuk, and co-workers (Goncharuk, Grebenyuk, Savranskii, Gorchev, and Chernega, 1981).

$$\text{HOMO-2 to LUMO } (n\text{-}\pi^*) \qquad\qquad \text{HOMO to LUMO } (\pi\text{-}\pi^*)$$
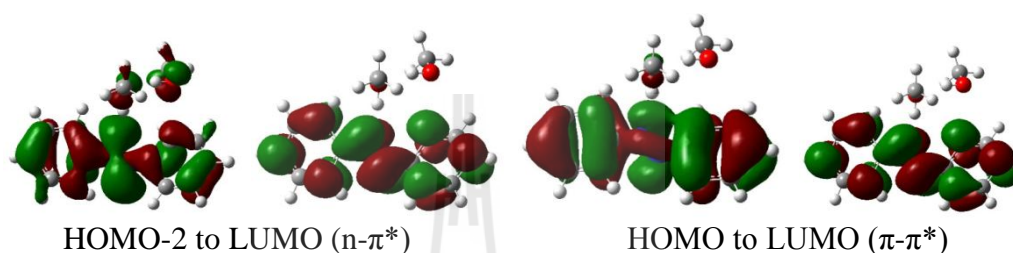
Figure 4.5 Frontier molecular orbital of *t*-azobenzene interacted with 2 molecules of CH$_3$OH calculated by TD-B3LYP 6-31 G(d,p).

We also confirmed the position and transition of the absorption peak by using TD-B3LYP 6-31 G(d,p). The absorption spectra of *t*-azobenzene in explicit solvent (CH$_3$OH) shows the first excitation states that corresponding to the electronic transition from HOMO-2 to LUMO combine with HOMO to LUMO that is corresponded to n-π* (see Figure 4.3b and Table 4.2). A weakly allowed peak with oscillation strength 0.0011 and 0.0224 appeared at 466 nm was assigned to be the interaction of one methanol with *t*-azobenzene, while in presence of 2 methanols, this peak was blue shifted to 455 nm with increasing of intensity This result was described by the strong interaction of *t*-azobenzene with solvent molecule which is in agreement with the experimental absorption spectrum of *t*-azobenzene in methanol that appeared the n-π* transition around 445 nm.

t-azobenzene in KLTL zeolite

Figure 4.6a and 4.6b show the diffuse reflectance spectra that shown in Kubelka-Munk unit of *t*-azobenzene adsorbed on round shape and ice hockey shape of K-LTL, respectively. It is clear that the spectrum shape of the incorporate *t*-azobenzene in zeolite K-LTL in both shapes with occupation probability (p; 0.05, 0.10, 0.25, 0.50, and 0.75) is similar to that in the solutions. However, there is a slight influence on the shift of the electronic spectra. The red shift for the 320 nm to 325 nm for *t*-azobenzene confined in K-LTL, is primarily π-π* transition in nature. In addition, the transition of n-π* in nature was observed at 455 nm which is in solution was appeared at 445 nm.

In the calculation by TD-DFT was used to predict the spectral properties of *t*-azobenzene confined in K-LTL. The maximum absorbance wavelengths calculated by TD-DFT were compared against experimental values (see Figure 4.6c). A reasonably good correlation was obtained between the theoretical and experimental values. From the calculation the first excited state of *t*- azobenzene in K-LTL is weakly allowed peak at 480 nm (the experimental values 455 nm) corresponded to the n-π* mixed with π-π* transition which transition from highest occupied molecular orbital (HOMO) to the lowest unoccupied molecular orbital (LUMO) combined with HOMO-1 to the LUMO (see Figure 4.7 and Table 4.2). Moreover, the slightly charge transfer from zeolite framework to dye mixed wth π-π* transition is also observed at 309 nm (experimental values 325 nm) corresponding to the transition from HOMO-3 to the LUMO, shown in Figure 4.7. This implies the weak interaction between dye and K-LTL due to charge transfer process.
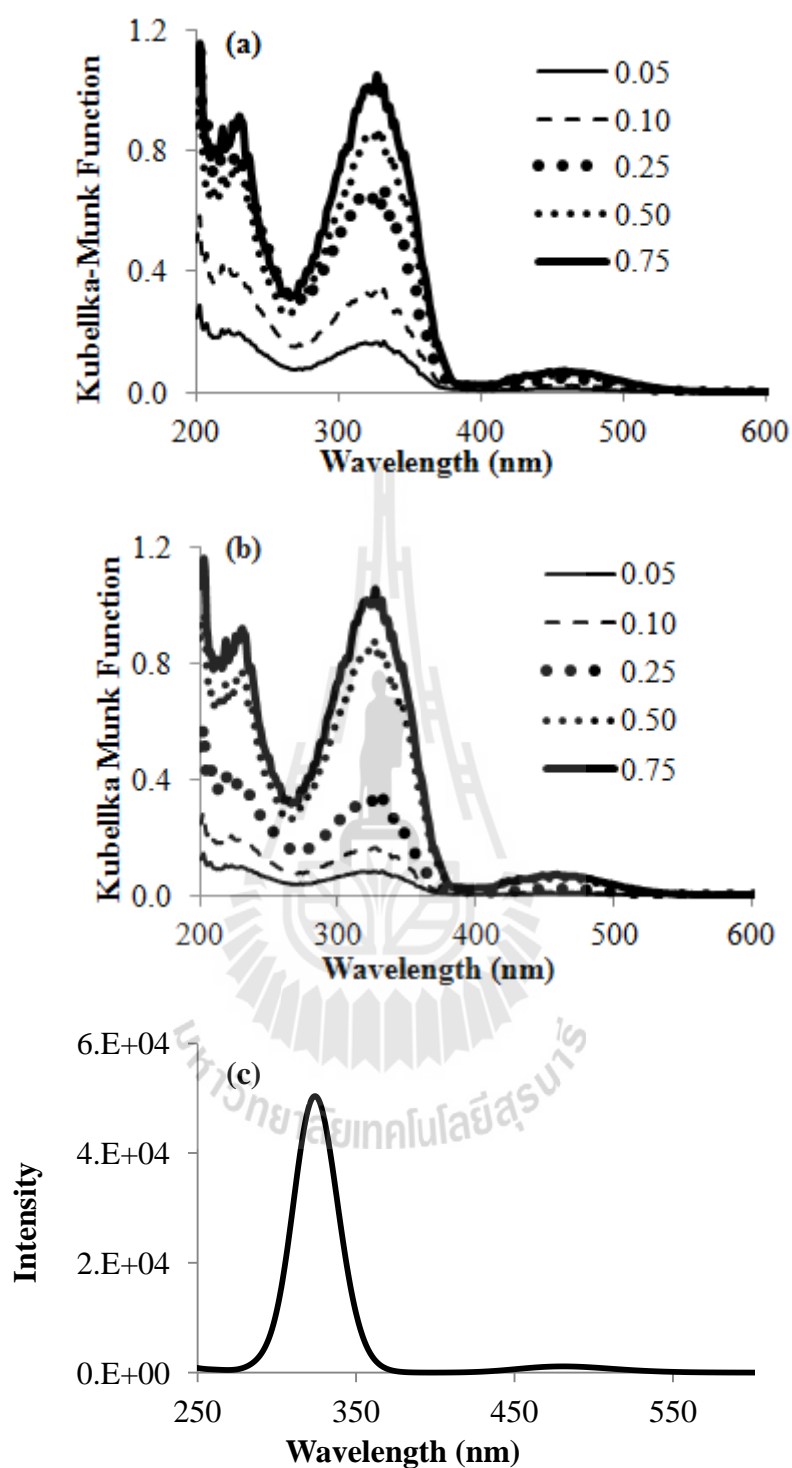
Figure 4.6 (a) Diffuse reflectance spectra of *t*-azobenzene loaded on round shape and

(b) ice hockey shape of K-LTL with occupation probability (ρ; 0.05, 0.10, 0.25, 0.50,

and 0.75) and (c) computational absorption spectra of *t*-azobenzene in K-LTL.

LUMO

HOMO (n; red)   HOMO-1(n; green)   HOMO-3
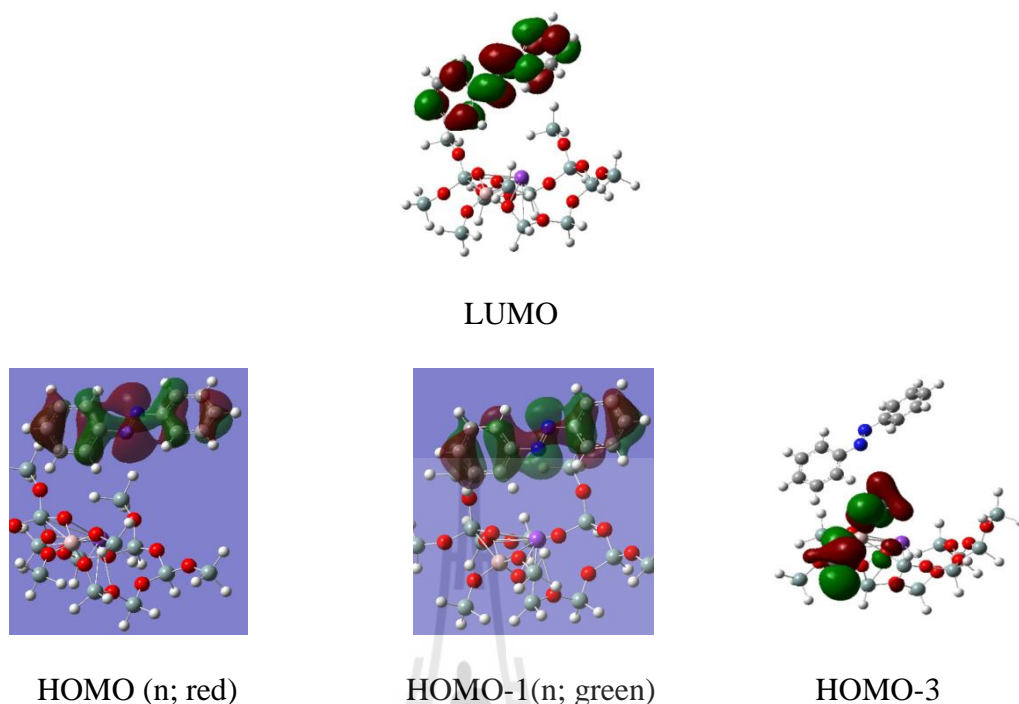
Figure 4.7 Frontier molecular orbital of *t*-azobenzene in K-LTL calculated by TD-B3LYP 6-31G(d,p).

t-azobenzene in H-LTL zeolite

Figure 4.8a and 4.8b show the diffuse reflectance spectra of *t*-azobenzene confined in round and ice hockey shape of H-LTL, respectively. The diffuse reflectance spectra of *t*-azobenzene in both shape of zeolite LTL and with occupation probability (p; 0.05, 0.10, 0.25, 0.50, and 0.75) are not significantly different. The red shift for the 320 nm to 330 nm for *t*-azobenzene confined in H-LTL, is the π-π* transition in nature. Moreover, the band at 425 nm was observed that described by the protonation of the azo groups with OH-brØnsted acid sites of H-LTL resulting in π-π* transition, which is consistent with the previously reported (Rao, 1990; Simomura and Kunitake, 1987). A similar finding was reported by Lei and co-worker, 1998). The

possible interactions between *t*-azobenzene with the framework acidic groups of AlPO$_4$-5 involve donation of the nitrogen lone pairs to the Lewis acid sites.

In addition, the computational calculation was also investigated the *t*-azobenzene confined in H-LTL (Figure 4.8c). This is predicted by computational approaches but the transition of n-π* state was not observed due to the lone pair electron of nitrogen forming bond with BrØnsted acid site of zeolite. The calculated absorption spectrum is in reasonable agreement with experimental observation. The first calculated absorption band at 571 nm (the experimental value 425 nm) is appeared, even though weakly allowed peak and very low oscillator strength. This band was assigned to be the charge transfer from zeolite framework to the dye. The calculated absorption band around 399 nm was combination of excited state at 5th, 6th and 7th which corresponded to the transition of π-π* (399 nm) involving an electronic transition from the HOMO to the LUMO (see Figure 4.9 and Table 4.2) together with the charge transfer from zeolite to dye (354 nm). This confirms that *t*-azobenzene in H-LTL was protonated.
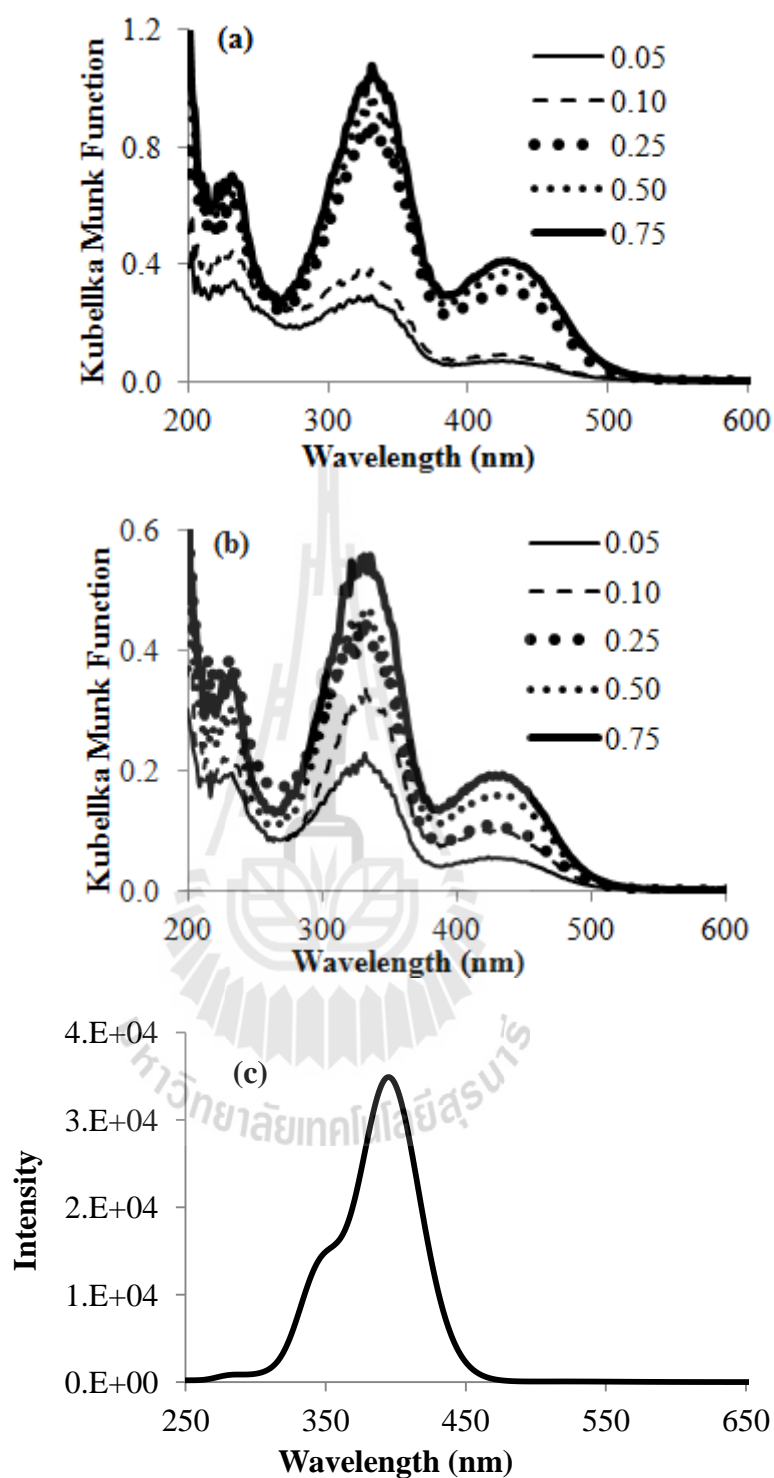
Figure 4.8 (a) Diffuse reflectance spectra of *t*-azobenzene loaded on round shape and

(b) ice hockey shape of H-LTL with occupation probability (ρ; 0.05, 0.10, 0.25, 0.50,

and 0.75) and (c) computational absorption spectra of *t*-azobenzene in H-LTL.

LUMO   HOMO   HOMO-3

HOMO-5   HOMO-8   HOMO-9
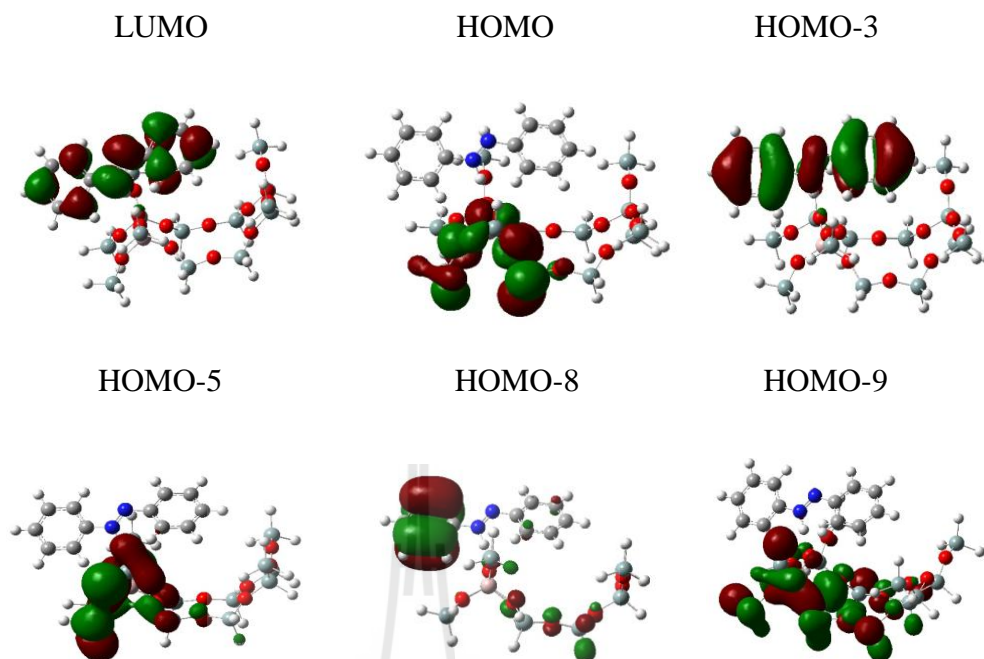
Figure 4.9 Frontier molecular orbital of *t*-azobenzene in H-LTL calculated by TD-B3LYP 6-31G(d,p).

From above mention we found that form of zeolite LTL (K-LTL and H-LTL zeolite) has influenced the photophysical property of *t*-azobenzene regardless of occupation probability of the dye and morphology of zeolite LTL. This situation is due to the channel diameter is 7.1 Å, it does not allow accommodate the dimer as well as aggregate of the dye molecule. Therefore, unusual photophysical property of the dye cannot be found.

Table 4.2 Summary the photophysical properties of *t*-azobenzene (*t*-AB) in the solvents and in H-LTL and K-KLTL.

Structure	λ(nm) (cal.)	Oscillator strength (*f*)	λ(nm) (Ex.)	Assignment
	-	0.0000	-	HOMO to LUMO
t-AB (g)	329	0.7716	-	HOMO-1 to LUMO (88%)
	466	0.0011	320	HOMO-1 to LUMO (80%)
t- AB -1CH₃OH	337	0.7194	445	HOMO to LUMO (69%)
	455	0.0224	-	HOMO-2 to LUMO (47%)
				HOMO to LUMO (37%)
t- AB -2CH₃OH	355	0.6124	-	HOMO to LUMO (41%)
				HOMO-2 to LUMO (37%)
	445	0.0421	420	HOMO-1 to LUMO (84%)
	408	0.6679	323	HOMO to LUMO (54%)
t- AB -H⁺				HOMO-2 to LUMO (12%)
	397	0.1447	-	HOMO-2 to LUMO (77%)
	439	0.0422	-	HOMO-2 to LUMO (36%)
				HOMO to LUMO (29%)
t- AB -K⁺	349	0.1412	-	HOMO-1 to LUMO+0 (66%)
				HOMO to LUMO (19%)
	480	0.0156	455	HOMO to LUMO (62%)
				HOMO-1to LUMO (25%)
t- AB -K-LTL	325	0.6613	325	HOMO-1 to LUMO (59%)
				HOMO to LUMO (20%)
	571	0.0001	425	HOMO to LUMO (99%)
	399	0.2049	330	HOMO-5 to LUMO (47%)
t- AB -H-LTL				HOMO-3 to LUMO (31%)
	354	0.0573	-	HOMO-9 to LUMO (42%)
				HOMO-8 to LUMO (24%)

(* more detail are shown in Appendix A: Table A.5 and A.6)

4.3.3 Emission Spectra of *t*-azobenzene in zeolite LTL

The emission spectra of *t*-azobenzene at ambient temperature were detected as shown in Figure 4.10a and 4.10b. Both of ice hockey and round shapes of zeolite LTL and occupation probability of *t*-azobenzene does not affect the feature of emission spectrum of *t*-azobenzene. The maxima intensity of the emission spectra at 380 nm was assigned to be protonated form of *t*-azobenzene that direct emission from S_2 to S_0 state (π-π*) (Fujino, Arzhansev, and Tahara 2001). The occurrence of this emission is possible only when lone pair electron of *t*-azobenzene is bonded. Consequently, the radiation transition to the ground state is orbital overlap allowed. In contrast to neutral *t*-azobenzene that the n-π* excited singlet state (S_1) is well known to be symmetry forbidden with a poor orbital overlap. Therefore, the emission from S_1 to S_0 state (n-π*) could not be detected. Azobenzene itself is not fluorescence (Tung and Guan, 1996) with the reason that the first singlet excited state of n-π* character of the compound not only the excited state lifetime is longer but the rate of intersystem crossing is faster. The faster rate of intersystem crossing is based on the fact that the singlet-triplet energy gap of the excited state of n-π* is smaller than that of π-π*. Additionally, the faster rate of intersystem crossing enhances spin-orbit coupling between singlet and triplet excited state. What we observed that *t*-azobenzene in K-LTL having no emission spectra is based on the lone pair electron of azo groups does not form coordinate bond with K-LTL framework. The fluorescent occurrence of *t*-azobenzene in H-LTL was found in agreement with *t*-azobenzene in AlPO4-5 crystals in which the complexation can be formed by the lone pair electrons and space confinement (Fujino, Arzhansev, and Tahara 2001).
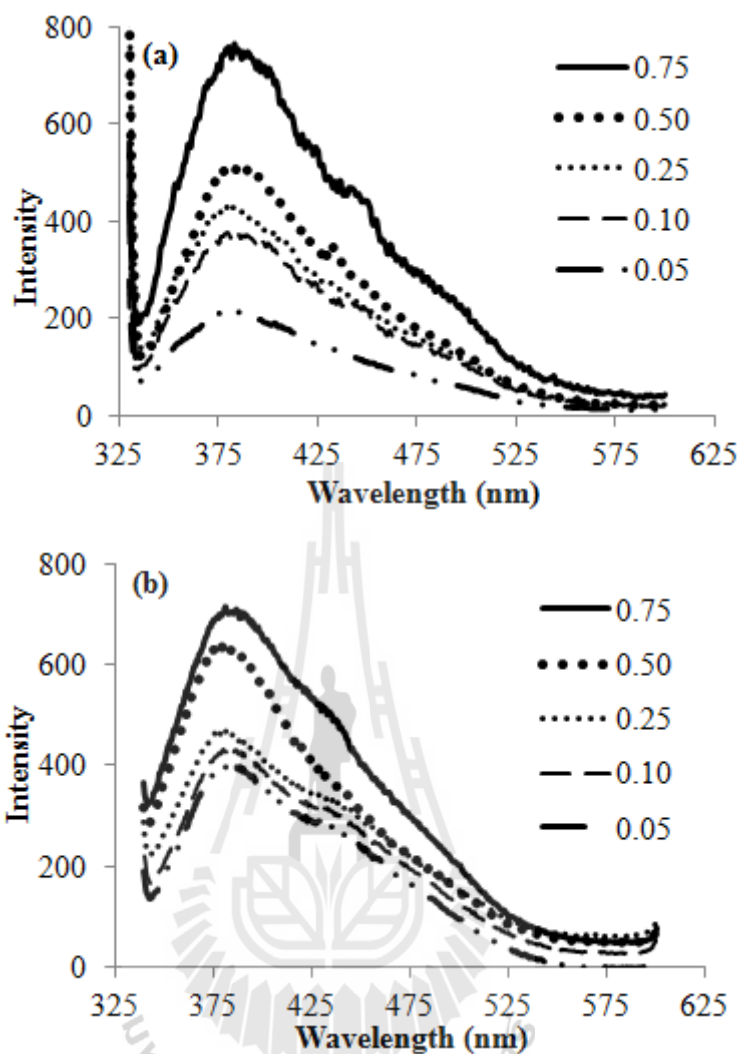
Figure 4.10 (a) Emission spectra of *t*-azobenzene loaded on round shape and (b) ice hockey shape of H-LTL with occupation probability (p; 0.05, 0.10, 0.25, 0.50 and 0.75), the samples were excited at 320 nm.

4.4 Conclusions

The photophysical properties of the *t*-azobenzene dye in solution and confined in the channel of round and ice hockey shape of zeolite LTL (K-LTL and H-LTL) were studied by experimental and theoretical methods. The experimental maximum absorption wavelength (λ_{max}) is at 320 (π-π*) and 445 nm (n-π*) for the dye in neutral

form (in organic solvent) and λ_{max} is at 323 (π-π*) and 420 nm for the dye in protonated form (in sulfuric solution). The n-π* and π-π* transitions of the neutral dye in the solutions were shifted from 445 to 455 nm and 320 to 325 nm for the dye in K-LTL, respectively and the similar trend was observed with the protonated dye in the solution shifted from 420 to 425 nm and 323 to 330 nm for the dye in H-LTL. The both forms of the dye showed the red shift of n-π* and π-π*. The red shift of the both transitions occurred when the dye was encapsulated into zeolite LTL indicating that the planarity of the dye was perturbed due to the confinement effect of the zeolite channels. Consistency to the structural properties of the dye was obtained from the calculation method. The both forms of the dye molecule in the solution can fully relax into the planar structure, while they are constrained by the framework of zeolite LTL and resulting in twisting. The emission spectrum (380 nm) was detected only from protonated *t*-azobenzene incorporated into H-LTL. It indicates that the requirements of a host for *t*-azobenzene which capable to emit fluorescence are both the existence of BrØnsted acid sites or Lewis acid sites and a rigidity of a medium like zeolitic framework. TD-B3LYP/6-31G(d,p) was employed to predict the λ_{max} of *t*-azobenzene in K-LTL and H-LTL. The calculated λ_{max} of the dye in K-LTL is 325 nm (π-π*) and 480 nm (n-π*), while in H-LTL the overlapping bands of 355 and 399 nm are assigned to be the π-π* mixed with charge transfer of the dye to the zeolite.

4.5 References

Bouwstra, J. A., Schouten, A., and Kroon, J. (1983). Structural studies of the symtem trans-azobenzene/trans-stilbene. **Acta Cryst. C**. 39: 1121-1123.

Bo, Q., and Zhao, Y. (2007). Fluorescence from an azobenzene - containing diblock copolymer micelle in solution. **Langmuir**. 23: 5746-5751.

Calzaferri, G. and Gfeller, N. (1992). Thionine in the cage of zeolite L. **J. Phys. Chem. A**. 96: 3428-3435.

Calzaferri, G., Maas, H., Pauchard, M., Pfeniger, M., Megelski, S., and Devaux, A. (2002). Supramolecularly organized dye molecules in the channels of zeolite L, **Adv. Photochem**. 27: 1-50.

Calzaferri, G., Huber, S., Devaux, A., Ruiz, A. Z., Li, H., Bossart, O., and Dieu, L.Q. (2006). Light-harvesting host-guest antenna materials for photonic device. **Proceedings of the SPIE, Organic Optoelectronics and Photonics II**. 619216-1- 619216-9.

Clazaferri, G., Bossart, O., Brühwiler, D., Huber, S., Leiggener, C.,. Van Veen, M. K., and Ruiz, A. Z. (2006). Light-harvesting host-guest antenna materials for quantum solar energy conversion devices. **C. R. Chimie**. 9: 214-225.

Calzaferri, G., and Devaux, A. (2010). Manipulation of energy transfer processes within the channels of zeolite L. **Int. J. Photoenergy**. ID 741834.

Devaux, A., Minkowski, C., and Calzaferri, G. (2004). Electronic and vibrational properties of fluorenone in the channels of zeolite L. **Chem. Eur. J**. 10: 2391-2408.

El Halabieh, R. H., Mermut, O., and Barrett, C. J. (2004). Using light to control physical properties of polymers and surfaces with azobenzene chromophores. **Pure Appl. Chem**. 76: 1445-1465.

Fujino, T., Arzhansev, S. Y., and Tahara, T. (2001). Femtosecond time - resolved Fluorescence study of photoisomerization of *trans*-azobenzene. **J. Phys. Chem A**. 105: 8123-8129.

Gfeller, N., Megelski, S., and Calzaferri. G. (1999). Fast energy migration in pyronine-loaded zeolite L microcrystals. **J. Phys. Chem. B**. 103: 1250-1257.

Goncharuk, V. V., Grebenyuk, A. G., Savranskii, L. I., Gorchev, V. F., and Chernega, A. N. (1981). Electronic spectra of azobenzene and p-dimethylaminoazobenzene adsorbed on surface of aluminosilicate catalysts and their quantum-mechanical interpretation. **J. Appl. Spectrosc**. 35(1): 754-757.

Hennessy, B., Megelski, S., Marcolli, C., Shklover, V., Bärlocher, C., and Calzaferri, G. (1999). Characterization of methyl viologen in the channels of zeolite L. **J. Phys. Chem. B**. 103: 3340-3351.

Hoffman, K., Marlow, F., and Caro, J. (1997). Photoinduced switching in nanocomposites of azobenzene and molecular sieves. **AdV. Mater**. 9: 567-575.

Kellerer, B., Hacker, H. H., and Brandmuller, J. (1971). Structure of azobenzene and tolane in solution. Raman spectra of azobenzene, azobenzene-d10, p,p'-azobenzene-d2, azobenzene-15N2, and tolane. **Ind. J. Pure Appl. Phys**. 9: 903-909.

Lei, Z., Vaidyalingam, A., and Dutta, P. K. (1998). Photochemistry of azobenzene in microporous aluminophosphate AlPO$_4$-5. **J. Phys. Chem. B**. 102: 8557-8562

Maas, H., and Calzaferri, G. (2003). Constructing dye-zeolite photonic nanodevices. **The spectrum**. 16(3): 18-24.

Megelski, S., and Calzaferri, G. (2001). Tuning the size and shape of zeolite L based inorganic organic host guest composites for optical antenna systems. **Adv. Funct. Mater**. 11(4): 277-286.

Meeprasert, J., Jungsuttiwong, S., and Namuangruk, S. (2013). Location and acidity of BrØnsted acid sites in isomorphously substituted LTL zeolite: A periodic density functional study. **Micropor. Mesopor. Mater**. 175(15): 99-106.

Park, Y. S., Lee, K., Lee, C., Yoon, K. B. (2000). Facile reduction of zeolite encapsulated viologens with solvated electrons and selective dispersion of inter- and intramolecular dimers of propylene-bridged bisviologen radical cation. **Langmuir**. 16(10): 4470-4477.

Park, S-K., Lee, C., Min, K-C., and Lee., N-S. (2005). Structural and conformational studies of *ortho-*, *meta-*, and *para-* methyl red upon proton gain and loss. **Bull. Korean Chem. Soc**. 26(8): 1170-1176.

Rao, H. (1990). Photochemistry and photophysics, Vol 9, J. F. Rabek (Ed), Chap. 4, CRC Press, Boca Patan.

Robin, M. B. and Simpson, W. T. (1962). Assignment of electronic transitions in azo dye prototypes. **J. Chem. Phys**. 36: 580-589.

Simomura, M., and Kunitake, T. (1987). Fluorescence and photoisomerization of azobenzene-containing bilayer membranes. **J. Am. Chem. Soc**. 109: 5175-5183.

Traetteberg, M., Hilmo, I., and Hagen, K. (1977). A gas electron diffraction study of the molecular structure of trans-azobenzene. **J. Mol. Struct**. 39: 231-239.

Tung, C.-H., and Guan, J. Q. (1996). Modification of photochemical reactivity by Nafion photocyclization and photochemical *Cis−Trans* isomerization of azobenzene. **J. Org. Chem**. 61: 9417-9421.

Vohra, V., Devaux, A., Dieu, L.Q., Catellani, M., Calzaferri, G., and Botta, C. (2009). Energy transfer in fluorescent nanofibers embedding dye loaded zeolites L crystals. **Adv. Mater**. 21: 1146-1150.

Zimmermann, G., Chow, L. Y., and Park, U. I. (1958). The photochemical isomerization of Azobenzene. **J. Am. Chem. Soc**. 80: 3528-3531.
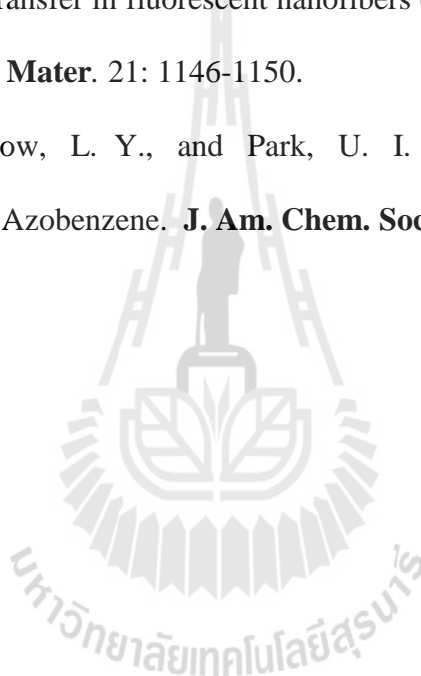
CHAPTER V

EVALUATION OF ADSORPTION OF CATIONIC DYES

ON K-LTL AND H-LTL ZEOLITE

Abstract

This article presents a study of the adsorption isotherms of acridine hydrochloride (Ac) and acriflavine hydrochloride (AF) on zeolite LTL (in form of H-LTL and K-LTL) including ice hockey and round shape. The study revealed that the adsorption isotherms are very well fitted with Langmuir model. Moreover, the thermodynamic quantities indicated that the adsorptions of both dyes on zeolite LTL are spontaneous, endothermic and highly disordered. The maximum loading (Θ_{max}) of AF and Ac on H-LTL and K-LTL with the both shapes was in the range of 4.03-6.44% and 0.45-2.80%, respectively. The higher amount of AF than that of Ac on zeolite LTL was explained in terms of the stronger interaction of amine groups (-NH_2) with BrØnsted acid sites in H-LTL and stronger interaction of cation-π in K-LTL. Moreover, the additional strong interaction of lone pair electron of amine groups (-NH_2) with K^+ ion is expected to be formed in K-LTL as well. In addition, the morphology of zeolite LTL was found to have an effect on the adsorption of AF and Ac.

5.1 Introduction

Zeolites are appealing inorganic microporous frameworks that possess a large variety of well-defined internal structures such as uniform cages, cavities, or channels (Auerbach, Carrado, and Dutta, 2003). One-dimensional channel of zeolite LTL is widely known as having an ability to inhibit dye molecules to form an aggregation which causes fast thermal relaxation of electronic excitation energy. Therefore, it is very appealing that zeolite LTL be used as a host material for intercalated dye molecule. In contrast to zeolite Y, zeolite LTL possesses supercages of 13 Å diameter with a pore opening of 7-8 Å that can aggregate within supercage (Ganesan and Ramaraj, 2001). The capacity of zeolite LTL framework to adopt an arrangement of the intercalated molecule has gained a great deal of interest for various applications, especially in regards of ice hockey and round shape where artificial antennas are commonly used (Calzaferri, 1998; Calzaferri, Huber, Maas, and Minkowski, 2003; Huber and Calzaferri, 2004; Maas and Calzaferri, 2003). The construction an artificial antenna system was studied by Calzaferri's group. In their study, the system was comprised of well-arranged monomeric dye with high luminescence quantum yield in zeolite crystals of 300 and 700 nm sizes in the dye concentration range of 10^{-4} mol/L up to 0.042 mol/L (Calzaferri, et al., 2003).

In artificial antenna systems, light is absorbed by dyes molecule along the channels. The shorter distances the dyes travel along the channels, the higher efficiency excitation energy is transported to a specific trap at the ends of the crystal. The study by Niklaus Gfeller's group revealed that energy transfer from donor (pyronine) to acceptor (oxonine) in zeolite LTL had more efficiency in terms of short donor-acceptor distances or increase loading of donor molecules together with short

in length of zeolite LTL. In addition, Calzaferri's group used donor (hostasol yellow 3G; HY3G) and acceptor (oxonine; Ox^+) in the ratio of 33:1. It was validity for light harvesting, transporting and trapping (Calzaferri et al., 2011). The intercalation of neutral dyes (resorufin and fluorenone) in zeolite LTL channel instead of cationic dyes (pyronine, oxonine, methylviologen and thionine) has also been researched (Lutkouskaya and Calzaferri, 2006; Gfeller, Megelski, and Calzaferri, 1999; Li, Devaux, Ruiz, and Calzaferri, 2006); Hennessy et al., 1999; Calzaferri and Gfeller, 1992).

Acridine hydrochloride (Ac) and acriflavine hydrochloride (AF) have been widely applied for OLED materials, photovoltaic cell (PVC), pH sensor and fluorescent probe (Chunxiang, et. al. 2008; Kaewsuya, et. al. 2008; Kazima, et. al. 2007; Misra et al., 2000). However, there is still a very small number of previous research exploring the possibility for application of Ac and AF in zeolite LTL as artificial antenna material. Investigation of an amount of inserted Ac and AF in zeolite LTL would provide crucial information on it able to be available or not. As a result of the lack of sufficient studies in this field, this research was intended to investigate the dye adsorption on zeolite LTL in order to estimate the amount of adsorbed Ac and AF on H-LTL and K-LTL including ice hockey and round shapes.

5.2 Experimental

5.2.1 Synthesis of Zeolite LTL (K-LTL)

All materials used in this study were of reagent grade. The typical procedure for the preparation of synthesis gel of K-LTL and H-LTL zeolite were modified according to a Chapter II in page 41.

5.2.2 Characterization

The products were analyzed through various techniques. The identification of phases of the resulting structures were determined using XRD (D5005, Bruker) CuK_{∞} radiations scanning from 3-35°. Scanning electron microscope (JSM6400, JEOL) at acceleration voltage ranging from 10-20 kV was used to examine zeolite LTL morphology. The chemical compositions were analyzed using ICP-OES. The samples for ICP-OES were digested in PTFE vessel developed in the laboratory. Concentrated nitric acid (65% w/v), hydrofluoric acid, hydrochloric acid (37% w/v) and boric acid (4% w/v) were utilized for the digestion and cleaning of the digestion tubes. Deionized water was used throughout the process. The specific surface area was evaluated by nitrogen gas adsorption at -196 °C using automated volumetric equipment (Autosorb 1-Quantachrome Instrument), U.S.A. Ammonia temperature programmed desorption (NH_3-TPD) was measured with a BEL Japan BELCAT-A equipped with a thermal conductivity detector (TCD) and a mass spectrometer (MS) for continuous analysis of the desorbed species. The sample (0.05 g) was placed in a quartz tube and purged with He, then heated with a temperature ramp of 3 °C/minutes to 500 °C under H_2 flow. After 3 hours at 500 °C, the sample was cooled down to 100 °C under He flow. Ammonia saturation was carried out at 100 °C using a 7% NH_3-He gas mixture for 0.5 hours. Then, excess ammonia was

removed by purging with He for 0.5 hours. The desorption step was carried out with the temperature ramp of 10 °C/minutes from 100 to 900 °C under He flow. The amount of desorbed ammonia was measured with a MS detector ($m/z = 16$). UV-vis spectra were recorded on a spectrophotometer (Carry 1E).

5.2.3 Adsorption isotherm studies

The adsorption was performed by batch experiments. The adsorption of the dyes was performed by shaking 0.1g of the zeolite in 25 mL of the solutions with varying concentrations (10^{-6}-10^{-5} M) at different temperatures (30, 40 and 50 °C, respectively). The samples were collected by separating the zeolites from solution using a centrifuge. The concentration of the dyes was determined spectrophotometrically by measuring absorbance at 355 and 440 nm for λ_{max} of Ac and AF, respectively. The data obtained from the adsorption tests were used to calculate the %w/v of the adsorbent by a mass-balance relationship, which represents the amount of adsorbed dye per the amount of dye adsorbent:

$$q_e = \frac{(C_0 - C_e)V}{m} \qquad (1)$$

Where qe (M/g) is the amount of dye adsorbed at equilibrium. V (L) is the volume of the solution. m (grams) is the mass of the zeolite LTL. C_0 and C_e (M) are concentrations of dyes in solution (M) at initial and equilibrium, respectively.

5.3 Results and discussion

5.3.1 Characterization of zeolite LTL

X-ray diffraction

Figure 5.1 shows the XRD patterns of H-LTL and K-LTL with different morphologies. The patterns were compared to a standard pattern of zeolite LTL (Treacy, Higgins, and Von Ballmons, 2001).
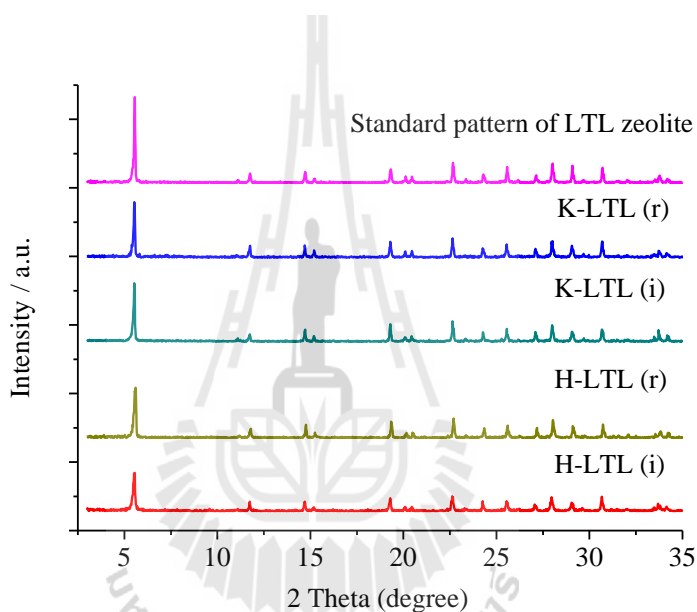
Figure 5.1 XRD patterns of H-LTL and K-LTL, ice hockey (i) and round shape (r).

The XRD patterns of all samples illustrate the same 2- theta (2θ) values for the main peaks located at 2θ = 5.5, 19.4, 22.7, 28.0, 29.1 and 30.7 degree. The XRD patterns indicate that the crystallinity of H-LTL is lower than that of K-LTL, and the percentage of crystallinity of H-LTL reduced to 25% of K-LTL. A possible explanation of this observation is that the calcination step led to destruction of the crystalline framework. The chemical composition shows that the exchange of NH_4^+

with K^+ in K-LTL was not complete and the NH_4^+ exchange level attained is about 77-79%. This is in line with the work of Dyer and co-worker (Dyer, Amini, Enamy, El-Naggar, and Anderson, 1993) on cation-exchange in K-LTL with NH_4^+ of about 80% of K-LTL.

Scanning electron microscopy

Zeolite LTL can be synthesized in various sizes and shapes. Y. Sig Ko and co-workers (Ko and Ahn, 2004) studied effects of starting materials and substrate compositions on the crystallization rate of zeolite LTL. In their experiment, the formation of ice hockey shaped crystals were obtained at the $(K_2O+Na_2O)/SiO_2$ ratio of 0.37 and the $H_2O/(K_2O+Na_2O)$ ratio of 50, and the formation of round- or disk-shaped were also observed (Ruiz, Brühwiler, Ban, and Calzaferri, 2005). The obtained zeolite K-LTL was synthesized in accordance with previous experiments (Insuwan and Rangsriwatananon, 2012). Ice hockey shape with the size 1.50 µm and round shape with the size 4.39 µm were shown in Figure 5.2.
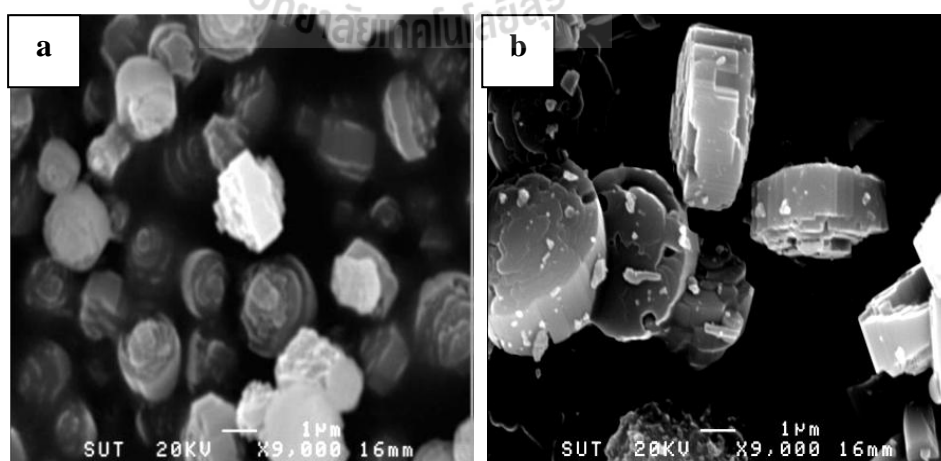
Figure 5.2 SEM images of K-LTL (a) ice hockey shape; (b) round shape.

Temperature programmed desorption (TPD)

The temperature-programmed desorption of NH_3 was used to monitor the changes in the surface coverage of probe molecules pre-adsorbed on the zeolite as a function of the temperature from which the strength and the amount of total acid sites were determined. The NH_3-TPD curves and the amount of total acid site of K-LTL and H-LTL were shown in Figure 5.3 and Table 5.1 The acidity of H-LTL shows two desorption peaks, indicating the existence of at least two types of acid sites. The first peak is called the weak acid sites at 179-190 °C and the second one was assigned to ammonia adsorbed directly on the BrØnsted acid site (Lónyi and Valyon, 2001), whereas the weak acid sites of K-LTL appeared at 165-167 °C.
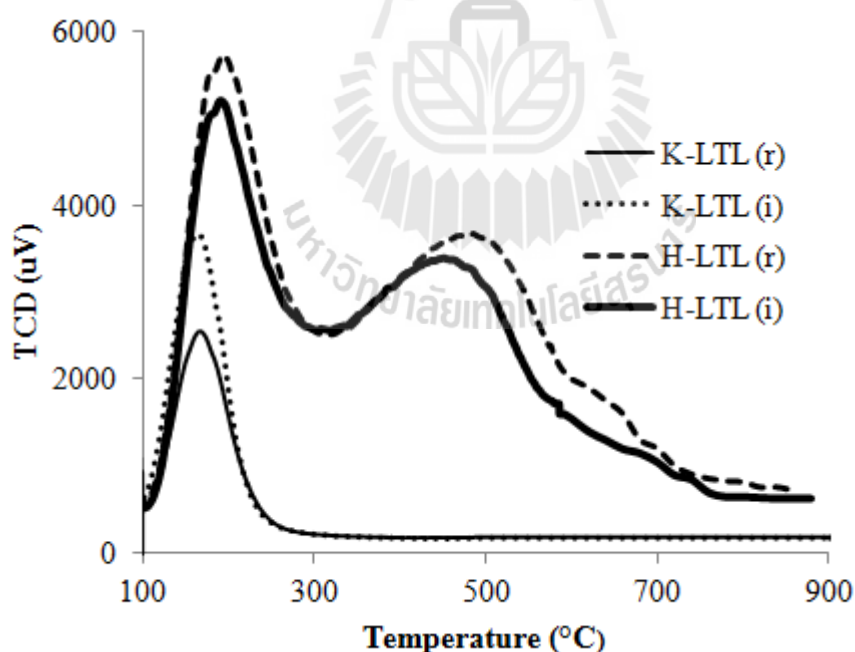
Figure 5.3 NH_3-TPD curves of K-LTL and H-LTL with ice hockey (i) and round shape (r).

Table 5.1 Acidity characteristics of the zeolite LTL.

Samples	Total	Number of acid sites (desorbed ammonia)/(mM/g sample)	
		Weak [a]	Strong [b]
K-LTL (i)	0.906	0.906	-
K-LTL (r)	0.694	0.694	-
H-LTL (i)	5.058	1.931	3.127
H-LTL (r)	5.960	2.351	3.609

[a] The weak acid sites correspond to the desorption peaks with maxima at about 166-190 °C and [b] is the strong acid sites at about 450-480 °C.

N$_2$ adsorption isotherm

The information of the surface area and micropore surface area are summarized in Table 5.2. The surface area and micropore surface area of zeolite LTL were increased upon the replacement of K$^+$ by H$^+$ ion. The increase in the micropore surface area was due to the smaller size of H$^+$ compared to K$^+$ ion, resulting in the increment of space for N$_2$-adsorption.

Table 5.2 Textural properties of zeolite LTL.

Samples	Surface area (m^2/g)	Micropore surface area (m^2/g)	Crystal sizes (μm)
K-LTL(i)	348.4	322.3	1.50
K-LTL(r)	324.9	309.7	4.39
H-LTL(i)	390.4	353.4	2.06
H-LTL(r)	404.5	368.7	5.10

5.3.2 Adsorption isotherms of dyes

The adsorption isotherm was performed at 30, 40, and 50 °C, respectively (see Figure 5.4 and 5.5). It was found that the experimental data were well-fitted with the Langmuir model. One of the assumptions of Langmuir model is that the adsorption occurs at specific homogenous sites within the adsorbent. The equation is as follows:

$$qe = \frac{q_m K_L C_e}{1 + K_L C_e} \tag{2}$$

Where qe (M/g) is the amount of dyes adsorbed on zeolite LTL at equilibrium and q_m (M/g) is the maximum adsorption monolayer capacity. K_L is the Langmuir constant related to the affinity between adsorbate and adsorbent and is related to the free energy of adsorption. Ce (M) is the concentration of dyes at equilibrium. The linear form of Langmuir model is expressed as the following equation (Hameed, Ahmad, and Aziz, 2007).

$$\frac{Ce}{q_e} = \frac{1}{q_m} Ce + \frac{1}{K_L q_m} \tag{3}$$

Linear plots of Langmuir isotherms of dyes adsorbed on H-LTL and K-LTL were shown in Figure 5.6 and 5.7. The correlation coefficient values of the linearity were found to be satisfactory. The maximum adsorption monolayer capacity (q_m) and the Langmuir constant (K_L) calculated from the slope and the intercept of the linear plot are shown in Table 5.2 and 5.3. Acriflavine hydrochloride is a larger molecule (0.91 nm in long and 0.37 nm in thick) than acridine hydrochloride (see

Scheme 5.1) (Charles, Ladoulis, Thomas, and Gill III, 1970). However, both molecules can diffuse into the channel of zeolite LTL with a free diameter of 0.71 nm.

Acridine hydrochloride (Ac)   Acriflavine hydrochloride (AF)
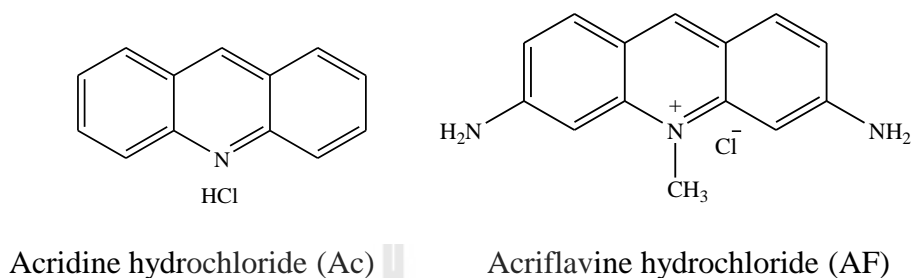
Scheme 5.1 Structure formula of cationic dyes.

As seen in Figure 5.4 and 5.5, the higher temperature the higher amount of dye was adsorbed indicating the endothermic characteristic of the adsorption. Additionally, the increasing temperatures raised the rate of diffusion of the dye molecules through the one dimension of an internal pore of zeolite, owing to the decrease in the viscosity of the solution (Tan and Hameed, 2010). A number of studies reported that it may produce a swelling effect within the internal structure of the zeolite enabling dyes to penetrate further into the pore (Tan and Hameed, 2010; Wang, Boyjoo, Choueib, and Zhu, 2005; Wang, Boyjoo, and Choueib, 2005).
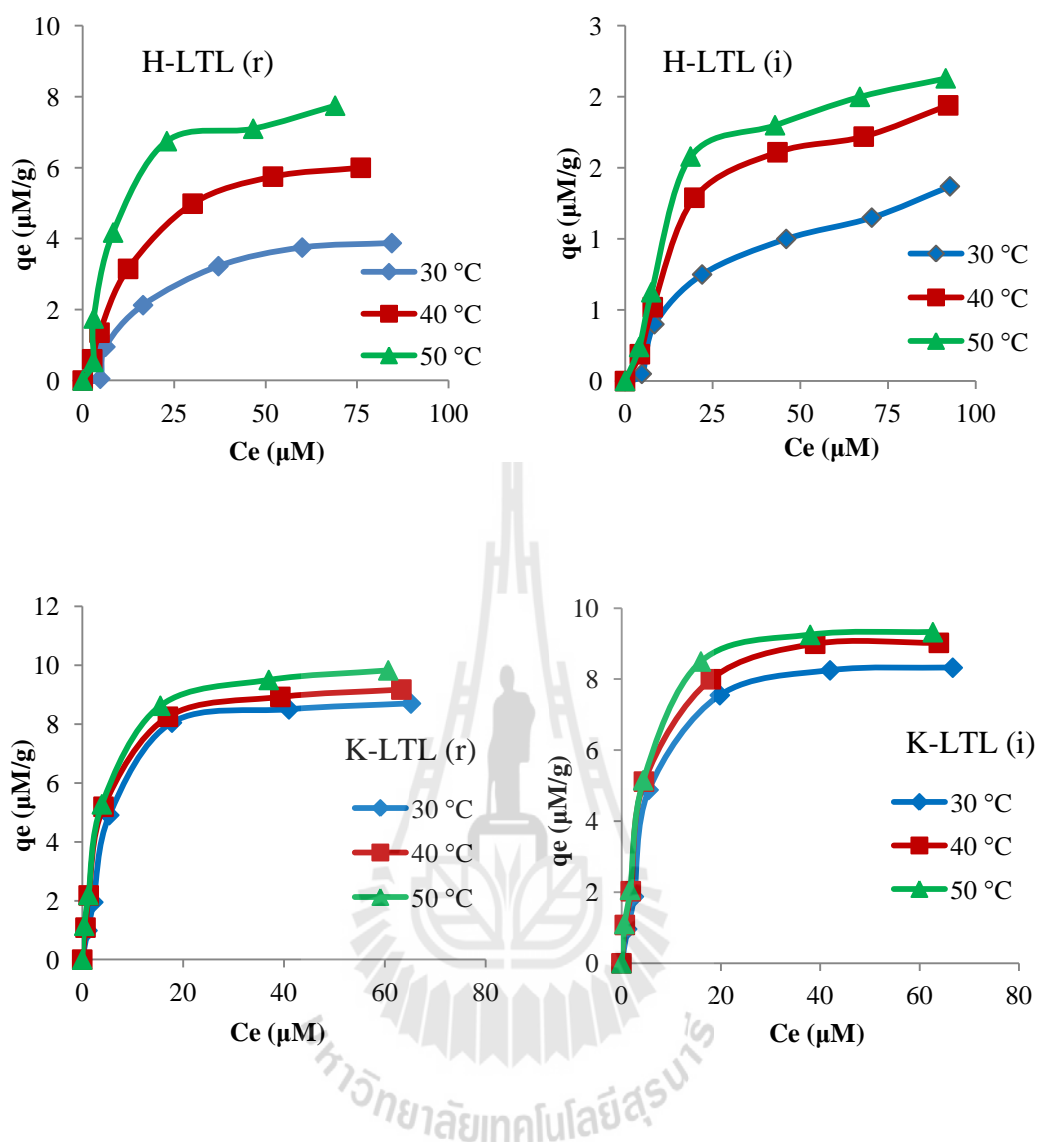
Figure 5.4 Adsorption isotherms of Ac on H-LTL and K-LTL including ice hockey punk and round shape at 30, 40 and 50 °C (qe and Ce values are shown in Appendix B: Table B.1).
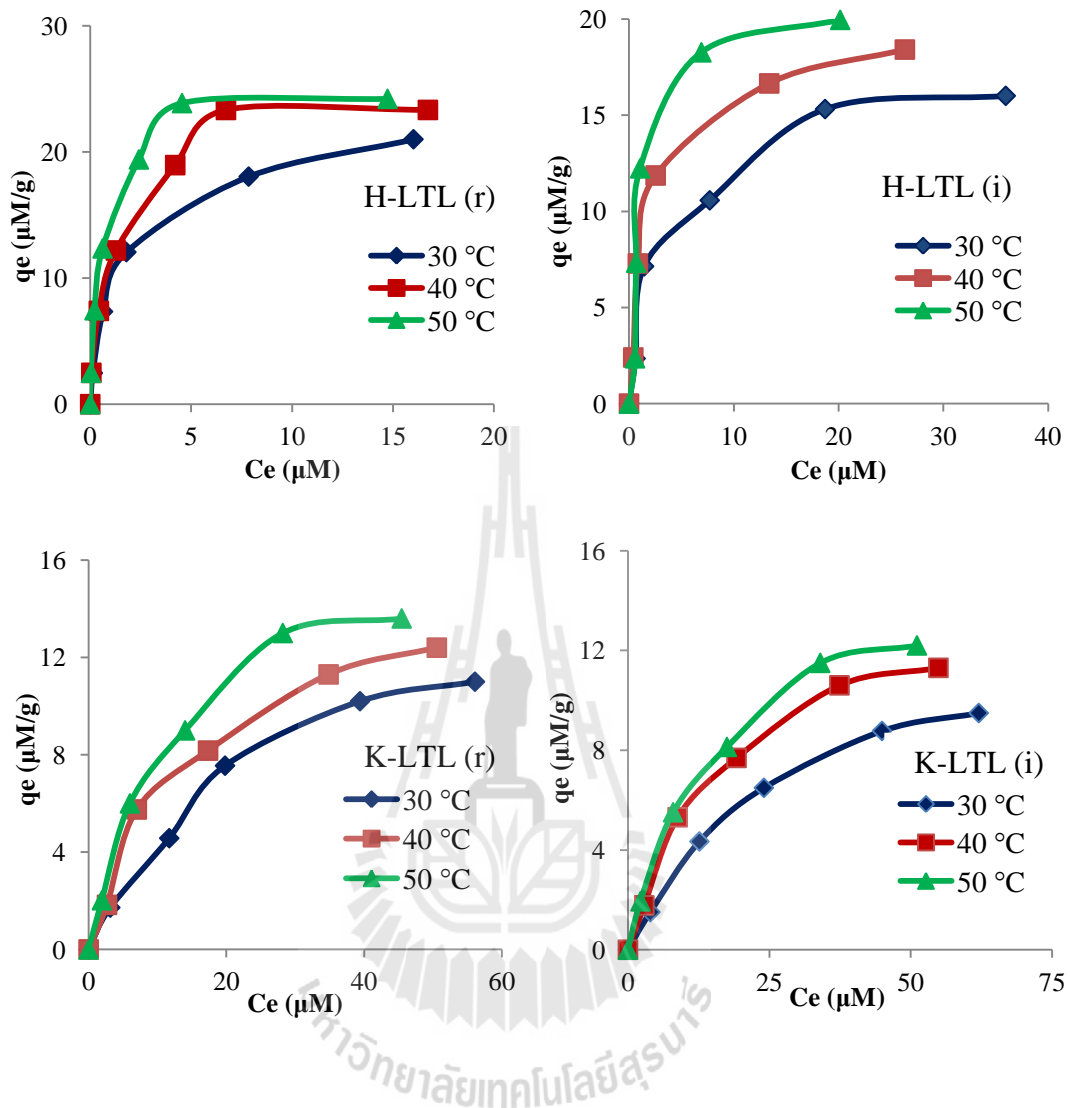
Figure 5.5 Adsorption isotherms of AF on H-LTL and K-LTL including ice hockey

and round shape at 30, 40, and 50 °C (qe and Ce values are shown in Appendix B:

Table B.2).
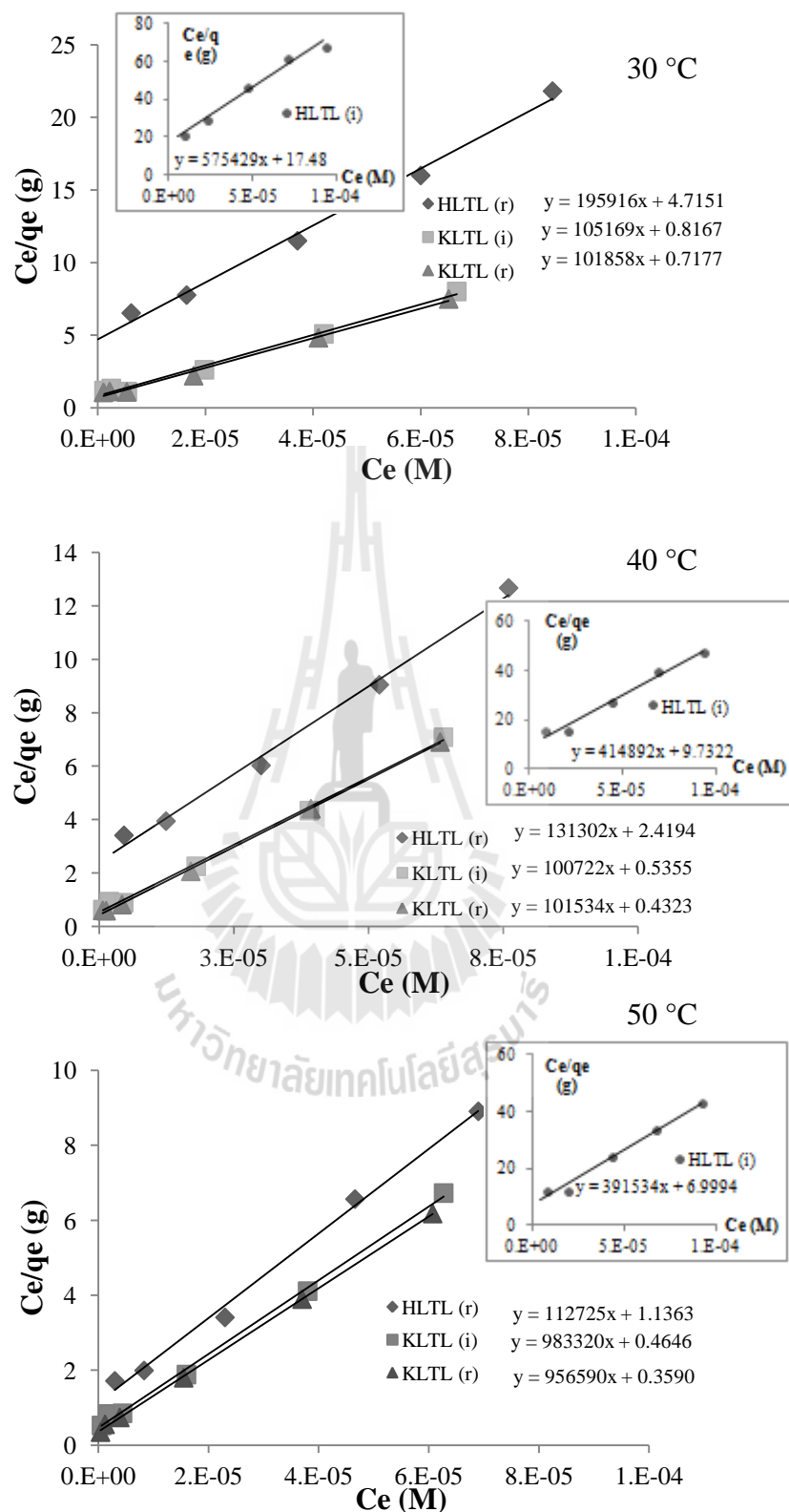
Figure 5.6 Linear plot of Langmuir isotherm of Ac on H-LTL and K-LTL including

ice hockey and round shapes at 30, 40, and 50 °C.
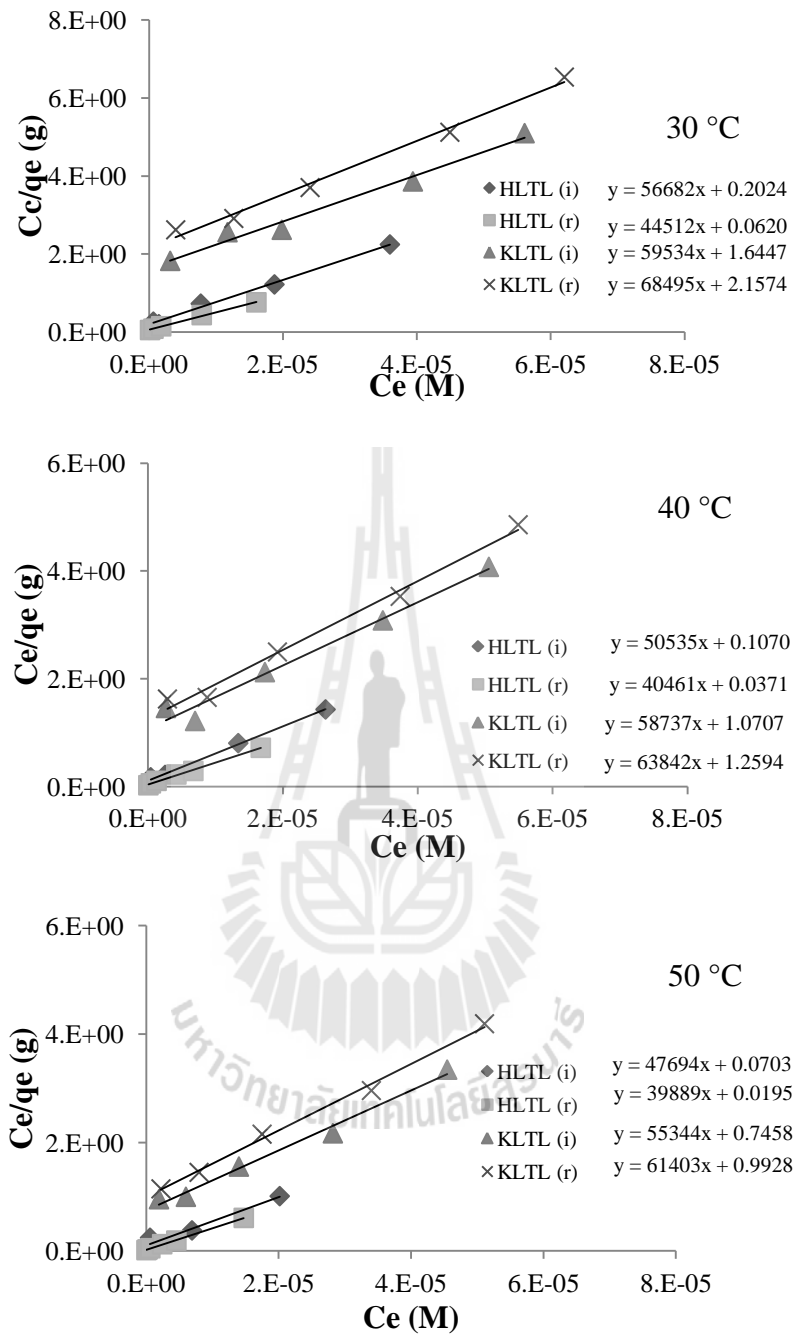
Figure 5.7 Linear plot of Langmuir isotherm of AF on H-LTL and K-LTL including ice hockey and round shapes at 30, 40, and 50 °C.

The adsorption parameters of Ac and AF calculated from Langmuir equation are shown in Table 5.3 and 5.4. According to the data presented in the tables, the maximum adsorption monolayer capacity (q_m) of Ac inside the channel of zeolite LTL is in the following order: H-LTL(i) < H-LTL(r) < K-LTL(i) < K-LTL(r), whereas AF is as follows: K-LTL(r) < K-LTL(i) < H-LTL(i) < H-LTL(r).

5.3.3 The maximum loading (%Θ_{max}) of dyes

The maximum loading (%Θ_{max}) of dyes on the H-LTL and K-LTL can be calculated according to the report (Hennessy et al., 1999).

$$\Theta_{max} = \frac{\text{number of molecules intercalated}}{\text{number of sites available}} = \frac{n_{D+}}{n_S} \tag{4}$$

The number of molecules intercalated (n_{D+}) can be obtained from adsorption study (q_m) that was fitted and described by the Langmuir model. The number of sites available in zeolite LTL can be calculated by eq (5).

$$n_s = \frac{W_Z}{Mw_z \text{ g/mol}} \tag{5}$$

Where W_z is amount of zeolite LTL in grams and Mw_z is a molecular weight/unit cell of sample.   The values of maximum loading (%Θ_{max}) of dyes inside zeolite LTL are shown in Table 5.5.

Table 5.3 Parameters for adsorption of Ac on K-LTL and H-LTL with ice hockey and round shape.

Samples	Temperature ($^{\circ}$C)	Langmuir isotherm		
		q_m (M/g)	K_L(M^{-1})	R^2
K-LTL (i)	30	9.51×10^{-6}	1.29×10^5	0.991
	40	9.93×10^{-6}	1.88×10^5	0.997
	50	1.02×10^{-5}	2.11×10^5	0.999
K-LTL (r)	30	9.82×10^{-6}	1.42×10^5	0.993
	40	9.85×10^{-6}	2.35×10^5	0.999
	50	1.04×10^{-5}	2.68×10^5	0.999
H-LTL (i)	30	1.74×10^{-6}	3.29×10^4	0.983
	40	2.41×10^{-6}	4.26×10^4	0.982
	50	2.55×10^{-6}	5.59×10^4	0.985
H-LTL (r)	30	5.10×10^{-6}	4.16×10^4	0.993
	40	8.20×10^{-6}	4.10×10^4	0.994
	50	8.87×10^{-6}	9.92×10^4	0.995

Table 5.4 Parameters for adsorption of AF on K-LTL and H-LTL with ice hockey and round shape.

Samples	Temperature ($^{\circ}$C)	Langmuir isotherm		
		q_m (M/g)	K_L(M^{-1})	R^2
K-LTL (i)	30	1.68×10^{-5}	3.62×10^4	0.982
	40	1.70×10^{-5}	5.48×10^4	0.978
	50	1.81×10^{-5}	7.42×10^4	0.989
K-LTL(r)	30	1.46×10^{-5}	3.17×10^4	0.992
	40	1.56×10^{-5}	5.07×10^4	0.989
	50	1.63×10^{-5}	6.18×10^4	0.996
H-LTL (i)	30	1.76×10^{-5}	2.80×10^5	0.994
	40	1.98×10^{-5}	4.72×10^5	0.997
	50	2.10×10^{-5}	6.78×10^5	0.966
H-LTL(r)	30	2.25×10^{-5}	7.18×10^5	0.997
	40	2.47×10^{-5}	1.10×10^6	0.996
	50	2.50×10^{-5}	2.15×10^6	0.999

Table 5.5 Maximum loading (%Θ_{max}) of Ac and AF on H-LTL and K-LTL, ice hockey (i) and round (r) shapes.

Samples	Maximum loading (%Θmax of Ac)			Maximum loading (%Θmax of AF)			Ratio Ac/AF
	30°C	40°C	50°C	30°C	40°C	50°C	(average)
K-LTL (i)	2.61	2.72	2.79	4.64	4.70	5.00	0.57
K-LTL (r)	2.65	2.65	2.8	4.03	4.31	4.50	0.63
H-LTL (i)	0.45	0.61	0.66	4.54	5.1	5.41	0.11
H-LTL (r)	1.28	2.06	2.22	5.80	6.37	6.44	0.29

Table 5.5 shows the maximum loading (%Θ_{max}) of adsorbed Ac on H-LTL and K-LTL in both shapes in the range of 0.45-2.22% and 2.61-2.80% of the total active site in the channel, respectively. Moreover, the %Θ_{max} of adsorbed AF on H-LTL and K-LTL in both shapes was in the range of 4.54-6.44% and 4.03-5.00 %, respectively. The %Θ_{max} of Ac is smaller than that of AF, even though Ac has smaller size than the other one. The difference in the %Θ_{max} values of Ac and AF can be described by the interactions between the zeolite frameworks and dyes. The lone pair electron of amine group (-NH$_2$) of AF molecule interacts with HO-BrØnsted acid sites of H-LTL via a strong hydrogen bond formation and the interaction of Ac with H-LTL is aromatic hydrogen bond occurring from HO-BrØnsted acid site and π-electron of Ac (OH/π interaction) (see figure 5.8; a and b), which is weaker interaction than the other one. Additionally, it is possible that the BrØnsted acid sites of H-LTL donate a proton to the amine group (-NH$_2$) acting as proton acceptor to form protonated amino group (-NH$_3^+$) which would be attracted with anionic sites of zeolite frameworks.

In the case of AF and Ac in K-LTL the interaction can be described by cation-π interaction, which K^+ ion in zeolite pointing toward the face of electron-rich π system of dyes (see Figure 5.8c) (Silbernagel, Garcia, Newsam, and Hulme, 1989). Since amine group (-NH_2) is electron donating group (Keiluweit ang Kleber, 2009), it causes stronger interaction of cation-π of AF than that of Ac molecule. However, the other attractive interaction is expected to form via the interaction of lone pair electron of amine group (-NH_2) with K^+ ion (see figure 5.8d).
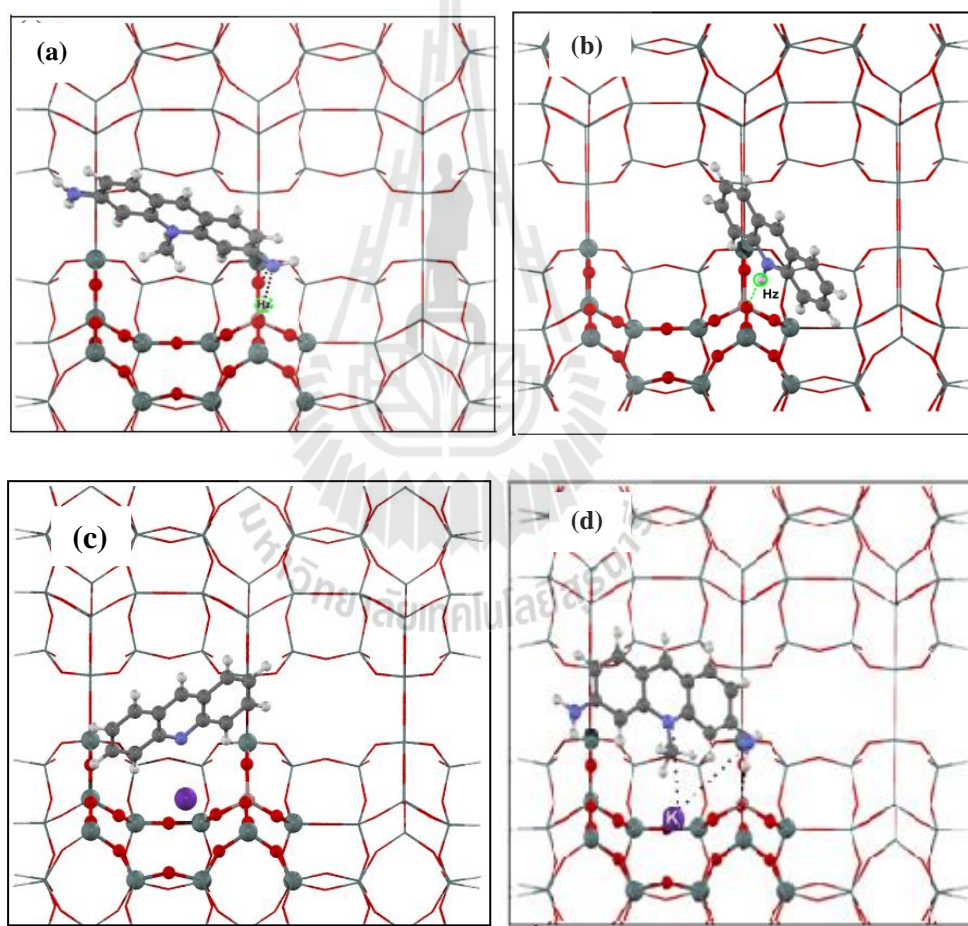
Figure 5.8 H-bond between AF and H-LTL (a), O-H/π interaction between Ac and H-LTL (b), and interaction between K-LTL with Ac (c) and AF (d).

Considering the morphology of zeolite LTL the adsorption of Ac and AF on H-LTL, these dyes can be adsorbed onto round shape more than ice hockey shape, even though the size of ice hockey shape is smaller than that of round shape. It may be explained by the existence of strong and weak acid sites of H-LTL. The present study also revealed that the total amount of acid sites of a round shape is over that of ice hockey shape (see Table 5.1). The differences of the average amount of $\%\Theta_{max}$ (see Table 5.5) in both shapes of adsorbed Ac and AF were 70 % and 20%, respectively. If the round and ice hockey shape have a similar size, higher dye adsorption capacity of round shape is expected. In the case of the dyes adsorbed on K-LTL, AF can be adsorbed on the ice hockey shape more than the round shape; and the different amount in both shapes is about 10%. It may be due to the higher an amount of acid sites and surface area or the smaller size of ice hockey shape resulting in the higher loading of AF (see Table 5.1 and 5.2). Whereas the morphology has no influence on the adsorption capacity of Ac onto K-LTL. It was possible Ac has a similar trend of diffusion to the both ice hockey and round shapes.

5.3.4 Thermodynamic parameters

The change in Gibbs free energy (ΔG°) of the adsorption process is related to the equilibrium constant by the following equation (Wang, Boyjoo, Choueib, and Zhu, 2005; Wang, Boyjoo, and Choueib, 2005).

$$\Delta G^{\circ} = -RTlnK_L \qquad (6)$$

Where R is the gas constant (8.314 J/mol·K), T is temperature (K), and K_L is adsorption constant in the Langmuir isotherm.

The values of ΔH° and ΔS° can be calculated from the slope and intercept of the linear variation of ln K_L with reciprocal of temperature (1/T) as in the following equation (see Appendix B: Figure B.1 and B.2).

$$\ln K_L = -\frac{\Delta H^{\circ}}{RT} + \frac{\Delta S^{\circ}}{R} \qquad (7)$$

The results of thermodynamic parameter are shown in Table 5.6 and 5.7. From the data, the more negative value of ΔG° was, the higher adsorption capacity is observed. The negative values of ΔG°, therefore, implied that the reaction occurs in the direction where adsorption takes place. The positive values of ΔH° indicate that the adsorption process is endothermic. This result agrees with the several reports on endothermic adsorption of reactive dyes on different types of adsorbents (Netpradit, Thiravetyan, and Towprayoon, 2004; Namasivayam and Kavitha, 2002; Fungaro, Yamaura, and Carvalho, 2011).

Table 5.6 Thermodynamic parameters for adsorption of Ac on K-LTL and H-LTL with ice hockey and round shape.

Samples	Temperature ($^\circ$C)	ΔG° (KJ/mol)	ΔH° (KJ/mol)	ΔS° (J/mol/K)
K-LTL (i)	30	-29.62		165.25
	40	-31.59	20.45	166.26
	50	-32.92		165.23
K-LTL (r)	30	-29.88		185.05
	40	-32.19	26.19	186.52
	50	-33.57		185.02
H-LTL (i)	30	-26.20		157.59
	40	-27.74	21.55	157.48
	50	-29.35		157.58
H-LTL (r)	30	-26.80		202.61
	40	-27.64	34.59	198.82
	50	-30.88		202.69

Table 5.7 Thermodynamic parameters for adsorption of AF on K-LTL and H-LTL with ice hockey and round shape.

Samples	Temperature ($^\circ$C)	ΔG° (KJ/mol)	ΔH° (KJ/mol)	ΔS° (J/mol/K)
K-LTL (i)	30	-26.45		182.74
	40	-28.39	28.92	183.10
	50	-30.10		182.72
K-LTL (r)	30	-26.10		176.47
	40	-28.18	27.37	177.48
	50	-29.62		176.44
H-LTL (i)	30	-31.60		222.64
	40	-33.99	35.86	223.16
	50	-36.04		222.60
H-LTL (r)	30	-33.96		259.34
	40	-36.17	44.62	258.12
	50	-39.15		259.35

Based on the magnitude of ΔH^o (20.45 - 44.62 kJ/mol), the adsorption of these dyes onto zeolite L (H-LTL and K-LTL) was classified as a physical adsorption process. In addition, the positive value of ΔS^o indicates an increase in randomness at the solid/solution interface following the adsorption process and an increase in degree of freedom of the adsorbed species (Bhattacharyya and Gupta, 2006).

5.4 Conclusions

AF and Ac can occupy the one-dimensional channels of H-LTL and K-LTL by ion exchange process. The maximum loading ratio of Ac to AF was found to be in the range of 0.11-0.29 in H-LTL and 0.57-0.63 in K-LTL. Based on the photophysical properties of AF and Ac, the system of zeolite incorporated with AF and Ac can be utilized for artificial antenna materials in which Ac and AF act as electron donor and acceptor, respectively. This system would perform efficiently if zeolite LTL had contained higher amount of Ac compared to AF. Based on the adsorption capability of these dyes, we would suggest that Ac and AF do not make effective donor-acceptor pairs in zeolite LTL. Additionally, the importance of the morphology of zeolite LTL should be recognized in terms of dye adsorption capability besides the physical property for proper fixation on the supporter.

5.5 References

Auerbach, S. M., Carrado, K. A., and Dutta, P. K. (2003). Handbook of Zeolite Science and Technology. Marcel Dekker. New York. p. 1.

Bhattacharyya, K. G., and Gupta, S. S. (2006). Adsorption of chromium (VI) from water by clays. **Ind. Eng. Chem. Res**. 45: 7232 -7240.

Calzaferri, G., and Gfeller, N. (1992). Thionine in the cage of zeolite L. **J. Phys. Chem**. 96(8): 3428-3435.

Calzaferri, G. (1998). Zeolite microcrystals as host for supramolecular organization of dye molecules. **Chimia**. 52: 525-532.

Calzaferri, G., Huber, S., Maas, H., and Minkowski, C. (2003). Host – guest antenna materials. **Angew. Chem. Int. Ed**. 42: 3732-3758.

Calzaferri, G.,Méallet-Renault, R., Brühwiler, D., Pansu, R., Dolamic, I., Dienel, T., Adler, P.,Li, H., and Kunzmann, A. (2011). Designing dye-nanochannel antenna hybrid materials for light harvesting, transport and trapping. **ChemPhysChem**. 12: 580-594.

Charles, T. Ladoulis, Thomas. J., and Gill III. (1970). Physical chemical studies on the specific interaction of an acriflavine-phosphotungstic acid complex with double stranded nucleic acids. **J. Cell Biol**. 47: 500-511.

Chunxiang, L., Peipei, S., Lijun, Y., Yi, P., and Chien-Hong, C. (2008). Synthesis and electroluminescent properties of Ir complexes with benzo[c]acridine or 5,6-dihydro-benzo [c]acridine ligands. Thin Solid Films. **Thin Solid Films**. 516: 6186-6190.

Dyer, A., Amini, S., Enamy, H., El-Naggar, H. A., and Anderson, M.W. (1993). Zeolites. 13: 281-290.

Fungaro, D. A., Yamaura, M., and Carvalho, T. E. M. (2011). Adsorption of anionic dyes from aqueous solution on zeolite from fly ash-iron oxide magnetic nanocomposite. **J. At. Mol. Sci**. 2: 305-316.

Ganesan, V., and Ramaraj, R. (2001). Spectral properties of proflavin in zeolite-L and zeolite-Y. **J. Lumin**. 92: 167-173.

Gfeller, N., Megelski, S., and Calzaferri, G. (1999). Fast energy migration in pyronine loaded zeolite L microcrystals. **J. Phys. Chem. B**. 103: 1250-1257.

Hameed, B. H., Ahmad, A. A., and Aziz, N. (2007). Isotherm, Kinetics and thermodynamics of acid dye adsorption on activated plam ash. **Chem. Eng**. 133: 195-203.

Hennessy, B., Megelski, S., Marcolli, C., Shklover, V., Bä1rlocher, C., and Calzaferri, G. (1999). Characterization of methyl viologen in the channels of zeolite L. **J. Phys. Chem. B**. 103: 3340-3351.

Huber, S., and Calzaferri, G. (2004). Energy transfer from dye-zeolite L antenna crystals to bulk silicon. **Chem Phys Chem**. 5: 239-242.

Insuwan, W., and Rangsriwatananon, K. (2012). Morphology controlled synthesis of zeolite L and physicochemical properties. **Engineering Journal**. 16(3): 1-12.

Kaewsuya, P.,Miller, J. D., Danielson, N. D., Sanjeevi, J., and James, P. F. (2008). comparison of N-alkyl acridine orange dyes as fluorescence probes for the determination of cardiolipin. **Analytica Chimica Acta**. 626: 111-118.

Kazima, S., Zulfequar, M., Mazharul Haq, M., Bhatnagar, P. K., and Husain, M. (2007). Electrical and optical properties of thin films based on poly [2-methoxy-5(20-ethyl hexyloxy)- 1,4-phenylene vinylene] doped with acridine orange dye with possible photovoltaic applications. **Sol. Energ. Mat. Sol. C**. 9: 1462-1466.

Keiluweit, M., and Kleber, M. (2009). Molecular-level interactions in soils and sediments: The role of aromatic π-systems. **Environ. Sci. Technol**. 43: 3421-3429.

Ko, Y. S., and Ahn, W. S. (2004). Crystallization of zeolite L from Na_2O–K_2O– Al_2O_3–SiO_2–H_2O system. **Powder Technol**. 145: 10-19

Li, H., Devaux, A., Ruiz, A. Z., and Calzaferri, G. (2006). Electronic excitation energy transfer from dye-loaded zeolite L monolayers to a semiconductor. **Nanophotonics**. 6195: 61951G.

Lónyi, F., and Valyon, J. (2001). On the interpretation of the NH_3-TPD patterns of H- ZSM-5 and H-mordenite. **Micropor. Mesopor. Mater**. 47: 293-301.

Lutkouskaya, K., and Calzaferri, G. (2006). Designing dye-nanochannel antenna hybrid materials for light harvesting, transport and trapping. **J. Phys. Chem. B**. 110: 5633-5638.

Maas, H., and Calzaferri, G. (2003). Constructing dye-zeolite photonic nanodevices. **The spectrum**. 16: 18-24.

Misra, V., Mishra, H., Joshi, H.C., and Pant, T.C. (2000). Excitation energy transfer between acriflavine and rhodamine 6G as a pH sensor. **Sensor Actuat B**. 63: 18-23.

Namasivayam, C., and Kavitha, D. (2002). Removal of congo red from water by adsorption onto activated carbon prepared from coir pith, an agricultural solid waste. **Dyes and Pigments**. 54: 47-58.

Netpradit, S., Thiravetyan, P., and Towprayoon, S. (2004). Adsorption of three azo reactive dyes by metal hydroxide sludge: effect of temperature, pH, and electrolytes. **J. Colloid Interface Sci**. 270: 255-261.

Ruiz, A. Z., Brühwiler, D., Ban, T., and Calzaferri, G. (2005). Synthesis of zeolite L: Tuning Size and Morphology. **Monatshefte für Chemie**. 136: 77-89.

Silbernagel, B.G., Garcia, A. R., Newsam, J. M., and Hulme, R. (1989). Molecular motion of benzene, *n-* hexane, and cyclohexane in potassium zeolite L studied by deuterium NMR. **J. Phys. Chem**. 93: 6506-6511.

Tan, I. A. W., and Hameed, B.H., (2010). Adsorption isotherms, kinetics, thermo-dynamics and desorption studies of basic dye on activated carbon derived from oil palm empty fruit bunch. **J. Appl. Sci**. 10: 2565-2571.

Treacy, M. M. J., Higgins, J. B., and Von Ballmons, R. (2001). Collection of simulated XRD power Diffraction pattern of zeolites. Elsevier. pp. 497-498.

Wang, S., Boyjoo, Y., Choueib, A., and Zhu, Z.H. (2005). Removal of dyes from aqueous solution using fly ash and red mud. **Water Res**. 391: 129-138.

Wang, S., Boyjoo, Y., and Choueib, A. (2005). Comparative study of dye removal using fly ash treated by different methods. **Chemosphere**. 60: 1401-1407.

CHAPTER VI

PHOTOPHYSICAL PROPERTIES OF *t*-STILBENE

CONFINED IN ZEOLITE LTL

Abstract

This work continues research of photophysical properties of *t*- stilbene which is structure of molecules similar to *t*-azobenzene. In this work *t*-stilbene was inserted into the channels of zeolite LTL (K-LTL and H-LTL including ice hockey and round shape) by using gas phase method. The absorption and emission spectra of *t*-stilbene incorporated into K-LTL and H-LTL were reported. It was found that the absorption maximum appeared at 308 nm and emission spectrum at 354 and 380 nm for K-LTL and H-LTL, respectively. This result indicates that the behavior of *t*-stilbene incorporated into H-LTL is much more polar than that in K-LTL. Additionally, the morphologies of zeolite LTL does not influence on the photophysical properties of the dyes confined in the zeolite. When compared of the photophysical properties of *t*-stilbene and *t*-azobenzene loaded on zeolite LTL, it was found that the influence of microenvironment within zeolite LTL affecting the photophysical properties of *t*-stilbene less than that of *t*-azobenzene.

6.1 Introduction

The name for stilbene (1,2-diphenylethylene) was derived from the Greek word stilbos, which means shining. There are two isomeric forms of 1,2-diphenylethylene: (E)-stilbene (trans-stilbene), which is not sterically hindered, and (Z)-stilbene (cis-stilbene), which is sterically hindered and therefore less stable.

trans-stilbene   *cis*-stilbene
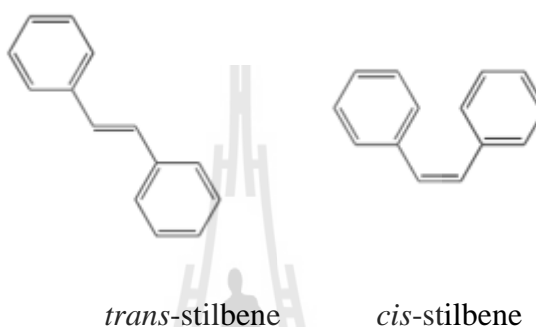
(E)-Stilbene has a melting point of about 125 °C, while the melting point of (Z)-stilbene is 6 °C. Stilbene is a relatively unreactive colorless compound practically insoluble in water. Because of unique features of trans-stilbene, including a fluorescence, phosphorescence, photochrome, and photochemical properties, have long been a matter of great interest to researchers. Recent years have seen the accumulation of new facts and ideas in the following areas: (i) stilbenes have proved for experimental and theoretical investigations of detailed mechanisms of photochemical and photophysical processes including photochromism phenomena (Haskins-Glusac, Ghiviriga, Abboud, and Schanze, 2004); (ii) stilbene derivatives have been used as molecular probes and labels for investigation of dynamic properties of proteins and biomembranes (Likhtenshtein et al., 1996); (iii) stilbenes are used as dyes, brighteners, whiteners of paper and textile, and photobleachers; (iv) stilbene and its combination with polymers and inorganic materials have been made a basis for numerous optical and measuring instruments, devices, and apparatuses for dye lasers,

organic solid lasers, and scintillators, phosphorus, neutron, and radiation detectors, electrophotographic photoconductor and image-forming apparatus, and photochromic, light-transmitting, dichroic, electroluminescent nonlinear optic, and organic–inorganic hybrid multichromophoric optical limiting materials. (Grabowski, Rotkiewicz, and Rettig, 2003; Meier et al., 1998; Morrall, Dalton, Humphrey, and Samoc, 2008). Moreover, stilbene is of interest not only because it features interesting singlet state and triplet state photophysics, but also because it undergoes efficient trans-cis photoisomerization. t-stilbene isomerizes to cis-stilbene under the influence of light. The reverse path can be induced by heat or light. The excited singlet state behavior of t-stilbene is governed by fluorescence from the S_1 state that effectively competes with isomerization. The isomerization reaction is characteristic of stilbene that proceeds in excited molecules via different mechanism. Firstly, the singlet mechanism is an internal conversion from the first excited state to the higher excited vibrational levels of the ground stated. Another is triplet mechanism, the excitation of an electron shell weaken the double ethylene C=C bond, transforming it into a single bond, which allows for free rotation of the phenyl rings. In addition, Kawagochi, (1994) assumed that in t-stilbene molecule there is a specific bond between ethylene and phenyl H-atoms to be approximately 2.5 Å which is on the same order of magnitude as the van der waals radius. So they assume that the structure of t-stilbene is planar. The attractive force between ethylene and phenyl H-atoms are weaken interaction and energy to break bond that the same order of magnitude as the energy of rotational of phenyl rings around the C=C bond. From above mentioned, the isomerization mechanism is suggested.

The appropriate molecular width of t-stilbene (~0.54 nm) can be incorporated into the channels of zeolite LTL which has pore diameter about 0.71 nm. The accommodation and distribution of guest molecules within the channel frameworks of zeolite are important factors in photochemical reaction. Hureau, Moissette, Vezin, Brémard, and Orio, (2012) have been explored the confinement effect on the stabilization of charge separation and on electron transfer of t-stilbene by using a probe adsorbtion in three types of zeolite (ferrierite (H-FER), H-MFI, and mordenite (H-MOR). They reported that electron transfer behaviors are dependent on the zeolite structure. t-stilbene radical cation (t-st$^{\bullet+}$) is stabilized for mounts in the narrow pore of H-FER because of it high electric filed and the tight fit of t-st$^{\bullet+}$ in the 10 memberd ring pore. Whereas, t-st$^{\bullet+}$ evolves to a charge-transfer complex though hole transfer in H-MFI and H-MOR. In addition, t-stilbene was incorporated as an intact molecule without solvent in the medium-size channel of nonacidic aluminium-rich Na$_{6.6}$ ZSM-5 zeolite with Na$_{6.6}$ (SiO$_2$)$_{89.4}$(AlO$_2$)$_{6.6}$ formula per unit cell (Moissette, Bremard, Hureau, and Vezin, 2007). It was found that the interaction between Na$^+$ cation and stilbene occurs through one phenyl group facially coordinated to the Na$^+$ cation near the O atoms binding Al atoms. A fast generation of primary t-st$^{\bullet+}$ pair occurred by the laser UV (266 nm) photoionization. The charge carriers exhibit lifetimes about 1 hour at room temperature and disappeared according to direct charge recombination and electron transfer. This subsequent electron transfer took place between the electron-deficient radical cation and the electron donor oxygen atom of the zeolite framework.

One of the most intriguing properties of zeolites is their ability to promote spontaneous ionization through mere incorporation of t-stilbene in their porous networks. The spontaneous incorporation of t-stilbene in the pore of zeolites was

determined by direct exposure under dry and inert atmosphere of solid *t*-stilbene to dehydrated porous material without any solvent. The basis of the spontaneous ionization phenomena upon mere incorporation in zeolites was reviewed recently (Morrall, Dalton, Humphrey, and Samoc, 2008; Strat, Buruiana, Buruiana, Pohoata, and Strat, 2005). Many reviews demonstrated that the sorption occurs in parallel with spontaneous ionization process in acidic zeolite such as H-AlZSM-5 (Moissette et al., 2010). They described that *t*-stilbene presents a relatively low ionization potential values (I.P. = 7.65 eV), which is known to induce readily spontaneous ionization in acidic zeolite. Whereas it is incorporated as an intact molecule in nonacidic Na-AlZSM-5. The presence of the acid proton (H^+) and the framework aluminum greatly promotes the spontaneous ionization because of the high electrostatic field of protron and tight fit offered by the pore structure of the ZSM-5 zeolite (Moissette, Lobo, Vezin, Al-Majnouni, and Bre´mard, 2010).

Ellison and Thomas (2001) have been also studied the fluorescence lifetime of *t*-stilbene adsorbed on NaY under various conditions in order to gain information about motion of *t*-stilbene in the adsorbed state. They reported that in dehydrated NaY and small amount of water added, lifetime was decreased whereas saturation of the zeolite NaY by either water or cyclohexane lifetime increased, indicating a decrease in mobility of trans-stilbene due to blocking effects of the solvent because *t*-stilbene in bathing the zeolite in H_2O should be trapped *t*-stilbene in particle interior and considerably weaken by the presence of H_2O. In contrast to the other studies have been shown that when the zeolite voids are filled with H_2O, an increase in the mobility of aromatic species such as antharcene included them was observed. This

situation led to weaken the π electron-cation interaction and lifetime of aromatic species should be decreased (Hashimoto, Hagiri, Matsubara, and Tobita, 2001).

In addition the steady-state fluorescence spectra obtained from stilbenes incorporated in various medium have been present. For example, the excimer fluorescence of *t*-stilbene in ternary aqueous solution of γ-cyclodextrin was reported by Agbaria and co worker (Agbaria, Roberts, and Warner, 1995). They reported that excimer bands of *t*-stilbene involving an ternary complex of *t*-stilbene / γ-cyclodextrin/cyclohexane was observed. They suggest that cyclohexane plays a key role in increasing the fluorescence intensity at 420 nm. It can provide a unique environment for the transformation of the *t*-stilbene excimer that may act as a spacer between the double bonds of adjacent *t*-stilbene molecules. In addition, the experimental and computational studies of *t*-stilbene which was encapsulated to capsules was investigated. The experimental results are agreed with the computational data. The results show that the fluorescence of *t*-stilbene persists in the large cage which is similar to free stilbene. The geometry of *t*-stilbene in ground state as well as first excited state is unaffected by encapsulation in large cage. While in small cage ground stated of *t*-stilbene is distorted by the phenyl group twisted. The geometry of the excited state lies at the conical intersection with ground state. In this manner, the excited state of stilbene in small cage does not emit, but it can decay nonradiatively through the conical intersection to the ground state that is similar to the experiment (Tzeli, Theodorakopoulos, Petsalakis, Ajami, and Rebek, 2012; Ams et al., 2009). The ability to record phosphorescence from stilbenes, even at room temperature is significant as only very weak phosphorescence from *t*-stilbene. However, inclusion *t*-stilbene in zeolites makes the T_1-S_0 radiative processes operative, when the small

cations of the zeolite are exchanged by larger cations, such as Rb^+, Cs^+, and Tl^+, possessing higher spin-orbit coupling parameters, which may induce efficient spin interconversion between excited stated (Ramamurthy and Turro, 1995). Ciorba and coworker showed that, with the use of zeolites as a medium, can detect phosphorescence from systems which have traditionally escaped detection. They presented that after inclusion of some aza-stilbenes in commercial NaY and cation-exchanged TlY faujasites to get information on the triplet properties induced by the heavy atom effect. The research was successful in detecting the phosphorescence spectrum of *t*-stilbene in TlY whereas did not show any phosphorescence when included in NaY (Ciorba, Clennan, Mazzucato, and Spalletti, 2011). The triplet emission can also agree well with the literature reports (Ramamurthy, Caspar, Eaton, Kua, and Corbin, 1992). Phosphorescence spectra at 298 K of *t*-stilbene included in TlX and in Tl ZSM-5 (excitation λ at 290 nm) can be detected triplet emission band at 579, 639, and 697 nm for TlX and 567, 623, and 691 nm for Tl ZSM-5. The above observations demonstrate that zeolite as a new medium for turning on the external heavy-atom perturbation of *t*-stilbene in which intersystem crossing (ISC) occurs between π-π* states.

The purpose of the present work is to investigate influences of the microenvironment of zeolite LTL in acidic form (H-LTL) and potassium form (K-LTL) including ice hockey and round shape on the photophysical properties of *t*-stilbene molecule.

6.2 Materials and method

Experimental procedure of *t*-stilbene loaded on zeolite LTL and physical measurements are explained in the Chapter IV, pp. 108-110 (insertion temperature of *t*-stilbene is 125 °C).

6.3 Results and discussion

6.3.1 UV-Vis absorption spectra of *t*-stilbene in solution

UV-Vis absorption spectra of the *t*-stilbene in hexane show the absorption band around 250-350 nm with the maximum at 297 nm (see Figure 6.1). This peak is believed to be largely due to π-π* transition. The π orbital is localized in the region of the olefinic double bond to a large extent, but it is affected by conjugative effects of the phenyl rings (Waldeck, 1991).

When *t*-stilbene in hexane was exposed to UV and visible light (360 nm), it results in spectral changes that absorption is weaker and shifted to shorter wavelength (see Figure 6.1 inset). The difference between two isomers has been associated with structural differences, trans isomer being planar but the cis isomers being twisted. Moreover, the emission spectrum of *t*-stilbene dissolved in hexane at λ_{max} 360 nm and exhibit mirror relationships with the absorption spectrum, consistent with fluorescence from the monomers. Considering transition probability between states of differing multiplicities, singlet-triplet absorption intensities may be increased by the use of solvent containing a heavy atom such as bromide or iodine (Chaudhuri and Gakguly, 1969).
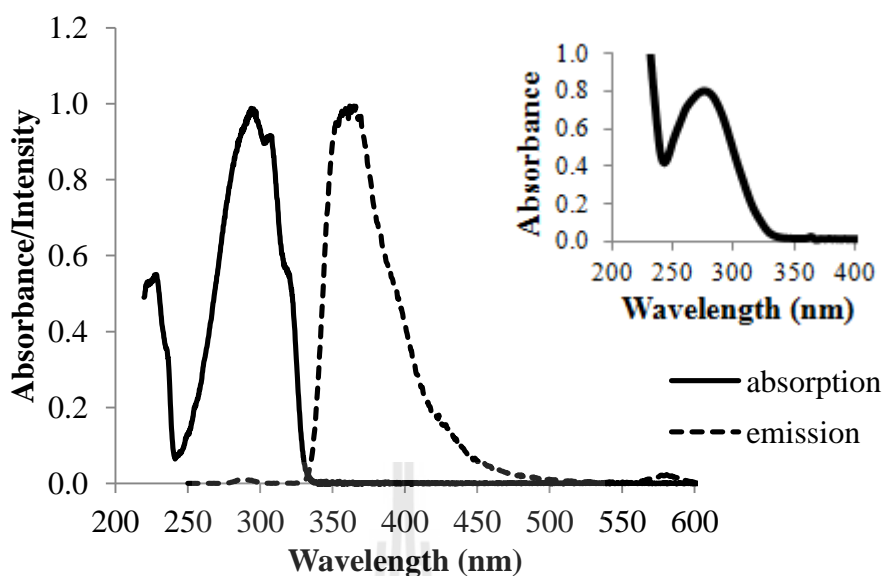
Figure 6.1 Absorption and emission spectrum of *t*-stillbene dissolved hexane (λ_{ex}=290 nm), inset is *t*-stilbene exposed to UV light.

6.3.2 Diffuse reflectance spectra of *t*-stilbene in zeolite LTL

Diffuse reflectance UV-Visible (DR-UV) spectra of *t*-stilbene in K-LTL and H-LTL including ice hockey and round shape were presented in Figure 6.2 and 6.3, respectively. All spectra show an intense and broad absorption band in the UV region between 250-350 nm with a maximum at 308 nm. This absorption band is characteristic of the *t*-stilbene molecule in neutral form (Obrzut and Karasz, 1987).
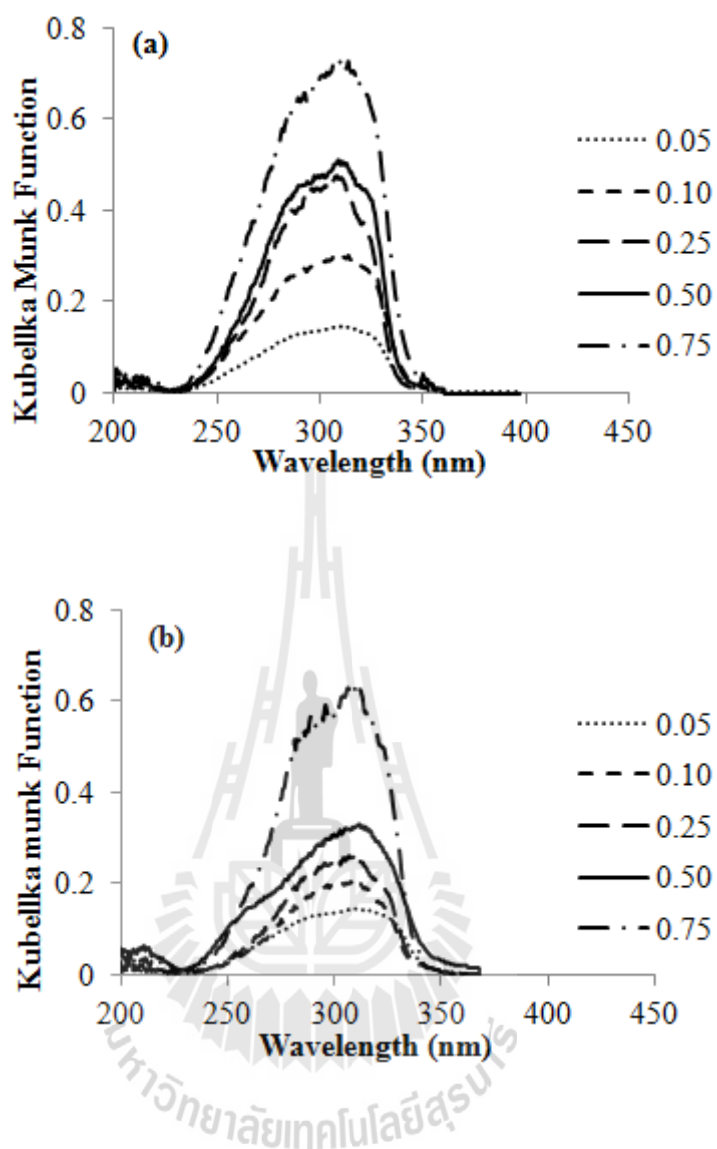
Figure 6.2 Diffuse reflectance spectra of *t*-stilbene adsorbed on K-LTL in ice hockey

(a) and round shape (b) with occupation probability (ρ; 0.75, 0.50, 0.25, 0.10, 0.05).
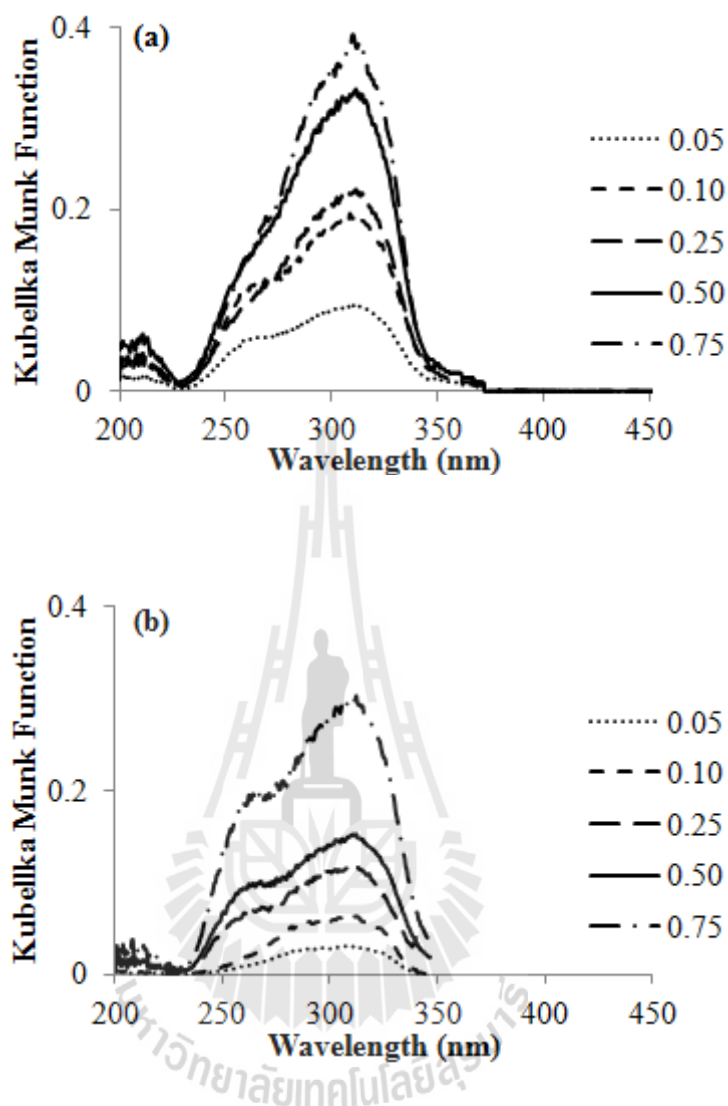
Figure 6.3 Diffuse reflectance spectra of *t*-stilbene adsorbed on H-LTL in ice hockey

(a) and round shape (b) with occupation probability (ρ; 0.75, 0.50, 0.25, 0.10, 0.05).

While *t*-stilbene adsorbed on H-LTL show a new shoulder band observed at 263 nm. This situation will be described by interaction between dye and zeolite framework in which BrØnsted acid site is interacted with *t*-stilbene through the central double bonds of *t*-stilbene that is similar to the literature (Hureau et al., 2012), shoulder band obtained after mixing *t*-stilbene with H-FER zeolite.
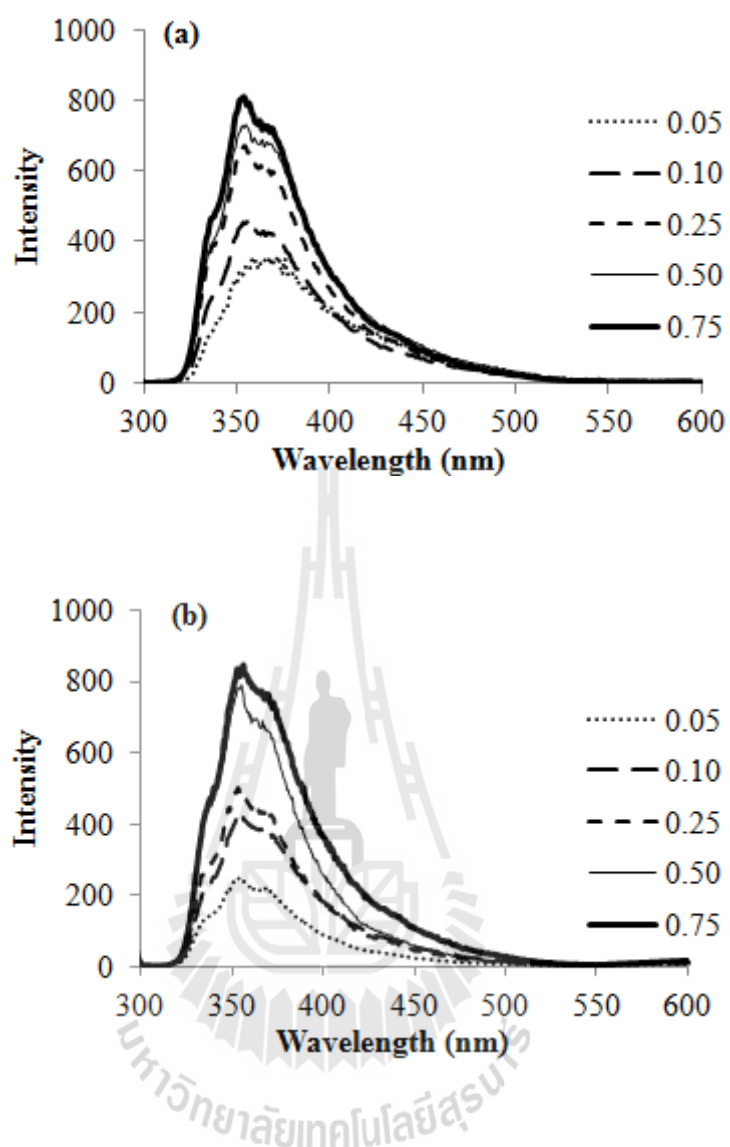
Figure 6.4 Emission spectra of *t*-stilbene adsorbed on K-LTL in ice hockey (a) and

round shape (b) with occupation probability (ρ; 0.75, 0.50, 0.25, 0.10, 0.05).
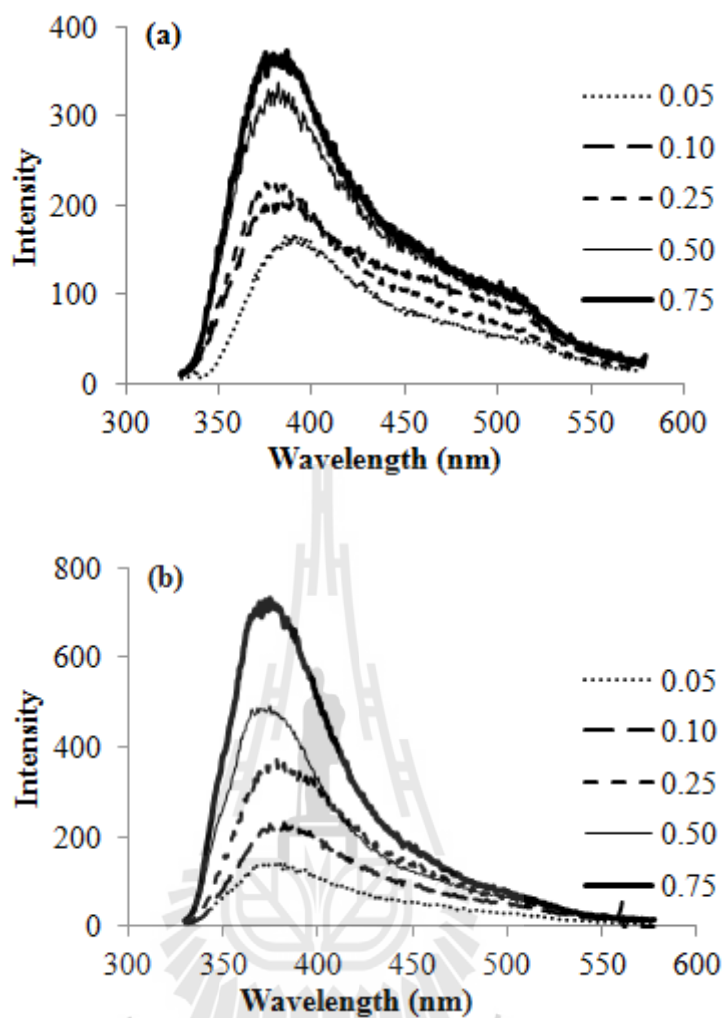
Figure 6.5 Emission spectra of *t*-stilbene adsorbed on H-LTL in ice hockey (a) and round shape (b) with occupation probability (ρ; 0.75, 0.50, 0.25, 0.10, 0.05).

6.3.3 Emission spectra of *t*-stilbene in zeolite LTL

The emission spectra of *t*-stilbene dissolved in various solvents were shown in Figure 6.1, the band maximum around 360 nm. Normally, the emission spectra exhibit an ambiguous vibronic structure in organic solvents at room temperature. In this work the emission spectra of *t*-stilbene adsorbed on K-LTL including ice hockey and round shape were shown in Figure 6.4. The excitation

wavelength was 290 nm for all of the samples. The band maximum is centered at 354 nm and the shoulder peak is at 368 nm that appeared in the both shapes. This result indicates that the harder restriction of the K-LTL zeolite on the motion of *t*-stilbene could maintain the conformation of the *t*-stilbene molecule unchanging during the photo exciting. However, the shoulder peak of *t*-stilbene may be attributed to the interaction of phynyl group and central C=C double bond with K^+ ions in K-LTL. The similar result is also observed as *t*-stilbene was doped in Sol-Gel system that unchanged the emission spectra (Perng, 2002). In the case of *t*-stilbene adsorbed on H-LTL including ice hockey and round shape shown in Figure 6.5, the maximum are about 375-380 nm in the both shapes. The different between the emission spectra of *t*-stilbene adsorbed on K-LTL and H-LTL were discussed. The change in the emission spectra to red shift of the *t*-stilbene adsorbed on the H-LTL was suggested to be caused by a local polarity around the adsorbed species on H-LTL more polar than that on K-LTL. However, some paper reported that the red shift of the polyurethane with anchored *t*-stilbene is caused by the formation of small aggregates of *t*-stilbene molecules in thin films (Strat, Buruiana, hohoata, and Strat, 2005). In addition, Altomare et al have been observed the emission band of trans-4-vinylstilbene (4VS) polymer solution, at 100 mol% 4VS units, and *t*-stilbene chromophore attracted to polypeptides and polyacrylate at 450 and 420 nm, respectively. (Altomare, Carlini, Solaro, Houben, and Rosato, 1983).

6.4 Conclusions

The incorporation of *t*-stilbene into the channel of zeolite LTL was done by gas phases method. The experimental studies performed by the diffuse reflectance UV-visible absorption and fluorescence emission show that the *t*-stilbene molecule is adsorbed in zeolite LTL (K-LTL and H-LTL) including ice hockey and round shape is in a neutral form. The UV−visible spectra of the dye does not changes compared with in solution (hexane). These results indicated that the perturbation of the electronic and vibrational states of the dye upon sorption in zeolite LTL.

6.5 References

Agbaria, R. A., Roberts, E., and I. M. Warner. (1995). Excimer fluorescence of trans-stilbene in ternary aqueous solutions of cyclodextrin. **J. Phys. Chem**. 99: 10056-10060.

Altomare, A. Carlini, F. Solaro, R. Houben. J. L. Rosato, N. (1983). Photochemistry and photophysics of copolymers of (-)-menthyl acrylate with 4-hydroxystilbene acrylate. **Polymer**. 24: 95-100.

Ams, M. R., Ajami, D., Craig, S. L., Yang, J.S., Rebek, J., and Beilstein, Jr. (2009). Control of stilbene conformation and fluorescence in self-assembled capsules. **J. Org. Chem**. 5: 79-82.

Chaudhuri, M. K., and Gakguly, S. C. (1969). Absorption and fluorescence spectra of crystalline trans-stilbene. **J. Phys. C: Solid State Phys**. 2: 1560-1568.

Ciorba, S., Clennan, E. L., Mazzucato, U., and Spalletti, A. (2011). Induced phosphorescence of some aza- and thio-stilbenes embedded in thallium-exchanged zeolites. **J. Lumin**. 131: 1193-1197.

Ellison, E. H., and Thomas, J. K. (2001). Single-pulse measurements of fluorescence lifetimes: The influence of solvent on the isomerization of *trans*-Stilbene included in zeolites. **J. Phys. Chem. B**. 105: 2757-2760.

Grabowski, R., Rotkiewicz, W., and Rettig, W. (2003). Structural changes accompanying intramolecular electron transfer: Focus on twisted intramolecular charge-transfer states and structures. **Chem. Rev**. 103, 3899-4032.

Haskins-Glusac, K., Ghiviriga, I., Abboud, K. A., and Schanze, K. S. (2004). Photophysics and photochemistry of stilbene-containing platinum acetylides. **J. Phys. Chem. B**. 108: 4969-4978.

Hashimoto, S., Hagiri, M., Matsubara, N., and Tobita, S. (2001). Photophysical studies of neutral aromatic species confined in zeolite L: Comparison with cationic dyes. **Phys. Chem. Chem. Phys**. 3: 5043-5051.

Hureau, M., Moissette, A., Vezin, H., Brémard, C., Orio, M. (2012). Influence of confinement effect on electron transfers induced by t-stilbene sorption in medium pore acidic zeolites. **J. Phys. Chem. C**. 116: 1812-1825.

Kawaguchi, Y. (1994). The new photoisomerization mechanism of stilbene. **J. Chem. Phys**. 100: 8856-8869.

Likhtenshtein, G. I., Bishara, R., Papper, V., Uzan, B., Fishov, I., Gill, D., and Parola, A. H. (1996) Novel fluorescence-photochrome labeling method in the study of biomembrane dynamics. **J. Biochem. Biophys. Methods**. 33(2): 117-133.

Meier, H., Stalmach, U., Fetten, M., Seus,P., Lehmann, M., and Schnorpfeil, C.(1998). Photochemistry of stilbenoid compounds-ways from photochemistry to materials science. **J . Inform. Rec**. 24: 47-60.

Morrall, J. P., Dalton, G. T., Humphrey, M. G., and Samoc, M. (2008). Organotransition Metal Complexes for Nonlinear Optics. **Adv. Organomet. Chem**. 55: 61-136.

Moissette, A., Bremard, C., Hureau, M., and Vezin, H. (2007). Slow interfacial electron hole transfer of a *trans*-Stilbene radical cation photoinduced in a channel of nonacidic aluminum rich ZSM-5 zeolite. **J. Phys. Chem. C**. 111: 2310-2317.

Moissette, A., Lobo, R. F., Vezin, H., Al-Majnouni, K. A., and Bre´mard, C. (2010). Long lived charge separated states induced by *trans*-Stilbene incorporation in the pores of Brønsted acidic HZSM-5 zeolites: Effect of Gallium on the spontaneous ionization process. **J. Phys. Chem. C**. 114: 10280-10290.

Obrzut, J., and Karasz, R. E. (1987). Ultraviolet and visible spectroscopy of poly(paraphenylene vinylene). **J. Chem. Phys**. 87: 2349-2358.

Perng, J. H. (2002). Luminescence Study of *cis*- and *trans*-stilbenes in the sol-gel system. **J. Fluorescence**. 12 (3): 311-316.

Ramamurthy, V., and Turro, N. J. (1995*).* Photochemistry of organic molecules within zeolites: Role of cations. **J. Incl. Phenom. Mol. Rec. Chem**. 21: 239-282.

Ramamurthy, V., Caspar, J. V., Eaton, D. F., Kua, E. W., and Corbin, D. R. (1992). Heavy-atom-induced phosphorescence of aromatics and olefins induced within zeolites. **J. Am. Chem. Soc**. 114: 3892-3896.

Tzeli, D., Theodorakopoulos, G., Petsalakis, I. D., Ajami, D., and J. Rebek. (2012). Conformations and fluorescence of encapsulated stilbene. **J. Am. Chem. Soc**. 134: 4346-4354.

Strat, G., Buruiana, E., Buruiana, T., Pohoata, V., and Strat, M. (2005). Fluorescence properties of the polyurethane with anchored stilbene chromophore. **J. Optoelectron**. **Adv. Mater**. 7: 925-928.

Waldeck, D. H. (1991). Photoisomerization dynamics of stilbenes. **Chem. Rev**. 91: 415-436.

CHAPTER VII

CONCLUSIONS

In this research, zeolites with framework Linde L (LTL) are synthesized successfully by a hydrothermal method, from molar compositions of 2.62-3.78 K_2O: 0.8-1.4 Al_2O_3: 8-12 SiO_2: 80-200 H_2O. Their morphologies varied from ice hockey to cylindrical shapes and their crystal sizes varied from 1.50-7.53 µm, as determined by scanning electron microscopy and particle size analyzer.

The zeolites LTL (K-LTL and H-LTL) with ice hockey and round shape have been used as a host and acridine hydrochloride (Ac) and acriflavine hydrochloride (AF) as guest molecules. This system is referred as a supramolecular chemistry in which two or more molecules or ions that are held together in structural relationships by chemical bonding. Cationic dyes and neutral dyes were incorporated into the channels of zeolite LTL by ion-exchange and gas phase method, respectively to obtain dye loaded zeolite LTL systems for using as artificial antenna system. To build an artificial antenna device which consists of monomeric dye, it is necessary to know the behavior of the dyes within zeolite LTL. The results from the experiment showed that the photophysical properties of Ac and AF are very sensitive to the form of zeolite LTL (K-LTL and H-LTL) regardless of morphology. Moreover, this result agreed with the theoretical calculations that density function theory (DFT) and time dependent density function theory (TD-DFT) were performed. In addition, the energy migration in Ac loaded on zeolite LTL, modified with AF as acceptor molecules

follows requirements expected for fluorescence resonance energy transfer (FRET) mechanism.

In this thesis the photophysical property of neutral dye (*t*-azobenzene) was studied because of less information on the photophysical properties of the neutral dye. The experimental data are in line with the calculation results. *t*-Azobenzene was protonated by the Brønsted acid site of H-LTL, while *t*-azobenzene interacts only with the zeolite framework of K-LTL. However, both forms are constrained by the framework and the *t*-azobenzene is therefore twisted. Moreover, the emission spectrum (380 nm) was detected only from protonated *t*-azobenzene incorporated into H-LTL while *t*-azobenzene was evidently not found confined in the K-LTL framework from the experiment, as judged by no observation of fluorescence. The results of the study lead to the conclusion that the zeolite framework affects the photophysical properties of *t*-azobenzene.

Finally, the amount of adsorbed Ac and AF on zeolite LTL (K-LTL and H-LTL) including ice hockey and round shape was estimated by studying the adsorption isotherms. The result showed that the maximum loading (Θ_{max}) of AF on H-LTL and K-LTL with the both shapes was higher than that of Ac molecule. In addition, the thermodynamic quantities indicated that the adsorptions of both dyes on zeolite LTL are spontaneous, endothermic and highly disordered. Considering the spectral properties of AF and Ac loaded on zeolite LTL indicates that it can be used as artificial antenna material. The adsorption capability of Ac and AF indicates that Ac and AF used as donor-acceptor pair in zeolite LTL is not effective in energy transfer. However, we expected that these dyes can be used effectively in an artificial system if

the Ac molecule served as acceptor molecule together with a suitable donor molecule and AF is used as donor molecule together with a suitable acceptor molecule.

APPENDICES

APPENDIX A

SUPPORTING INFORMATION FOR CHAPTER

III AND IV

Table A.1 The electronic properties of AF, AFH$^+$, AF-H-LTL and AFH$^+$-H-LTL calculated by TD-B3LYP/6-31G(d,p) level of theory.

Structures	States	E_{Exc} (eV)	λ (nm)	Oscillator strength (*f*)	Assignment
AF	S1	3.17	390.8	0.5522	H-0 → L+0 (74%) & H-1 → L+1 (9%)
	S5	4.72	262.6	0.1219	H-0 → L+1 (43%) & H-2 → L+0 (24%)
	S6	5.09	243.4	0.5549	H-1 → L+1 (38%) & H-0 → L+3 (33%)
AFH$^+$	S1	2.85	434.6	0.1537	H-0 → L+0 (73%) & H-1 → L+0 (10%)
	S2	3.55	349.4	0.1604	H-1 → L+0 (65%) & H-0 → L+1 (19%)
	S4	4.59	270.4	0.5369	H-0 → L+1 (52%) & H-2 → L+0 (16%)
	S6	4.90	252.9	0.2796	H-1 → L+1 (44%) & H-3 → L+0 (30%)
	S7	5.31	233.3	0.1903	H-1 → L+2 (55%) & H-1 → L+1 (14%)
AF-H-LTL	S1	3.08	403.0	0.1482	H-0 → L+0 (42%) & H-2 → L+0 (33%)
	S3	3.23	384.1	0.3441	H-2 → L+0 (44%) & H-0 → L+0 (31%)
	S18	4.83	256.8	0.1393	H-0 → L+1 (47%) & H-0 → L+2 (20%)

Table A.1 The electronic properties of AF, AFH$^+$, AF-H-LTL and AFH$^+$-H-LTL calculated by TD-B3LYP/6-31G(d,p) level of theory (Continued).

Structures	States	E_{Exc}(eV)	λ (nm)	Oscillator strength (f)	Assignment
AFH$^+$-HLTL	S1	2.22	558.1	0.0001	H-0 → L+0 (100%)
	S4	2.74	451.9	0.1358	H-3 → L+0 (76%) & H-8 → L+0 (5%)
	S8	3.55	349.3	0.0839	H-8 → L+0 (29%) & H-7 → L+0 25%)
	S9	3.56	348.3	0.0582	H-9 → L+0 (51%) & H-8 → L+0 (31%)
	S27	4.58	270.8	0.4951	H-3 → L+1 (53%) & H-3 → L+2 (12%)

Table A.2 The electronic properties of AF, AF_K$^+$ ion and AF_K-LTL and calculated

by TD-B3LYP/6-31G(d,p) level of theory.

Structures	States	E_{Exc} (eV)	λ (nm)	Oscillator strength (*f*)	Assignment
AF	S1	3.17	390.8	0.5522	H-0 → L+0 (74%) & H-1 → L+1 (9%)
	S5	4.72	262.6	0.1219	H-0 → L+1 (43%) & H-2 → L+0 (24%)
	S6	5.09	243.4	0.5549	H-1 → L+1 (38%) & H-0 →L+3 (33%)
	S7	5.26	235.6	0.6401	H-0 → L+3 (48%) & H-1 →L+1 (37%)
	S12	6.08	203.8	0.1885	H-4 → L+0 (51%) & H-2 → L+1 (25%)
AF_K$^+$	S1	3.02	405.6	0.2169	H-0 → L+0 (69%) & H-1 → L+0 (14%)
	S2	3.49	355.0	0.2707	H-1 → L+0 (69%) & H-0 → L+2 (8%)
	S6	4.49	275.9	0.1120	H-0 → L+2 (38%) & H-2 → L+0 (38%)
	S7	4.74	261.5	0.2034	H-0 → L+2 (35%) & H-0 → L+3 (21%)
	S8	5.04	246.0	0.4733	H-0 → L+3 (48%) & H-1 → L+2 (17%)
	S9	5.32	233.1	0.5363	H-1 → L+2 (47%) & H-0 → L+4 (7%)
AF_K-LTL	S1	3.03	405.0	0.4281	H-0 → L+0 (66%)
	S3	3.26	380.3	0.1103	H-3 → L+0 (74%) & H-2 → L+0 (7%)
	S11	4.60	269.4	0.1156	H-0 → L+6 (23%) & H-0 → L+2 (19%)
	S20	5.12	242.3	0.2818	H-2 → L+1 (31%) & H-0 → L+4 (29%)
	S21	5.16	240.4	0.1381	H-2 → L+1 (44%) & H-3 → L+1 (24%)
	S24	5.26	235.7	0.4101	H-0 → L+3 (31%) & H-3 → L+1 (21%)

Table A.3 The electronic properties of acridine in the gas phase, acridine in various solvent, protonated acridine (AcH$^+$) and acridine_H$_2$O calculated by TD-B3LYP/6-31G(d,p) level of theory.

Structures	States	E_{Exc} (eV)	λ (nm)	Oscillator strength (f)	Assignment
Ac	S1	3.35	370.5	0.0511	H-0 → L+0 (82%)
	S2	3.74	331.6	0.0009	H-2 → L+0 (95%)
	S3	3.94	314.4	0.0464	H-1 → L+0 (63%) &
					H-0 → L+1 (39%)
	S6	5.31	233.3	0.0423	H-0 → L+2 (81%)
AcH$^+$	S2	3.80	326.3	0.128	H-1 → L+0 (47%) &
					H-2 → L+0 (35%)
	S3	3.92	316.3	0.07	H-2 → L+0 (57%) &
					H-1 → L+0 (24%)
	S5	5.27	235.2	1.1722	H-0 → L+1 (61%) &
					H-1 → L+0 (10%)
Ac in acetonitrile	S1	3.31	374.6	0.0662	H-0 → L+0 (83%)
	S2	3.85	322.2	0.0011	H-2 → L+0 (96%)
	S3	3.94	315.0	0.0715	H-1 → L+0 (66%) &
					H-0 → L+1 (36%)
	S5	5.18	239.4	1.9248	H-0 → L+1 (55%) &
					H-1 → L+0 (21%)
Ac in methanol	S1	3.29	376.5	0.0703	H-0 → L+0 (83%)
	S2	3.92	316.3	0.0012	H-2 → L+0 (96%)
	S3	3.93	315.3	0.0794	H-1 → L+0 (67%) &
					H-0 → L+1 (35%)
	S5	5.14	241.4	1.9518	H-0 → L+1 (56%) &
					H-1 → L+0 (21%)
Ac in butanol	S1	3.29	376.6	0.0706	H-0 → L+0 (83%)
	S2	3.92	316.0	0.0012	H-2 → L+0 (96%)
	S3	3.93	315.3	0.0802	H-1 → L+0 (67%) &
					H-0 → L+1 (35%)
	S5	5.13	241.5	1.9544	H-0 → L+1 (56%) &
					H-1 → L+0 (21%)

(x) = calculated by using cpcm model.

Table A.3 The electronic properties of acridine (Ac) in the gas phase, acridine in various solvent, protonated acridine (Ac_H_3O^+) and acridine_H_2O calculated by TD-B3LYP/6-31G(d,p) level of theory (Continued).

Structures	States	E_{Exc} (eV)	λ (nm)	Oscillator Strength (*f*)	Assignment
Ac_H_2O	S1	3.31	374.6	0.0538	H-0 → L+0 (82%)
	S2	3.92	316.5	0.0007	H-4 → L+0 (57%) & H-2 → L+0 (38%)
	S3	3.94	314.7	0.0526	H-1 → L+0 (64%) & H-0 → L+1 (38%)
	S6	5.31	232.2	1.0705	H-0 → L+1 (34%) & H-0 → L+2(29%)
	S7	5.36	231.3	0.6242	H-0 → L+2 (55%) & H-0 → L+1 (18%)
Ac_H_3O^+	S1	3.03	409.7	0.0390	H-0 → L+0 (98%)
	S2	3.84	322.5	0.1368	H-1 → L+0 (64%) & H-2 → L+0 (21%)
	S3	3.95	313.8	0.0305	H-2 → L+0 (76%) & H-1 → L+0 (15%)
	S4	5.28	234.8	1.2431	H-0 → L+1 (71%) & H-1 → L+0 (20%)
	S6	5.62	220.6	0.2005	H-0 → L+2 (88%) & H-0 → L+1 (5%)

(x) = calculated by using cpcm model.

Table A.4 The electronic properties of acridine in the gas phase, Ac_K-LTL and Ac_ H-LTL calculated by TD-B3LYP/6-31G(d,p) level of theory.

Structures	State	E_{Exc} (eV)	λ (nm)	Oscillator Strength (*f*)	Assignment
Ac-H-LTL	S1	2.18	568.3	0.0000	H-0 → L+0 (99%)
	S4	3.01	411.9	0.0185	H-3 → L+0 (92%)
	S5	3.03	408.8	0.0293	H-4 → L+0 (88%)
	S10	3.83	324.4	0.0941	H-9 → L+0 (59%) & H-4 → L+1 (12%)
	S12	3.93	315.4	0.0163	H-13→L+0 (33%) & H-14→L+0 (17%)
	S40	5.22	237.4	0.7003	H-3 → L+0 (30%) & H-4 → L+1 (26%)
	S41	5.23	237.2	0.4448	H-3 → L+0 (53%) & H-4 → L+1 (16%)
Ac-K-LTL	S1	3.25	381.4	0.0561	H-0 → L+0 (97%)
	S2	3.91	317.4	0.0524	H-3 → L+0 (54%) & H-0 → L+1 (30%)
	S11	5.19	238.9	0.0513	H-0 → L+3 (84%)
	S12	5.22	237.7	1.1258	H-0 → L+1 (55%) & H-3 → L+0 (23%)
	S14	5.36	231.4	0.0513	H-0 → L+4 (56%) & H-0 → L+5 (35%)
	S15	5.38	230.4	0.1561	H-0 → L+5 (56%) & H-0 → L+4 (29%)

Table A.5 The electronic properties of bare t-azobenzene (t-AB), t-azobenzene_H$^+$ (t-ABH$^+$) and t-azobenzene_H-LTL in the gas-phase calculated by TD-B3LYP/6-31G(d,p) level of theory.

Structures	States	E_{Exc} (eV)	λ (nm)	Oscillator strength (f)	Assignment
t-AB	S1	2.55	486.0	0.0000	H-0 → L+0 (88%)
	S2	3.77	328.9	0.7716	H-1 → L+0 (79%)
	S4	4.11	301.6	0.0535	H-2 → L+0 (89%) & H-1 → L+1 (7%)
	S10	5.52	224.8	0.1321	H-1 → L+1 (77%) & H-3 → L+3 (12%)
t-ABH$^+$	S1	2.78	445.2	0.0421	H-1 → L+0 (84%) & H-0 → L+0 (9%)
	S2	3.04	407.7	0.6697	H-0 → L+0 (54%) & H-2 → L+0 (12%)
	S3	3.13	396.7	0.1447	H-2 → L+0 (77%) & H-0 → L+0 (8%)
	S11	5.64	219.8	0.0515	H-6 → L+0 (87%)
t-AB _H-LTL	S1	2.17	571.4	0.0001	H-0 → L+0 (99%)
	S5	3.11	399.0	0.2049	H-5 → L+0 (47%) & H-3 → L+0 (31%)
	S6	3.13	396.4	0.2106	H-5 → L+0 (51%) & H-3 → L+0 (26%)
	S7	3.23	383.9	0.0677	H-6 → L+0 (80%)
	S9	3.50	354.7	0.0573	H-9 → L+0 (42%) & H-8 → L+0 (24%)
	S10	3.55	349.0	0.0743	H-7 → L+0 (27%) & H-8 → L+0 (26%)

Table A.6 The electronic properties of bare t-azobenzene (t-AB), t-azobenzene_K$^+$ (t-AB_K$^+$), and t-azobenzene_K-LTL (t-AB_K-LTL) in the gas-phase calculated by TD-B3LYP/6-31G(d,p) level of theory.

Structures	States	E_{Exc} (eV)	λ (nm)	Oscillator strength (f)	Assignment
t-AB	S1	2.55	486.0	0.0000	H-0 → L+0 (88%)
	S2	3.77	328.9	0.7716	H-1 → L+0 (79%)
	S4	4.11	301.6	0.0535	H-2 → L+0 (89%) & H-1 → L+1 (7%)
	S10	5.52	224.8	0.1321	H-1 → L+1 (77%) & H-3 → L+3 (12%)
t-AB_K$^+$	S1	2.83	438.8	0.0422	H-2 → L+0 (36%) & H-0 → L+0 (29%)
	S2	3.55	349.2	0.1412	H-1 → L+0 (66%) & H-0 → L+0 (19%)
	S3	3.71	334.2	0.4843	H-2 → L+0 (43%) & H-0 → L+0 (32%)
	S5	4.33	286.3	0.0490	H-0 → L+1 (94%)
t-AB_K-LTL	S1	2.58	480.6	0.0156	H-0 → L+0 (62%) & H-1 → L+0 (25%)
	S2	3.81	325.0	0.6613	H-1 → L+0 (59%) & H-0 → L+0 (20%)
	S3	4.01	309.5	0.0664	H-3 → L+0 (88%)
	S4	4.21	294.7	0.0217	H-5 → L+0 (89%)

APPENDIX B

SUPPORTING INFORMATION FOR CHAPTER V

Table B.1 Ce and qe values of acridine hydrochloride (Ac) adsorbed on zeolite LTL.

30 °C

H-LTL (r)		H-LTL (i)		K-LTL (i)		K-LTL (r)	
Ce (μM)	qe (μM/g)	Ce (μM)	qe (μM/g)	Ce (μM)	qe (μM/g)	Ce (μM)	qe (μM/g)
4.8	0.1	4.8	0.1	1.2	1.0	1.1	1.0
6.2	1.0	8.4	0.4	2.5	1.9	2.2	2.0
16.5	2.1	22.0	0.8	5.5	4.9	5.4	4.9
37.1	3.2	46.0	1.0	19.8	7.6	17.8	8.1
60.0	3.8	70.4	1.2	42.0	8.3	41.0	8.5
84.5	3.9	92.7	1.4	66.7	8.3	65.2	8.7

40 °C

H-LTL (r)		H-LTL (i)		K-LTL (i)		K-LTL (r)	
Ce (μM)	qe (μM/g)	Ce (μM)	qe (μM/g)	Ce (μM)	qe (μM/g)	Ce (μM)	qe (μM/g)
2.6	0.6	4.2	0.2	0.7	1.1	0.7	1.1
4.6	1.4	7.9	0.5	1.9	2.0	1.3	2.2
12.4	3.1	19.8	1.3	4.5	5.1	4.2	5.2
30.1	5.0	43.5	1.6	18.0	8.0	17.0	8.3
52.0	5.8	68.1	1.7	39.0	9.0	39.3	8.9
76.0	6.0	92.2	1.9	63.9	9.0	63.3	9.2

Table B.1 Ce and qe values of acridine hydrochloride (Ac) adsorbed on zeolite LTL (Continued).

50 °C

H-LTL (r)		H-LTL (i)		K-LTL (i)		K-LTL (r)	
Ce (μM)	qe (μM/g)	Ce (μM)	qe (μM/g)	Ce (μM)	qe (μM/g)	Ce (μM)	qe (μM/g)
2.9	0.5	4.0	0.2	0.6	1.1	0.4	1.2
3.0	1.8	7.5	0.6	1.7	2.1	1.2	2.2
8.3	4.2	18.7	1.6	4.4	5.2	3.9	5.3
23.0	6.8	42.8	1.8	16.0	8.5	15.5	8.6
46.6	7.1	67.0	2.0	38.0	9.3	37.0	9.5
69.0	7.8	91.5	2.1	62.7	9.3	60.7	9.8

Table B.2 Ce and qe values of acriflavine hydrochloride (AF) adsorbed on zeolite LTL.

30 °C

H-LTL (r)		H-LTL (i)		K-LTL (i)		K-LTL (r)	
Ce (μM)	qe (μM/g)	Ce (μM)	qe (μM/g)	Ce (μM)	qe (μM/g)	Ce (μM)	qe (μM/g)
0.1	2.5	0.6	2.3	3.1	1.7	4.0	1.5
0.6	7.3	1.4	7.1	11.7	4.6	12.6	4.3
1.8	12.1	7.7	10.6	19.8	7.6	24.0	6.5
7.8	18.0	18.7	15.3	39.4	10.6	44.9	8.8
16.0	21.0	36.0	16.0	56.1	11.0	62.0	9.5

40 °C

H-LTL (r)		H-LTL (i)		K-LTL (i)		K-LTL (r)	
Ce (μM)	qe (μM/g)	Ce (μM)	qe (μM/g)	Ce (μM)	qe (μM/g)	Ce (μM)	qe (μM/g)
0.1	2.5	0.4	2.4	2.7	1.8	2.9	1.8
0.4	7.4	0.8	7.3	7.0	5.8	8.8	5.3
1.3	12.2	2.5	11.9	17.3	8.2	19.2	7.7
4.2	18.9	13.4	16.7	34.8	11.3	37.4	10.6
6.7	23.3	26.3	18.4	50.6	12.4	54.9	11.3

50 °C

H-LTL (r)		H-LTL (i)		K-LTL (i)		K-LTL (r)	
Ce (µM)	qe (µM/g)	Ce (µM)	qe (µM/g)	Ce (µM)	qe (µM/g)	Ce (µM)	qe (µM/g)
0.1	2.5	0.6	2.4	1.9	2.0	2.2	1.9
0.2	7.4	0.7	7.3	6.0	6.0	8.0	5.5
0.6	12.3	1.1	12.2	14.0	9.0	17.5	8.1
2.4	19.4	6.9	18.3	28.2	13.0	34.0	11.5
4.5	23.9	20.2	20.0	45.5	13.6	51.1	12.2
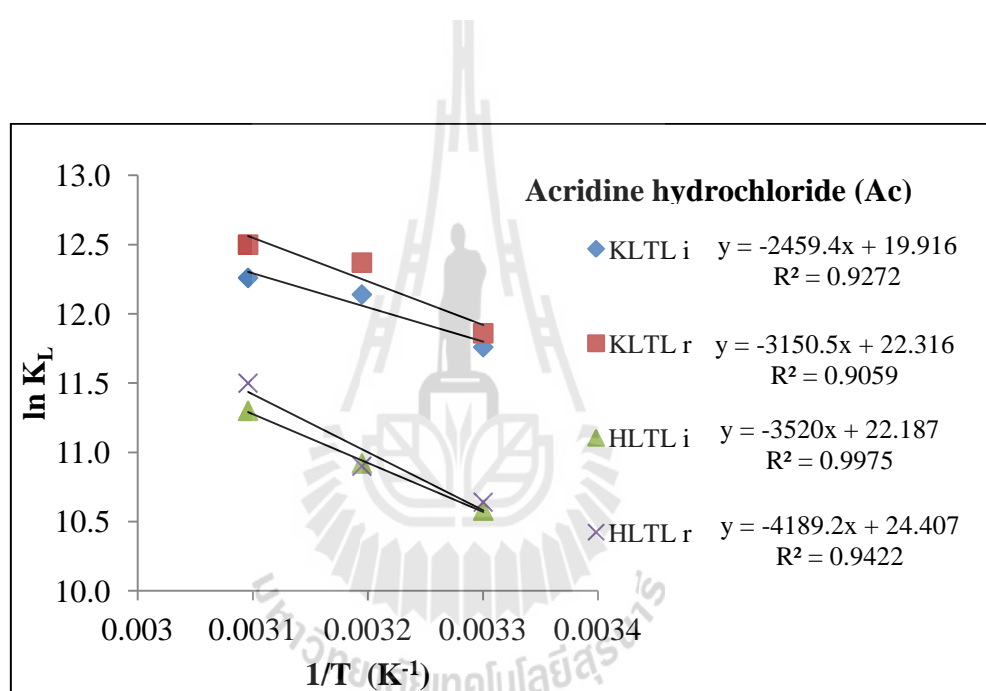
Figure B.1 The linear variation of ln K_L with reciprocal of temperature (1/T) of Ac adsorbed on zeolite LTL.
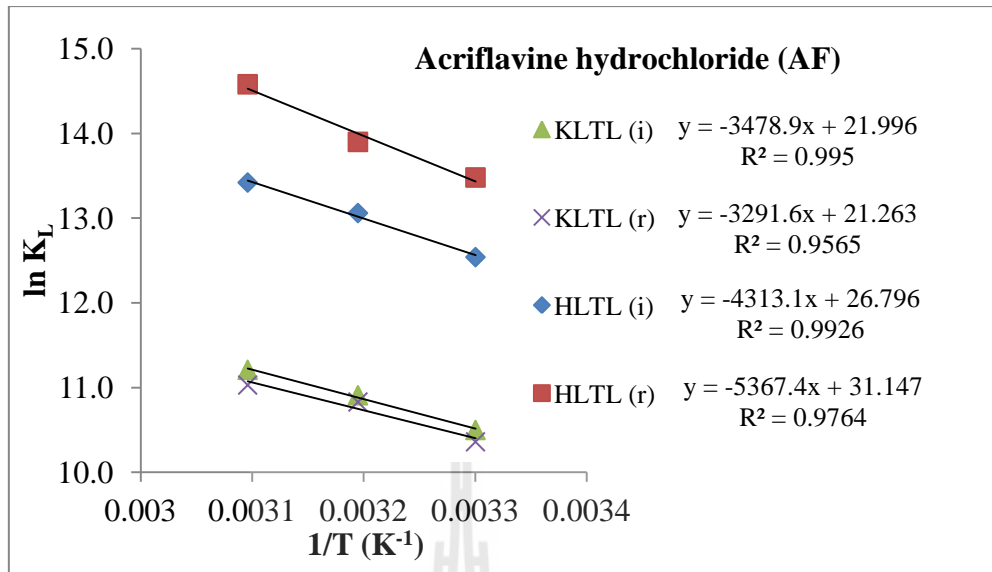
Figure B.2 The linear variation of ln K_L with reciprocal of temperature (1/T) of AF adsorbed on zeolite LTL.

APPENDIX C

THESIS RELEVANT PRESENTATIONS

Conferences presentations

Oral presentation

Wilaiporn Insuwan and Kunwadee Rangsriwattananon. Morphology-controlled Synthesis of Zeolite L and Physicochemical Properties, *German-Thai Symposium on Nanoscience and Nanotechnology (GTSNN 2011)*. 13-16 September 2011. Nakorn Ratchasima, Thailand. (Accepted)

Poster presentations

Wilaiporn Insuwan and Kunwadee Rangsriwattananon. Adsorption of Acriflavine on HLTL and KLTL Zeolite, International Association of Colloid and Interface Scientists Conference (IACIS 2012), 13-18 May 2012. Sendai, Japan.

Wilaiporn Insuwan, and Kunwadee Rangsriwattananon. Synthesis characterization of zeolite L with different morphology and crystals size. *Pure and Applied Chemistry International Conference (PACCON 2010)*, 21-23 January 2010. Ubon Ratchathani, Thailand.

Wilaiporn Insuwan and Kunwadee Rangsriwattananon. Synthesis of zeolite L with different morphology and crystals size, *The 35th Congress on Science and Technology of Thailand (STT'35)*. 15-17 October 2009. Chonburi, Thailand.

Jittima Meeprasert, Supawadee Namuangruk, **Wilaiporn Insuwan**, Kunwadee Rangsriwatananon, and Siriporn Jungsuttiwong. Photophysical properties of *trans*-azobenzene confined in H-LTL zeolite: DFT/TD-DFT investigations, *Pure and Applied Chemistry International Conference (PACCON 2013)*, 23-25 January 2013. Chon buri, Thailand.

Publication:

1. Insuwan, W., and Rangsriwatananon, K. (2012). Morphology controlled synthesis of zeolite and physicochemical properties. **Engineering Journal**.16, (3): 1-12. (accepted)

2. Wilaiporn Insuwan, and Kunwadee Rangsriwattananon. Evaluation of adsorption of cationic dyes on H-LTL and K-LTL Zeolite. **Journal of Porous Materials**. (submitted).
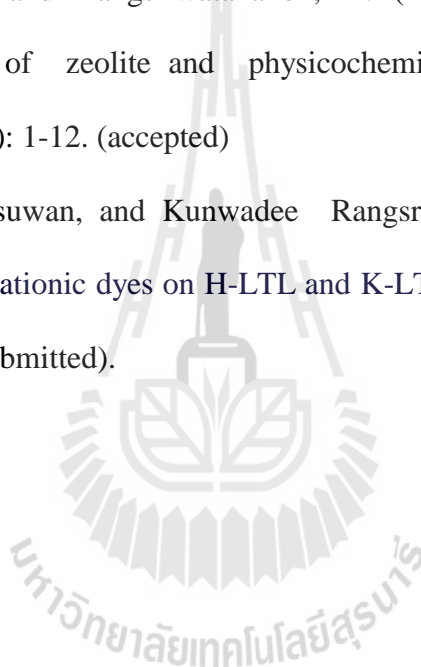
CURRICULUM VITAE

Name   Wilaiporn Insuwan

Date of Birth   March 10, 1984

Place of Birth   246 Moo 2, Tumbon Phosai, Phosai, Ubon Ratchathani, 34340,

Thailand

Education:

2006   B.Sc. in Chemistry, Ubon Ratchathani University, Thailand

2007-2013   Ph. D. candidate, Suranaree University of Technology,

Thailand

Relevant Experience:

2008-2012   Teaching Assistant, Courses: Fundamental Chemistry laboratory

I and II, Institute of Science, Suranaree University of

Technology

Scholarship:

2007-2010   The Commission on Higher Education (CHE), Thailand